Integration of Renewable Generation in Power System Defence Plans

Das, Kaushik

Publication date:
2016

Document Version
Publisher's PDF, also known as Version of record

Integration of Renewable Generation in Power System Defence Plans

Department of Wind Energy PhD Report 2016

Kaushik Das

DTU Wind Energy PhD-0058(EN)

March 2016

DTU Vindenergi
Institut for Vindenergi

Author: Kaushik Das

Title: Integration of Renewable Generation in Power System Defence Plans

Division: Department of Wind Energy

Summary:

Increasing levels of penetration of wind power and other renewable generations in European power systems pose challenges to power system security. The power system operators are continuously challenged especially when generations from renewables are high thereby reducing online capacity of conventional controllable generations to minimum. In such operation hours, the system is typically more vulnerable to disturbances in general and major disturbances in particular. This was the case in the major disturbance on 4th November 2006, where the Central European power system was split into 3 areas, one of them being the North East area with high share of wind power generation.

The aim of this study is to investigate how renewable generations like wind power can contribute to the power system defence plans. This PhD project “Integration of Renewable Generation in Power System Defence Plans” develops a new methodology to analyse the adequacy of reserves for future power systems with high penetration of wind power generation. This methodology assesses the requirements of frequency restoration reserves in order to contain the power imbalance caused by forecast errors within the designed frequency containment reserves. A set of sensitivity studies of the frequency containment process are performed where reserves are deployed from different power plant technologies including wind turbine.

Recommendations for protection and control strategies from wind turbines during overfrequency emergency are developed and discussed. Optimal underfrequency load shedding schemes for power systems with high penetration of distributed generation are developed and assessed through simulations. Results show the ability of such schemes to prevent additional load shedding, have minimum generation disconnection and better frequency response.

The PhD research work is carried out at Wind Energy Department in Technical University of Denmark. This work has been done as a part of EU-FP7 iTesla project.

DTU Wind Energy PhD-0058(EN)
March 2016

ISBN: 978-87-93278-77-6

Project Period:
2013.04.01 – 2016.03.31

Education:
PhD

Division:
Wind Energy

Supervision:
Poul Ejnar Sørensen, DTU Wind Energy
Anca Daniela Hansen, DTU Wind Energy
Hans Abildgaard, Energinet.Dk

Contract number:
n°. 283012

Sponsorship:
iTesla- R&D project co-funded by the EC 7th Framework Programme

Project Website:
http://www.itesla-project.eu/

Pages: 160
Figures: 82
Tables: 24
References: 105

Technical University of Denmark
Department of Wind Energy
DTU Risø Campus Frederiksborgvej 399
Building 115
4000 Roskilde
Denmark

www.vindenergi.dtu.dk

Abstract

Increasing levels of penetration of wind power and other renewable generations in European power systems pose challenges to power system security. The power system operators are continuously challenged especially when generations from renewables are high thereby reducing online capacity of conventional controllable generations to minimum. In such operation hours, the system is typically more vulnerable to disturbances in general and major disturbances in particular. This was the case in the major disturbance on 4^{th} November 2006, where the Central European power system was split into 3 areas, one of them being the North East area with high share of wind power generation.

The aim of this study is to investigate how renewable generations like wind power can contribute to the power system defence plans. This PhD project "Integration of Renewable Generation in Power System Defence Plans" develops a new methodology to analyse the adequacy of reserves for future power systems with high penetration of wind power generation. This methodology assesses the requirements of frequency restoration reserves in order to contain the power imbalance caused by forecast errors within the designed frequency containment reserves. A set of sensitivity studies of the frequency containment process are performed where reserves are deployed from different power plant technologies including wind turbine.

Recommendations for protection and control strategies from wind turbines during overfrequency emergency are developed and discussed. Optimal underfrequency load shedding schemes for power systems with high penetration of distributed generation are developed and assessed through simulations. Results show the ability of such schemes to prevent additional load shedding, have minimum generation disconnection and better frequency response.

The PhD research work is carried out at Wind Energy Department in Technical University of Denmark. This work has been done as a part of EU-FP7 iTesla project.

This page would be intentionally left blank if we would not wish to inform about that.

Dansk Resume

Den stadig voksende andel af vindkraft og anden vedvarende energi i Europa er en udfordring for at sikre stabil og sikker forsyning i fremtidens elsystemer. Udfordringen er særlig stor for netoperatørerne når produktioner fra vedvarende energikilder er høj og dermed reducerer andelen af konventionel styrbar produktion til et minimum. I sådanne driftssituationer er elsystemer typisk mere sårbare over for forstyrrelser i almindelighed og større forstyrrelser i særdeleshed. Dette var f.eks. tilfældet i de store forstyrrelser den 4. november 2006 hvor det centraleuropæiske elsystem blev opdelt i 3 områder, hvoraf det nordøstlige område havde en høj andel af vindkraft.

Det overordnede formål med PhD projektet "Integration of Renewable Produktion in Power System Defence Plans" er at undersøge hvordan vedvarende energi som vindkraft kan bidrage til systemværnet i elsystemet, dvs. til at sikre at større forstyrrelser ikke udvikler sig til kollaps af hele eller dele af elsystemet.

Først udvikles en ny metode til at vurdere tilstrækkeligheden af reserver til fremtidige elsystemer med høj andel af vindkraft. Denne metode vurderer behovet for reserver for at håndtere ubalancer forårsaget af vindkraft prognosefejl. Til det formål undersøges hvordan frekvensen påvirkes af reguleringen af forskellige kraftværksteknologier, herunder vindmøller.

Derefter udvikles strategier og anbefalinger vedrørende beskyttelse og styring af vindmøller under nødsituation. Anbefalingerne omfatter såvel overfrekvens som underfrekvens situationer, altså både situationer med produktionsoverskud som 4. november og med produktionsunderskud. I overfrekvens tilfælde anbefales at nedregulere vindmøller frem for at udkoble dem helt. I tilfælde af underfrekvens udvikles nye optimerede metoder til udkoblinger i distributionssystemet som tager hensyn til at der i dag ikke kun er forbrug koblet til distributionssystemet men også distribueret produktion fra vedvarende energikilder som vind og sol. Simuleringer af de foreslåede nye metoder viser at de både reducerer udkoblingen af distribueret produktion og forbedrer frekvensstabiliteten sammenlignet med nuværende praksis.

Ph.d. forskningen udføres på Institut for Vindenergi på Danmarks Tekniske Universitet. Dette arbejde er blevet udført som en del af EU-FP7 projektet iTesla.

This page would be intentionally left blank if we would not wish to inform about that.

Acknowledgements

I would like to express my special gratitude and thanks to my supervisors; main supervisor - Poul Ejnar Sørensen, and co-supervisors - Anca Daniela Hansen and Hans Abildgaard, for their guidance, support, encouragement, and valuable contributions throughout my doctoral study.

I would also like to thank Müfit Altin from DTU Wind Energy for his support, contributions and encouragements. This PhD work would not be possible without the continuous supports from my supervisors and Müfit Altin.

I would like to acknowledge that the CorWind outputs which I have applied in my research were obtained from Marisciel Litong-Palima and Petr Maule of DTU Wind Energy.

Special thanks and acknowledgements to Martin Høgdahl Zamastil, Knud Johansen and others from Energinet.Dk, for their valued contributions to my doctorate study.

I am thankful to Damian Flynn and Michael Power from University College Dublin, Ireland where I stayed for three months as an external PhD student. I have received valuable inputs and feedbacks from them during my external stay.

I am thankful to my colleagues at Integration and Planning section at DTU Wind Energy, for their knowledge sharing, support and friendship. It has been a privilege to work along with such esteemed and friendly colleagues. I cherish the experience of being a PhD student at DTU Wind Energy. I will also take the opportunity to thank Abdul Basit an alumnus of our section for his help and support.

I gratefully acknowledge that this doctoral study was financially supported by iTesla - R&D project co-founded by the EC 7^{th} Framework Programme. The collaborative research experiences with colleagues in iTesla project has not only been beneficial for my PhD research but also helped me in broadening my knowledge.

Last but not the least, a special thanks to my family. I would like to mention my thanks to my wife Moumita for her support in every form throughout the thesis. Words cannot express how grateful I am to my mother for all the sacrifices that she made on my behalf. I would also like to thank all my relatives for supporting me throughout my life.

Contents

List of Figures

This page would be intentionally left blank if we would not wish to inform about that.

List of Tables

Acronyms

BRP Balance Responsible Parties.

CE Continental Europe.

DG Distributed Generation.

DSO Distribution System Operator.

ENTSO-E European Network Transmission System Operators for Electricity.

FCP Frequency Containment Process.

FCR Frequency Containment Reserve.

FRP Frequency Restoration Process.

FRR Frequency Restoration Reserve.

FSWT Fixed Speed Wind Turbine.

LFC Load Frequency Controller.

LLSP Linear Least Square Problem.

NC-LFCR Network Code on Load-Frequency Control and Reserves.

NERC North American Electric Reliability Corporation.

NRMSE Normalised Root Mean Square Error.

PEGASE Pan European Grid Advanced Simulation And State Estimation.

PV Photovoltaics.

RMSE Root Mean Square Error.

RoCoF Rate of Change of Frequency.

RP Replacement Process.

RR Replacement Reserve.

SCADA Supervisory Control and Data Acquisition System.

SPP Southwest Power Pool.

SpPS Special Protection Schemes.

SyPS System Protection Schemes.

TSO Transmission System Operator.

UCTE Union for the Co-ordination of Transmission of Electricity.

UFLS Underfrequency Load Shedding.

VSWT Variable Speed Wind Turbine.

WPP Wind Power Plant.

WT Wind Turbine.

Chapter 1

Introduction

This chapter briefly introduces the background and motivation for this research project. The project objectives, limitations and contributions are summarized as well. The outline of the thesis is provided together with publication list related to this study.

1.1 Motivation

Majority of electrical power systems are aiming to reduce their dependencies towards fossil fuels in the face of growing concerns for environment, increasing fuel price, energy conservation, and sustainable development. As a result, there has been steady increase in renewable power generation in power systems all over the world and expected to grow further in future. In European power systems, among other renewables hydro power plants' net generation capacity is expected to remain stable until 2025, the installed wind power and solar net generation capacity can increase by 80% and 60%, respectively. Biomass and other renewable generation technologies will have a marginal role [9]. Wind power generations are connected both at high voltage transmission networks and medium/low voltage distribution networks. Whereas, during the last years, 80 % of the installed generation capacity of solar Photovoltaics (PV) panels is connected to low voltage grids [10]. A high proportion of Wind turbine (WT) and PV generations are converter based generations. These generations do not add any inertia to the system. Therefore, power systems with high penetration of these generations face new challenges.

Striving for utilization of power system infrastructure to its maximum capacity, reliability of network is compromised. Figure 1-1 depicts different power system states. Figure 1-1 illustrates that most of the power systems are operated with n-1 security constraints, which implies that the grid will remain viable with the outage of any one system element. It ensures that most credible contingencies affecting generating units or transmission system elements must not lead to severe consequences i.e. in "normal"

or “secure” state [2]. If the system parameters are still within admissible ranges but the system does not meet n-1 criteria any more, power system is considered to be in “alert” state (or endangered state).

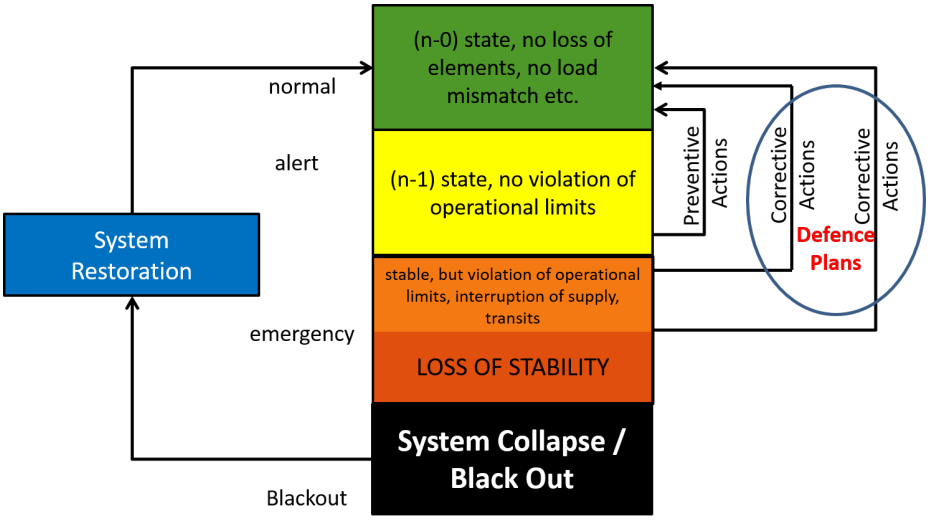

Figure 1-1: Power System States

In alert state, as consequence of extreme or unforeseen contingencies (like cascading outages), admissible operational limits of power system parameters could be violated and power system would move to “emergency” state (a disturbed state). A system in emergency state might not be able to fulfil its function with respect to consumer supply and power transfers, but is not blacked out. However, there is the risk of blackout in case of loss of stability. Power system stability can be defined as the ability of an electric power system, for a given initial operating condition, to regain a state of operating equilibrium after being subjected to a physical disturbance, with most system variables bounded so that practically the entire system remains intact [11]. Instability can be of short term or long term, it can concern the rotor angle, voltage or frequency and may be caused due to small or large disturbance. Figure 1-2 [11] depicts the classification of different types of instabilities in terms of time scale and type of disturbances. When the system is in emergency state, relevant actions must be taken immediately to prevent blackout [6]. In order to minimize the impact of these rare but extreme contingencies defence plans have been developed and implemented by several utilities.

A defence plan can be considered as an additional level of protection, designed to initiate the final attempt at stabilizing the power system when a widespread collapse is imminent. Therefore, defence plan lies between emergency state and blackout as shown in Figure 1-1. System Protection Schemes (System Protection Schemes (SyPS)) or Special Protection Schemes (Special Protection Schemes (SpPS)) such as automatic generation run back schemes, load or generation rejection, load shedding, reactive switching, bus or system splitting, etc. are then regarded as coordinated elements used within a defence plan [12].

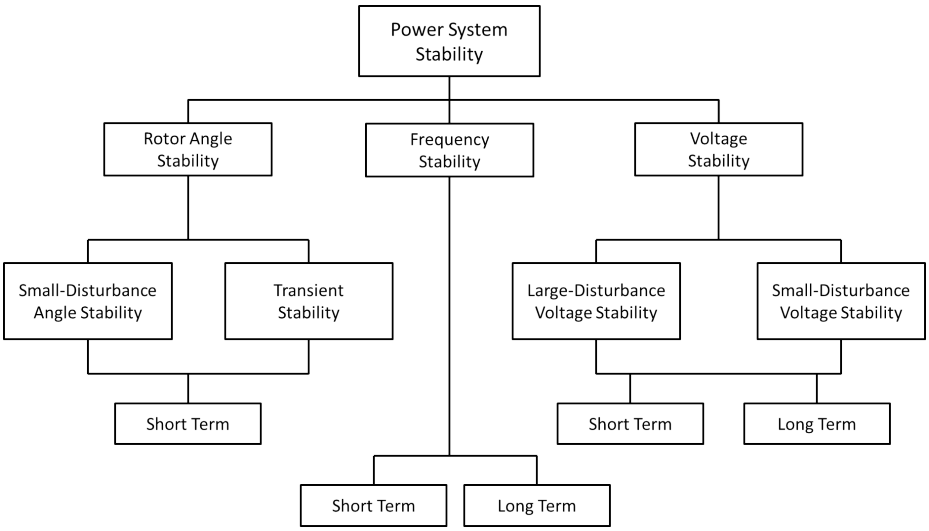

Figure 1-2: Classification of power system stability according to IEEE/CIGRE Joint Task Force on Stability Terms and Definitions. (©IEEE 2004)

This thesis is mainly concerned with defence plans for frequency stability. Therefore, studies are done for technical requirements of preventing the system frequency into entering alert and emergency state. Following which, defence strategies are developed as corrective measures to return the system frequency into normal or alert state if the system enters into emergency state to prevent frequency instability. As defined by Kundur et. al. [11], frequency stability is related to the ability of a power system to reach and maintain a stable operating frequency (sustainable from generators) following a severe disturbance (resulting in a significant imbalance between production and consumption) [11]. Instability that may result occurs in the form of sustained frequency swings leading to tripping of generating units and/or loads or in an aperiodic transient. In large interconnected power systems, this type of situation is most commonly associated with splitting of systems into islands. Stability in this case is a question of whether or not each island will reach a state of stable operating equilibrium with minimum unintentional loss of load. It is determined by the overall response of the island as evidenced by its mean frequency [6]. If frequency moves beyond pre-defined range, frequency protection can disconnect the power plants leading to separation of the interconnected systems or blackout of the power system [13]. As stated in "ENTSO-E - Technical Background and Recommendations for Defence Plans in the Continental Europe Synchronous Area" [6] frequency stability problems are associated with:

- inadequacies in regulation/control of power plants;
- poor coordination of control and protection equipment;
- unintentional protection trips leading to islands or high load-generation imbalance;
- out of step of plants;
- voltage instability;

- insufficient generation reserve respectively excessive power imbalance.

During frequency excursions, the time constants of the processes and devices participating in these excursions may range from fraction of seconds (corresponding to the response of devices such as underfrequency relays, generator controls and protections) to several minutes (corresponding to the response of devices such as prime mover energy supply systems and load voltage regulators) [6]. In this sense, frequency stability may be a short-term or long-term phenomenon.

There has been history of system collapse due to frequency instability. In most of the cases, either defence plans were not available or not sufficient to prevent the blackout.

- Italian Blackout of September 28, 2003 [14] is such an example where frequency decay was not controlled adequately to stop generation from tripping due to underfrequency. Thus, over the course of several minutes, the entire Italian system collapsed causing a nationwide blackout.
- In the blackout in Southern Sweden and Eastern Denmark at September 23, 2003 [15], the system experienced voltage collapse followed by frequency collapse.

There are also events where blackouts could be prevented by adequate defence plans.

- During 1999 storm in the South-West of France, spread of loss of synchronism and frequency instability could be avoided by correct activation of out-of-step relays.
- The disturbance on November 4^{th}, 2006 [1] at the "Union for the Co-ordination of Transmission of Electricity" (UCTE) network is one of the most important phenomenon seen related to cascading overload phenomena leading to a splitting of the UCTE network and large frequency deviations. Tripping of a 380 kV line due to overload and other cascading trippings led to the final separation of the entire UCTE network in three islands [1] as shown in Figure 1-3. The frequency excursions in these three islands after the split are shown in Figure 1-4.

  The countries in the Western part were in power deficiency situation of about 9 GW. That led to a frequency drop down to about 49 Hz stopped by automatic load-shedding and by tripping of pumping storage units. The tripping of small and/or distributed generation units due to underfrequency increased power/consumption unbalance. The countries in the South-Eastern area encountered a slighter deficiency of power which led to a frequency drop to about 49.7 Hz and were not seriously affected by the disturbance. The countries in the North-Eastern area encountered a surplus of generation. The value of frequency was over 50.5 Hz in most of the cases and it peaked at 51.4 Hz. It was observed that a more efficient and coordinated Underfrequency Load Shedding (UFLS) scheme among Transmission System Operator (TSO)s in Europe is required. It is evident that DGs need to be monitored and controlled appropriately in a coordinated way between TSOs during emergency situations. North-Eastern area of the UCTE network experienced overfrequency situation. This area had high proportion of wind power generation which were being disconnected and reconnected arbitrarily. It demonstrates the requirement for proper control and protections settings of wind power generations.

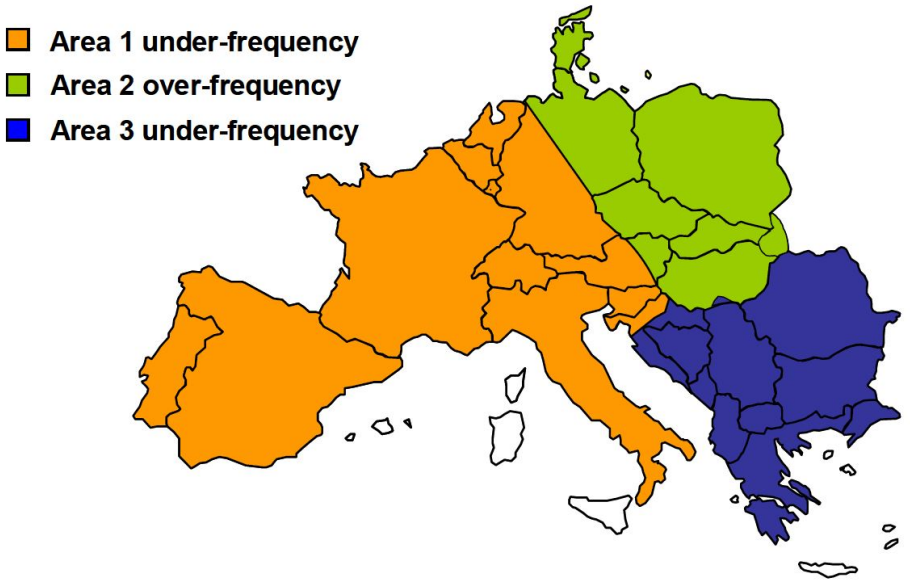

Figure 1-3: Schematic map of UCTE area split into three areas [1]

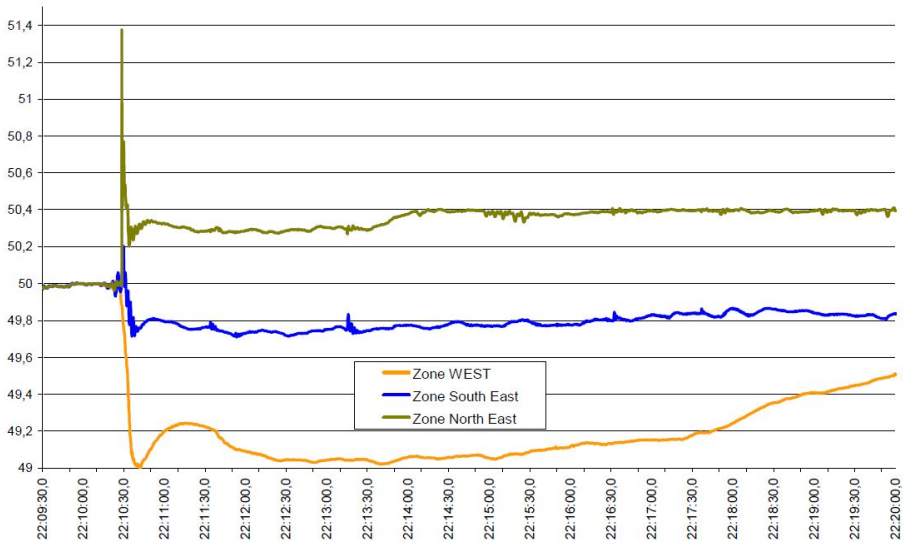

Figure 1-4: Frequency recordings after the split [1]

These examples show the importance of properly designed defence plans in any power system. Until now the existing defence plans have been planned and developed without considering the high penetration of renewable generation. Therefore, strong revisions of the traditional defence actions are required since characteristics of power system such as inertia, damping etc. change largely with high penetration of renewable generations. While every power system is operated close to its limits, increasing penetration

of renewable generation increases the vulnerability of the power system towards emergency. Therefore, modifications of design requirements for prevention of emergency & control and protection during emergency becomes more and more significant in present and future power systems. Detailed research should be performed to study the contributions and impact of renewable generations in power system defence plans. This is the motivation for this PhD project.

1.2 Project Objectives and limitations

The overall objective of this PhD project "Integration of Renewable Generation in Power System Defence Plans" is to investigate how wind power and other renewable generations can contribute to the power system defence plans ensuring that major disturbances do not develop into system blackouts.

The attention in the project is especially directed to the major and increasing role of wind power into the European power systems' stability and security. The role of other renewable generation especially PV generation is also taken into account sharing grid connection properties with converter connected WTs.The power system operators are continuously challenged especially when generations from renewables are high, thereby reducing online capacity of conventional controllable generation to minimum. In such operation hours, the system is typically more vulnerable to disturbances in general and major disturbances in particular. This was the case in the major disturbance on 4^{th} November 2006, where the Central European power system was split into 3 areas, one of them being the North East area with a very high share of wind power generation.

Specifically, the research objectives defined for this PhD project are:

- To review the state of the art-
  - To review the defence plans - definitions, descriptions and the state of art of power system defence plans from different organisations such as ENTSO-E, CIGRE, NERC etc.
  - To provide the state of the art for operating reserves - i.e. different types of frequency reserves in European power systems
  - To check wind power protection and control - the state of the art of wind power protection based on grid code requirements of different TSOs as well as control capabilities and strategies from converter connected WT models
- To study the adequacy of frequency reserves for future European power systems with high penetration of wind power generation
- To study the sensitivity of frequency containment process when frequency containment reserves are delivered from different technologies such as fossil steam generator, hydro generator, nuclear generator and wind turbine
- To develop and recommend overfrequency control and protection strategies for converter connected wind turbines during emergencies for different levels of wind power

penetration. To validate the proposed recommendations for a simulated Pan-European network.

- To develop an optimal underfrequency load shedding algorithm for power systems with large penetration of distributed generations. This algorithm should disconnect minimum amount of distributed generation while disconnecting required amount of consumption.

Project Limitations
Large penetration of renewable generations can have impacts in defence plans not only with respect to frequency stability but also rotor angle stability and voltage stability. This thesis work focuses only on frequency stability and not on other forms of stabilities.

While assessing the adequacy of reserves for future power systems, power imbalance caused by wind power forecasts are only considered. Therefore, power imbalances caused by other sources like loads, contingencies, other variable generations like solar PV etc. are not taken into account along this work.

Sensitivity studies of frequency containment process (FCP) are mainly concerned with the fast response capabilities of generators for power system for FCP assuming that volume of Frequency Containment Reserve (FCR) is sufficient. This sensitivity studies of frequency restoration process (Frequency Restoration Process (FRP)) is not considered in this work, therefore set-point of generators are kept constant.

1.3 Project Contributions

The main contributions of this PhD work are listed below:

- Overview of the state of art in defence plans as well as opportunities and threats of renewable generations towards existing defence plans.
- Proposal and development of a new methodology to assess adequacy of frequency reserves in future European power systems with high penetration of wind power is conducted, resulting in:
  - Development of an algorithm to estimate power imbalances due to wind power forecast errors.
  - Probabilistic risk assessment of power imbalances exceeding designed frequency containment reserves with activation of frequency restoration and replacement reserves.
  - Recommendations on volume and speed of frequency restoration reserve deployment for reducing probabilistic risk of power imbalances exceeding designed frequency containment reserves.
  - Investigation of the methodology for possible wind power generation scenarios in 2020 and 2030 for Continental Europe network.

- Sensitivity studies of frequency containment process when frequency containment reserves are delivered from different technologies of governor-turbine systems are conducted, resulting in:
  - Proposal and development of a mathematical analytical approach for frequency containment process.
  - Analytical studies of impacts of governor droop settings and system inertia on frequency containment process.
- Recommendations for protection and control settings of converter connected WTs during overfrequency emergency situations are discussed and proposed, as i.e.
  - Recommendations on power activation delays, ramping rate capabilities and droop settings of WTs for different degrees of wind power penetrations.
  - Validation of WT control and protection recommendations in large scale simulated Pan-European network.
- Development of new underfrequency load shedding schemes considering distributed WT and PV generation is conducted including:
  - Test of the proposed schemes on a simulated power system developed by Energinet.Dk

1.4 Thesis Outline

This PhD thesis is organised in 7 chapters as follows:

Chapter 1 provides an introduction by prescribing the motivations, project objectives and limitations, project contributions and thesis outline.

Chapter 2 gives an overview of the state of art in defence plans with respect to definitions, descriptions and existing practices. This chapter also discusses different types of operating frequency reserves used in European power systems. The opportunities and threats of WTs and PV generations towards existing defence plans are also discussed.

Chapter 3 proposes a new methodology to assess the adequacy of frequency reserves to handle power imbalances caused by wind power forecast errors. Challenges faced by future European power systems due to increased penetration of wind power generation are analysed. An algorithm is proposed and developed to estimate the power imbalances due to wind power forecast error following activation of different operating reserves. Assessment of probabilistic risk of power imbalances exceeding designed frequency containment reserves is estimated. Possibility of reducing this risk is investigated for different volumes and speed of frequency restoration reserve deployment in this chapter.

Having designed the volume requirements of reserves, it is important to decide the technology which can deploy frequency containment reserves. The choice of technology becomes crucial especially when the power system inertia is low due to high penetration of converter connected renewable generations. Chapter 4 is concerned with

frequency containment process (FCP). A mathematical analytical approach for FCP is proposed and discussed in this chapter. Capabilities of different technologies of generation sources in providing FCP are analysed through this mathematical analytical approach in this chapter. A set of simulations has been performed in a power system consisting of generic governor models or generic wind turbine model in order to study the impacts of droop settings and system inertia. Observations from these simulations are analyzed and explained in this chapter with the help of analytical model which provide the feasible range of droop settings for different values of system inertia.

Chapter 5 deals with protection and control settings of WTs during overfrequency emergency situations. Recommendations on power activation delays, ramping rate capabilities and droop settings of WTs for different degrees of wind power penetrations are proposed in this chapter. Following which, the success of frequency control from WTs with recommended settings are validated in a large scale simulated Pan-European network.

In chapter 6, new Underfrequency Load Shedding (UFLS) schemes are proposed considering the amount of Distributed Generation (DG) connected to the feeders in real-time and compares them with traditional UFLS scheme. The UFLS schemes proposed and discussed in this chapter are - i) traditional method using static relay ii) directional relay based UFLS using power flow direction in the feeders, iii) UFLS scheme using power flow magnitude and direction, iv) UFLS scheme using power flow and Distributed Generations (DG) data respectively. In order to use DG data, amount of DG connected to each feeder are estimated using power flow data in this chapter. Based on the real-time estimation of the amount of DG connected, each feeder is prioritized for UFLS. Following prioritization, feeders are selected for load shedding using mathematical optimization technique in this chapter. These methods are studied and compared on a simulated transmission system developed by Energinet.Dk in which distribution networks are incorporated. The results are compared over large number of random wind and PV generation scenarios.

Chapter 7 summarizes and concludes the thesis, providing suggestions for future research.

1.5 Publications

Journal Publications

P1 Kaushik Das, Antonios Nitsas, M. Altin, A. D. Hansen, P. E. Sørensen, "**Improved Load Shedding Scheme considering Distributed Generation**," in *IEEE Transactions in Power Delivery*, to be published in 2016.

P2 Kaushik Das, A. D. Hansen, P. E. Sørensen, "**Understanding IEC Standard Wind Turbine Models using SimPowerSystems**," in *Wind Engineering*, vol:40, issue:3, pp:212-227, 2016.

P3 S. D. Boeck, Kaushik Das, V. Trovato, J. Turunen, M. Halat, P. E. Sørensen, D.

V. Hertem,"**Review of Defence Plans in Europe: Current Status, Strengths and Opportunities**," in *CIGRE Science & Engineering*, vol:5, pp:6-16, 2016

Conference Publications

P4 J. N. Sakamuri, Kaushik Das, M. Altin, N. A. Cutululis, A. D. Hansen, P. Tielens, D. V. Hertem,"**Improved Frequency Control from Wind Power Plants Considering Wind Speed Variation**," in 19^{th} *Power System Computation Conference*, June 20 - 24, 2016, Genoa, Italy.

P5 Kaushik Das, M. Litong-Palima, P. Maule, P. E. Sørensen,"**Adequacy of Operating Reserves for Power Systems in Future European Wind Power Scenarios**," in *IEEE PES General Meeting*, July 26 - 30, 2015, Denver, CO, USA.

P6 Kaushik Das, M. Altin, A. D. Hansen, P. E. Sørensen, H. Abildgaard,"**Primary Reserve Studies for High Wind Power Penetrated Systems**," in *IEEE PowerTech*, June 29 - July 2, 2015, Eindhoven, The Netherlands.

P7 Kaushik Das, A. D. Hansen, P. E. Sørensen,"**Aspects of Relevance of Wind Power in Power System Defense Plans**," in *12th Int'l Workshop on Large-Scale Integration of Wind Power into Power Systems as well as on Transmission Networks for Offshore Wind Power Plants*, October 22-24, 2013, London.

Other Publications

P8 iTesla Deliverable D6.2-Ed.2, "**Improvement of defence plans in European power systems- Proposed harmonization, coordination and inclusion of renewables, distributed resources and PMU information**",2015 (Confidential to TSOs)

Chapter 2

State of the Art

This chapter gives an overview of the state of the art in the defence plans, as well as to underline the capabilities of modern wind turbines(WTs) to contribute actively into the power systems. The opportunities and threats of large WTs connected to the transmission networks as well as dispersed WT and photovoltaic (PV) generations connected to distribution networks towards existing defence plans against frequency instability are investigated. While the traditional Fixed Speed Wind Turbine (FSWT) can inherently contribute with inertia to the power system, they lack control capabilities of active and reactive power. While modern Variable Speed Wind Turbine (VSWT) do not inherently contribute to the system inertia but due to their advanced control features can emulate inertia and control independently active and reactive power. These capabilities make modern VSWTs capable of providing defence support in terms of inertia and active power support during emergency in a power system.

2.1 Wind Power Plant Capabilities

Among many control capabilities provided by Wind Power Plants (WPPs), the most relevant control capabilities with respect to this thesis work are as following:

- **Active power control capability during normal operation:**
  According to several national grid codes, WPPs must be able to regulate their power production to an imposed reference value, set remotely or locally. Hansen et. al. [16] demonstrates the capabilities of VSWT technology based WPPs to independently control active and reactive power.
- **Frequency-active power control capability:**
  As WPPs tend to substitute conventional units in the power system, they are often required to remain connected to the the power system during frequency variations; but

not only to remain connected but they also have to help actively with active power when wind power penetration is high [17]. WPPs have to adjust their power outputs according to frequency deviations although the fluctuating nature of wind poses serious constraints regarding the availability of active power. This feature becomes vital for non-interconnected weak power systems, like island systems, whose inertia is restricted and frequency variations often lead to severe load shedding [16].

2.2 Defence Plans

Several definitions on defence plans and restoration have been outlined by different utilities and organisations over the years. This project considers the definitions in as per CIGRE and North American Electric Reliability Corporation (NERC), but it is mainly focusing on definitions provided by European Network Transmission System Operators for Electricity (ENTSO-E).

ENTSO-E classifies the system operating conditions into states for the purpose of analyzing power system security [2]. Figure 2-1 illustrates different possible states of the power system: Normal, Alert, Emergency, Blackout and also shows defence plans as a fence protecting against Blackout.

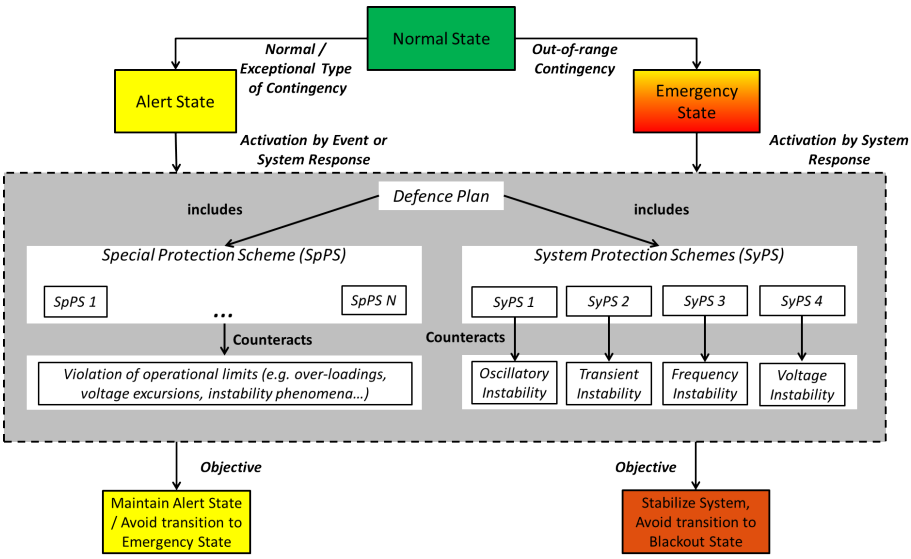

Figure 2-1: ENTSO-E Definition of Defence Plan, System Protection Scheme, Special Protection Scheme [2]

As long as the normal and exceptional(multiple contingencies like cascading) type of contingencies are "secured" by means of redundancy and the "normal" power system control capabilities, the system remains either in "normal" or "alert" state. In such cases, automatic protection measures (like PST, HVDC controls, FACTS controls etc.) are not required to preserve the system integrity. However, manual actions should be

taken if the system is in “alert” state to re-establish the “normal” state.

However, if the system is not secured by redundancy, other measures known as “Special Protection Schemes (SpPS)” are required to restore the system to acceptable condition i.e. to “normal” or “alert” state. SpPS are often designed for a particular combination of events triggered by limited number of pre-identified (through off-line studies) critical contingencies. In these situations, SpPS are called “event based”. They aim to stabilize the system in the alert state by means of dedicated automatic controls as shown in Figure 2-1. SpPS can also be triggered if certain system quantities exceeds some threshold values when they are called “response based”. It should to be noticed that also selected system quantities can be monitored and used to trigger the SpPS (response based), but in contrary to SyPS, which will be discussed in the following, the power system is not necessarily in a emergency state or close to instability, even though there might be a risk to enter the emergency state when SpPS are triggered. Therefore, SpPS maintain “alert” state and prevent entering into ”emergency” state as depicted in Figure 2-1.

“System Protection Schemes (SyPS)” as shown in Figure 2-1 are developed and implemented by the utilities to minimize the impact of extreme contingencies to prevent system blackout. SyPS mostly include a set of coordinated and automatic measures initiated as a final attempt when a wide spread collapse is imminent. Since system collapse is caused by loss of stability, SyPS are generally designed as response based corrective actions to avoid a specific instability.

SpPS and SyPS together constitute a **Defence Plan** as shown in Figure 2-1. According to ENTSO-E report on “Special Protection Schemes”[2], a Defence Plan thus can include (not necessarily must include) :

- A set of specific, event-based SpPS in order to avoid the violation or operational limits or the loss of stability after normal or exceptional contingencies
- A set of co-ordinated, response-based and/or event based SyPS in order to avoid the loss of stability after “out-of-range” or extreme contingencies.

According to CIGRE’s Technical Brochure “Defense Plans Against Extreme Contingencies” [12] - Defence plans are a set of coordinated automatic measures intended to ensure that the overall power system is protected against major disturbances involving multiple contingency events, generally not caused by natural calamity. Defence plans are used to minimize and reduce the severity and consequence of low probability and unexpected events and to prevent system collapse. These actions such as load shedding, generator rejection etc. are defined as System Integrated Protection Schemes. Defence plans are primarily used to increase power system security.

NERC defines Special Protection System as an automatic protection system designed to detect abnormal or predetermined system conditions, and take corrective actions other than and/or in addition to the isolation of faulted components to maintain system reliability. NERC definition of Special Protection System does not include (a) underfrequency or undervoltage load shedding or (b) fault conditions that must be isolated or (c) out-of-step relaying (not designed as an integral part of an Special Protection System) [18].

From these definitions, it is clear that CIGRE and NERC make defence actions as automatic but it is not clear whether these actions should be initiated in alert state or emergency state. ENTSO-E has relaxed the definition of defence actions to not being necessarily automatic, and to be initiated either in the emergency state (SyPS) or the alert state (SpPS).

This PhD thesis is mainly concerned with designing of defence plan against frequency stability.

Some of the traditional defence actions with respect to frequency stability are as follows [12]:

- **Defence actions against overfrequency instability**
  - Generator Rejection [19]: This scheme involves tripping of generating units especially hydro-generator units. Hydro-generator units are quite rugged as compared to thermal units and the risk of damage to hydro-generator unit from a sudden trip is less.
  - HVDC fast power change [12]: Since HVDC transmission links are highly controllable devices, they can be used for fast power flow change through the connecting systems. Power flow on HVDC links can be modulated by controlling the converters. The DC power can be either ramped down or ramped up (taking advantage of short-term overload capability) to assist power system frequency stability. The beneficial effect of DC modulation on the AC system is similar to the effect of generation rejection or load shedding. Taylor et. al. [20] describes dynamic HVDC modulation controls. An issue with this scheme is that imbalance from one AC system can be transmitted to neighbouring system. Frequencies of the two systems which are connected through HVDC are decoupled. However, frequency oscillations can start in any system in order to reduce frequency excursions in neighboring system. Therefore, proper attention should be taken to prevent such situation.
- **Defence actions against underfrequency instability**
  - Fast start-up [12]: Power support by fast unit (e.g. gas turbine) or pump storage start-up could be used at low frequencies. The gas turbine start-up process takes several minutes or tens of minutes whereas pump storage start-up can be even faster.
  - Underfrequency load shedding (UFLS)[12]: UFLS scheme is the last resort to prevent frequency instability. UFLS is initiated by underfrequency relays designed to trip blocks of load in distribution networks when the frequency drops below discrete frequency thresholds and/or the rate of change of frequency exceeds pre-set Rate of Change of Frequency (RoCoF) values. UFLS is generally done in several steps to prevent excessive load disconnection and to allow the frequency to recover before the next step.
  - Controlled opening of interconnection [12]: Controlled system separation is generally a last resort for saving the power system following a major disturbance involving loss of generation or imminent instability between areas. Controlled system separation is applied when specific load and generating areas can be defined

within a large interconnected system. The instability between areas is usually characterized by sudden change in tie-line power. However, it can be very difficult task to define system separation points for a large interconnected system since power flow through tie-lines change all the times. Therefore, this scheme is not widely applied.

- HVDC fast power change: This has been discussed before.

2.3 Relevance of renewable generations for defence plans

Since more and more renewable generations are connected into the power system, the defence plans need to be revised. For example, future defence actions pertaining to transmission networks should consider impacts of large VSWT based WPPs whereas, defence actions involving distribution networks should consider dispersed FSWT and PV generations.

In order to revise the defence plan regarding frequency stability, first consideration should be made on adequacy of reserves for power systems with high penetration of renewable generations. A power system should operate in a reliable and secured manner. In order to operate the system with stable frequency, the generation and load should always match. Since a power system has to deal with many uncertainties originating from variability of load, network topology, natural and technical disturbances, stochastic generation etc., there are always mismatches between consumption and generation. These mismatches are met with operating reserves in order to prevent frequency instability. Different types of operating reserves - both manual and automatic are used to handle these uncertainties.

Among the renewables, large WPPs connected to transmission networks are major contributor towards uncertainties. While small WT and PV generations connected to distributions networks are too dispersed to have large impacts on uncertainties in a large power system like CE. With increasing penetration of wind power generation, uncertainties in the system increase. Imbalance in wind power due to the variability of wind speed is mainly caused by error in wind forecasting. This imbalance could be quite high with high penetration of wind power generation. Therefore, it is required to estimate the amount of reserves required for future power systems with high penetration of wind power generation. This can be considered as precursory to design of defence plans against frequency instability, since frequency instability may occur in the absence of enough operating reserve in the system.

2.3.1 Frequency Reserves

Different nomenclatures for operating reserves can be found in literature. In UCTE operation handbook [21], different operating reserves are referred to as primary, secondary and tertiary reserves based on the type of control used to stabilize the frequency of the network. These reserves are referred as Frequency Containment Reserve(FCR),

Frequency Restoration Reserve(FRR) and Replacement Reserve (RR) based on their functionalities in recent ENTSO-E NC-LFCR[22]. Whereas, operating reserves are classified in Nordic Grid Code [23] as:

- Automatic active reserve (Frequency controlled normal operation reserve and Frequency controlled disturbance reserve)
- Fast active disturbance reserve
- Slow active disturbance reserve
- Reactive reserve

Milligan et. al. [24] provides a comprehensive overview of different nomenclatures of operating reserves used in different regions. In this thesis, the definitions of FCR, FRR and RR from NC-LFCR [22] are followed.

The overall goal of these reserves is basically to stabilize the system frequency following an imbalance. The purpose of FCR is to contain the system frequency deviation following a large disturbance within a pre-defined range. FCR is required to be activated within 30s after the disturbance [21]. After the frequency is contained FRR is activated. FRR is defined as the active power reserve which is activated to perform the function of restoring system frequency to its nominal value and maintaining area power balance to the scheduled value for synchronous area consisting of more than one Load Frequency Controller (LFC). In some networks, FRR is activated manually. FRR is limited and supported by RR to handle further imbalances. Generally, FRR are activated within 10-15 minutes following the imbalance. RR is used to replenish/support the used up FRR to handle further system imbalances. These reserves have activation time from minutes up to hours. RR are generally activated manually. Fig. 2-2 [3]

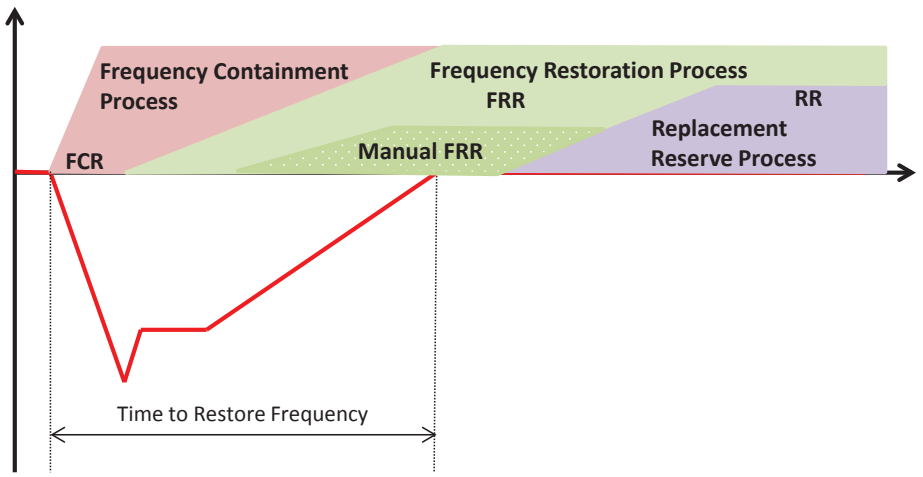

Figure 2-2: Operating Reserve Activation Structure [3]

shows reserve activation process for different operating reserves. Fig. 2-2 illustrates

that FCR is deployed to contain the frequency. After the frequency is stabilised, slowly FRR starts replenishing FCR and brings back the frequency to normal value. Following which, RR replenishes FRR.

In the future European power systems, wind power generation will have higher contribution resulting in an increase of uncertainties in the system. The uncertainty in wind power generation mainly comes from wind power forecast error. The accuracy of the wind forecast improves as time horizon is closer to the operation time. Better wind forecast means that the TSOs at the control center can take better decisions to reduce the imbalance closer to the real time operation. Thereby, closer to real-time operation, operators can predict imbalance prognoses with reduced forecast error based on which they can activate slow and manual RR. The remaining imbalance, if substantial, is handled by short-term FCR and FRR through Frequency Containment Process (FCP) and FRP respectively. These limited short-term reserves are replaced by RR already deployed. FCR and FRR are also needed to handle the imbalances caused due to any unforeseen contingency. **Therefore, it is very important to note that the reserves utilized to meet imbalance due to wind power generation will reduce the available reserve to handle any contingency as per n-1 security constraint.**

Many studies have been performed regarding requirements of operating reserves with integration of wind power generation. For example, Ela et. al. [25] and Milligan et. al. [24] provide comprehensive review of operating reserve requirements with integration of variable generations. Ela et. al. [26] and Holttinen et. al. [27] discuss about determination of requirements of operating reserves with integration of wind power generation. Kiviluoma et. al. [28], Botterud et. al. [29], discuss impacts of wind power integration in operating reserve requirements from power system market and unit commitment point of view. Menemenlis et. al. [30] shows the advantages of using dynamic operating balancing reserve at time horizon of 1-48 hours over static reserves with integration of wind power.

2.3.2 Frequency Support

Margaris et. al. [31] depicts that a WPP consisting of converter connected WTs with frequency-active power control capability can provide significant improvement in terms of frequency stability following a major power imbalance compared to the conventional generation plants.

Partial replacement of conventional generation capacity with wind power generation (without frequency control from WPP) may result in an erosion of system inertia resulting in increased RoCoF and larger frequency excursions. Supplementary control inside WTs are therefore needed to improve the inertial response. In island systems, high RoCoF frequency excursions are particularly challenging due to already low system inertia. These frequency excursions can trigger RoCoF based protection relays which in turn can invoke instability in these systems. Therefore, operators need to revise the frequency control strategies to avoid large RoCoF and/or large frequency excursions particularly if the wind power penetration is high.

Responses from renewable generations during an underfrequency event is different from than that of an overfrequency event. Therefore, relevance of renewable generations for overfrequency and underfrequency situations are discussed separately as following:

Overfrequency

The frequency in the high wind power generation area can also increase very fast if power system inertia is not high. The automatic overfrequency protection system prevents frequency increases above or equal to 51.5 Hz (typical value for a 50 Hz system) that can cause conventional generating units to trip causing frequency instability [32].

The fast active power control capability of modern WTs is a relevant option in the future defence plans as WTs can be down-regulated quite fast pertaining to fast control capabilities of power electronic converters . Although an important point to be considered is that since the RoCoF is very high when system inertia is reduced, there is a high possibility of tripping of instantaneous df/dt (RoCoF) based relays of system causing unintentional disconnections of generations. This aspect brings up the challenge of redesigning the protection settings meant for defence against extreme contingencies with high penetration of wind power generation. This issue has more pronounced effects in island systems like Ireland power system [33].

The grid code requirements with respect to active power and overfrequency control for different countries are listed below.

Grid code requirements generally require the WPPs to be capable to regulate their power output to a defined level either by an active power output command from TSOs or to down-regulate/up-regulate active power output when frequency increases/decreases. This can be achieved either by disconnecting WTs or by power control of WTs through power electronics controller / pitch controller action.

- In Germany, the TSO Tennet requires the WPPs to be capable of reducing power output with a power droop of 5% of the available power when frequency exceeds 50.2 Hz . The power plants should have ramping capability at least 10 % of the grid connection capacity per minute, without the plant being disconnected from the grid [34].
- According to Danish Grid Code [4], frequency control from WPPs above 1.5 MW is defined as illustrated in Figure 2-3. Droop is defined as a percentage of WPP to its nominal output. P_{Delta} refers to the WPP reserve and is set to provide upward regulation. If the power output is reduced below a certain value P_{min}, then the power plant can be disconnected. The maximum ramping up/down of active power allowed is 100 kW/s.
- According to grid code in Great Britain [35], all generators (including WPPs) if operating in frequency sensitivity mode (capable of frequency control) should have minimum requirement for frequency response of 10% of capacity, with droop 3-5%, and

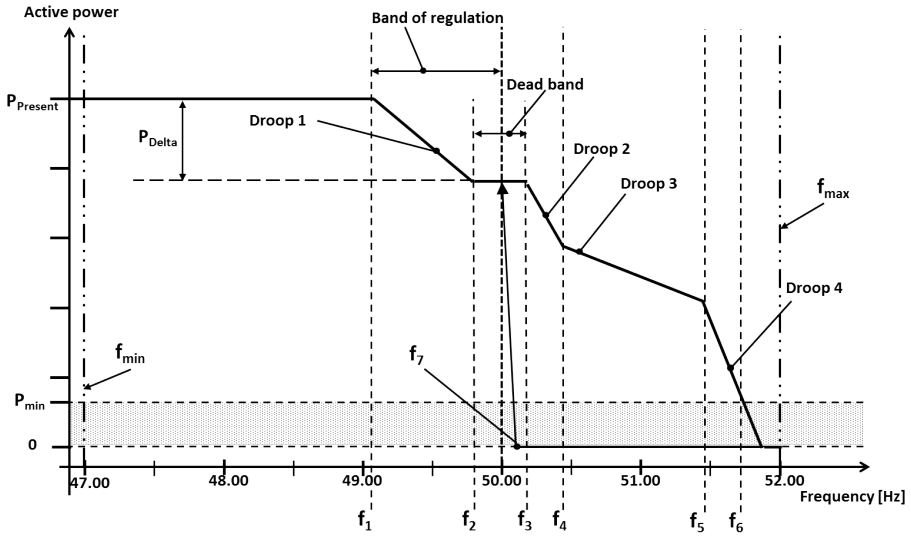

Figure 2-3: Frequency control for WPPs shown with a large downward regulation P_{Delta} [4]

deadband $\leq$ 0.03 Hz until frequency reaches 50.5 Hz. Beyond 50.5 Hz power output should be reduced at the rate of 2% of the power output per 0.1 Hz.

- Nordic grid code [36] requires that WPPs must be capable to down-regulate power output down from 100% to 20% of rated power in less than 5 seconds.
- WPPs in Québec [37] are required to be capable of ramping down of power output from rated power to 0 MW in adjustable 2 - 60 minute interval.
- Frequency response characteristics for Irish grid code [5] is shown in Figure 2-4. Power output from WPPs are decreased when frequency increases more than a deadband frequency (F_C) with certain droop (calculated with respect to WPP capacity). If the frequency increases beyond (F_D), WPP should reduce their power output to its minimum value, ($DMOL$). WPP should disconnect when frequency reaches (F_E).
- ENTSO-E has tabulated the grid code requirements for all type of generators with respect to current practices towards frequency control in [38].

Underfrequency

Quite a high proportion of dispersed generations (including converter connected renewable generations) are connected to distribution networks and are referred to as Distributed Generations (DGs).

A severe disturbance like loss of a large generating unit can cause fast decline of frequency which can result in frequency instability. In order to limit the frequency from decreasing too low, FCR are deployed from dedicated generators. If these reserves are

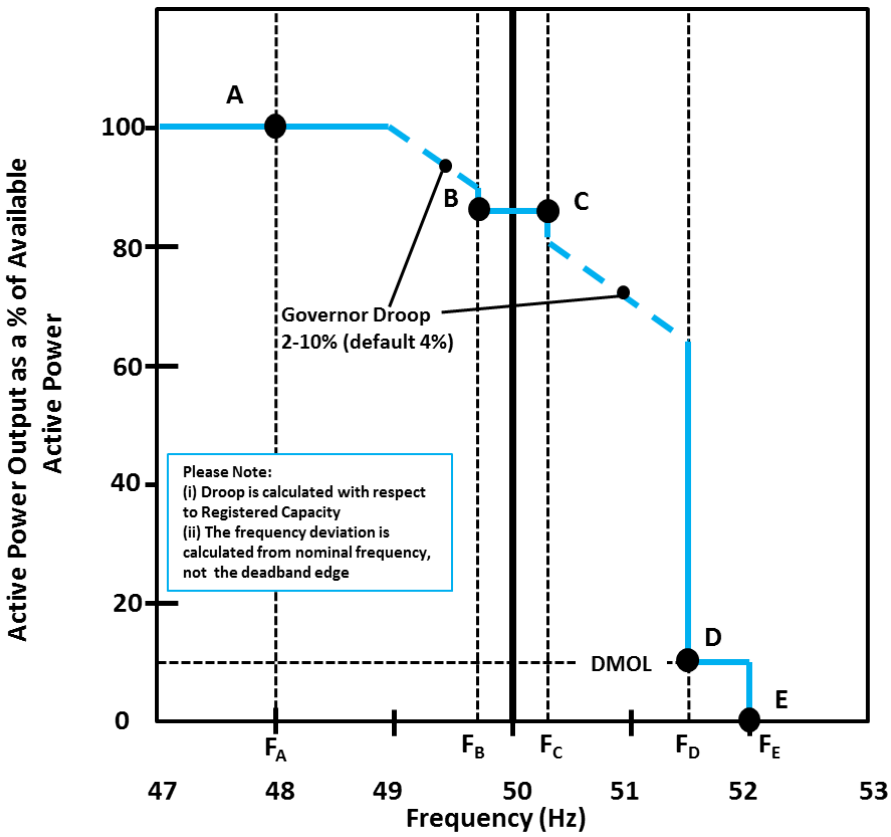

Figure 2-4: Example of Power-Frequency Response Curve for Wind Following Mode as per Irish Grid Code [5]

exhausted or unable to contain the frequency, the system enters in an emergency state invoking defence actions to prevent system collapse.

Underfrequency load shedding (UFLS) is a SyPS which is considered as last resort to prevent frequency instability [12]. ENTSO-E recommendation for UFLS for European networks [6] is shown in Figure 2-5. It can be observed from Figure 2-5 that minimum load shedding is recommended to start at 49 Hz and multiple steps of load shedding are continued until 48.1 Hz as represented by the red region. However, load shedding from 49.2 Hz until 48.4 Hz (as represented by the green region) is desirable. Although it should be noted that UFLS is the last resort to contain frequency decline and it causes economic loss and consumer discomfort. UFLS is generally performed by automatically disconnecting the feeders at distribution substations. Disconnecting feeders with large penetration of DG may disconnect substantial amount of generation. Consequently, the required amount of load disconnection as per design requirements (e.g. Figure 2-5) is not achieved. Traditional load shedding relays do not consider this effect. Thus high penetration of DG advocates for advanced UFLS approach which would take DG into account [39].

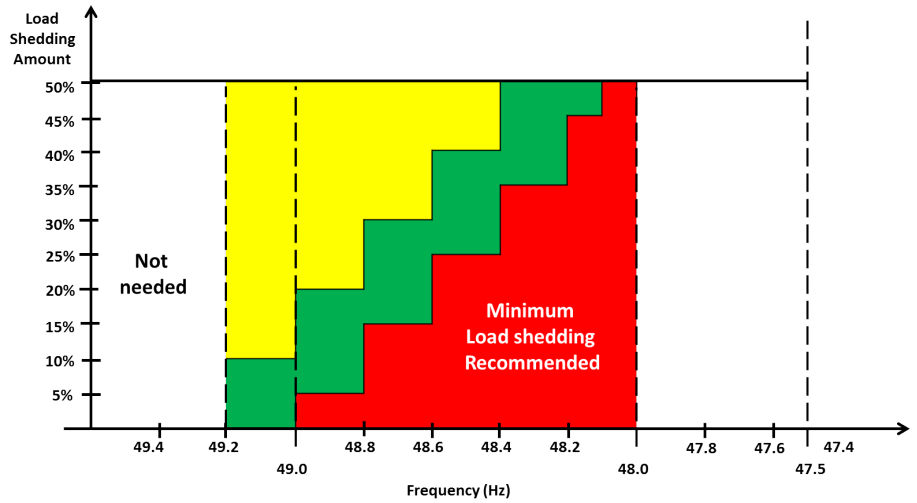

Figure 2-5: ENTSO-E Recommendation for UFLS [6]

In literature, there have been several works on UFLS. Delfino et. al. [40] has compared traditional, semi-adaptive and adaptive load shedding schemes. Anderson et. al. [41] and Rudez et. al. [42], [43] proposed adaptive UFLS schemes using RoCoF. Terzija [44] proposed an adaptive UFLS scheme considering magnitude of disturbance. Ceja-Gomez et. al. [45] solved UFLS problem using integer programming whereas, Luan et. al. [46] used genetic algorithm. Manson et. al. [47] has provided a case study of UFLS scheme considering communication challenges as well. Reddy et. al. [48] used PMU based sensitivity study to find location and amount of load to be shed. Mullen et. al. [49] and Chuvychin et. al. [50] proposed smart grid approaches for UFLS. However, these UFLS schemes do not take into account effects of high penetration of DG in their schemes. Therefore, during load shedding these methods may disconnect substantial amount of DG.

Recently some works have been done regarding UFLS considering DG. Liu et. al. [51] proposed an UFLS method where DG provides active power support to alleviate under-frequency problem. Xu et. al. [52] classified DG into different categories for their applicability for UFLS. Malekpour et. al. [53] optimized loads and losses to be minimum with integration of DG. Mahat et. al. [54] stabilized the frequency in an islanded system consisting of DG. However, all these methods suffer from an important drawback that none of these methods consider that if substantial amount of DG is disconnected during UFLS, frequency response will be very poor and may lead to frequency instability in extreme cases. These methods do not consider amount of DG connected to any feeder before disconnecting it. “IEEE Guide for the Application of Protective Relays Used for Abnormal Frequency Load Shedding and Restoration” [39], has clearly mentioned that tripping feeders that have active DG certainly diminishes the beneficial affect of load shedding, and can even have negative impact by eliminating sources of generation that supports system inertia. Therefore, new load shedding schemes need to be developed to minimize the amount of DG disconnection while disconnecting the required amount

of consumptions.

The inertia of power system will decrease with large penetration of converter connected WTs in power system replacing the synchronous conventional generations. In such a system, frequency will decrease with high RoCoF following a large disturbance, like disconnection of a large generator. In such situations, WPPs are expected to participate more and more in power system frequency control [55, 56]. However, there is no grid code specifying for how long the WPPs should contribute with additional power after under frequency events.

There are different frequency control methods for WPPs available in literature for underfrequency active power support [57–62]. The frequency control methods can generally be categorised as (i) inertial control and (ii) proportional control. Inertial or fast frequency control emulates inertia from WPPs thereby limiting the RoCoF during frequency events. Morren et. al. [63] and Conroy et.al. [64] proposes methods to emulate inertia based on RoCoF. Since, it is a derivative control, a low-pass filter is added to eliminate noise from the measurement. Ullah et. al. [65] and Keung et. al. [66] explain proportional control which provides an additional active power reference proportional to the frequency deviation from nominal value. Fischer et. al. [67], Asmine et. al. [68] and Wachtel et. al. [69] discuss fixed duration overloading method above initial actual power output of a WT following a frequency event. WT's capability to provide temporary overproduction depending on the initial pre-overproduction conditions, i.e. wind speed conditions, limits of the mechanical/electrical components and control strategy has been investigated by Hansen et. al. [70]. It has been observed by Hansen et. al. [70] that at low wind speeds there might be a risk of stopping the WT during long overproduction periods.

Reviews of state of art of defence plans and operating reserves depict that there are variety of definitions and nomenclatures of defence plans and operating reserves across different power systems. However, it is clear that defence plans of future power systems will face new challenges due to increased penetration of renewable generations. Fortunately modern converter connected renewable generations have control capabilities to support the power systems during emergencies. Therefore, new defence plans should be designed for future power systems with active participation from renewable generations. In following chapters, defence plans against frequency instability are developed considering large penetration of renewable generations.

Chapter 3

Adequacy of Active Power Reserve for Frequency Control

In this chapter, a new methodology is developed to assess the adequacy of frequency reserves to handle power imbalances caused by wind power forecast errors. Challenges faced by future European power systems due to increased penetration of wind power generation are analysed. An algorithm is proposed and developed to estimate the power imbalances due to wind power forecast error following activation of different operating reserves. Frequency containment reserve requirements for mitigating these power imbalances are studied. Possibility of reducing this frequency containment reserve requirement is investigated for different volumes and speed of frequency restoration reserve deployment. Wind power generation for 2020 and 2030 scenarios for Continental Europe (CE) network are investigated using this methodology.

3.1 Introduction

Uncertainties due to wind power forecast errors may increase in future European power systems with high wind power penetration. This may increase the power imbalances between generations and loads reflected by change in frequency. These power imbalances are handled using different operating reserves deployed in different time scales. These reserve requirements are determined based on network topology, dimensional fault, historical data, reliability studies etc. However, the accuracy of the wind forecast improves as time horizon is closer to the operation time. This allows the transmission system operators at the control center to take improved decisions to reduce the imbalance closer to the real time operation. Thereby, closer to real-time operation operators can prognose power imbalances with reduced forecast error based on which they can activate slow and manual Replacement Reserves (RR). However, since RR deployment

process is slow, certain amount of power imbalances need to be handled using fast and limited Frequency Containment Reserves (FCR) and Frequency Restoration Reserves (FRR). FRR can be activated manually or automatically. In Continental Europe (CE) network, FRR are activated using automatic Load Frequency Controller (LFC). ENTSO-E Network code on Load Frequency Control and Reserves (NC-LFCR) [22] requires that FRR should be dimensioned to be able to cover the power imbalances in 99 % of the time.

FRR are provided by dedicated generating units whose set-points are set by LFC. However, the frequency restoration process (FRP) has some inherent delay introduced mainly by LFC properties. It is required by ENTSO-E network code [22] that FRR should be activated and delivered within 15 minutes following a disturbance/imbalance to restore back frequency. Although, FRR are generally delivered much faster than 15 minutes. In real-time, the power imbalances are handled by FCR until FRR are activated. FCR are dimensioned based on reference incident in European networks. For example, according to UCTE Operations Handbook [71], reference incident for CE network is defined as the maximum instantaneous power deviation of 3000 MW which is defined considering system reliability and size of loads and generation units. In case the imbalance is greater than 3000 MW, the system frequency goes beyond the Standard Frequency Range ($\pm 50mHz$) and the system moves to either alert or emergency state. According to NC-LFCR [22], CE system is allowed to operate maximum of 15000 minutes outside the Standard Frequency Range every year. This number is derived from probabilistic risk calculation for exhaustion of FCR for CE. Table 3.1 illustrates that the number of minutes the frequency exceeded $\pm 50mHz$ from 2010-2012 for CE network [8]. It can be observed that the number of minutes outside Standard Frequency Range has been close to 15000 minutes and in 2012 it exceeded 15000 minutes by 0.1 %. As seen from the results in this chapter, this value can be much larger for future CE network with more and more penetration of wind power generation.

Table 3.1: Comparison of current and NC-LFCR target values for minutes outside the Standard Frequency Range for CE [8]

Year	Minutes outside the Standard Frequency Range	Deviation from the value defined by NC-LFCR (15000 min)	
		in minutes	in % of the year
2010	14189	811	0.15
2011	13400	1600	0.3
2012	15521	-521	-0.1

Therefore, it is essentially required to estimate power imbalances caused by wind power forecast error for future scenarios with high penetration of wind power. In these future scenarios, it might be possible to reduce power imbalances by activating higher volumes of FRR. Faster activation of FRR may also have impact on reduction of power imbalances.

The probabilistic risk of power imbalances exceeding dimensioned FCR with activation of FRR for future wind power generation scenarios are studied in this chapter. Probabilistic risk estimation will help in dimensioning FCR and FRR for future power

systems with large wind power penetration. In order to estimate the probabilistic risk, wind power forecasts for different time horizons like hour-ahead forecasts, online prognoses, real-time available power are simulated for wind power scenarios. Based on these forecasts, the decisions taken by operators to activate slow RR at the advent of power imbalances are emulated. Automatic FRR deployment to handle the power imbalances in real-time are analyzed by simulating LFC response. Probabilistic estimation and risk assessment of the requirements of FCR in order handle the remaining power imbalances are investigated.

3.2 Wind Power Scenarios of 2020 and 2030

A set of anticipated wind power installation scenarios for ENTSO-E networks for 2020 and 2030 are developed and simulated in the following based on data from different sources such as [72–74]. These scenarios are adjusted according to EWEA report [75]. Table 3.2 depicts the anticipated installed onshore and offshore wind power capacity in GW of different ENTSO-E networks for 2020 and 2030. In 2020 scenario, offshore wind power capacity is more than 3 times smaller than the onshore wind power capacity. While in 2030 scenario, offshore wind power capacity is less than 2 times of the onshore wind power capacity. Furthermore, in some countries, offshore wind power capacity becomes more dominant than onshore wind capacity in 2030.

Table 3.2: Installed Capacity of Wind Power Generation in GW

Network	2020		2030	
	Onshore	Offshore	Onshore	Offshore
UK	12.5	9	19	32
CE	166	25	217	94
Baltic	0.5	0	0.5	5
Nordic	8	9	10	28
Ireland	2	2.5	1.5	3
Total	189	46	248	162

Figure 3-1a and 3-1b show all the wind power plants of UK, CE, Baltic, Nordic and Ireland Networks for 2020 and 2030 respectively. 2030 scenario has more number of wind power plants (WPPs) as compared to 2020 scenario. This is more evident in the North Sea area, where many new WPPs are expected to be installed in 2030 scenario.

In order to calculate the power imbalances in European networks for these scenarios, power forecasts and available power from WPPs are needed to be generated using CorWind (Appendix A). As indicated in Figure 3-1a and 3-1b, large amount of WPPs (more than 15000 in 2030) will be installed in Europe and this in fact may drastically increase the computational burden making it impossible to simulate power forecasts. Therefore, simplified wind power scenarios, as indicated in Figure 3-2a and 3-2b have been defined in order to reduce computational burden by accumulating nearby onshore WPPs

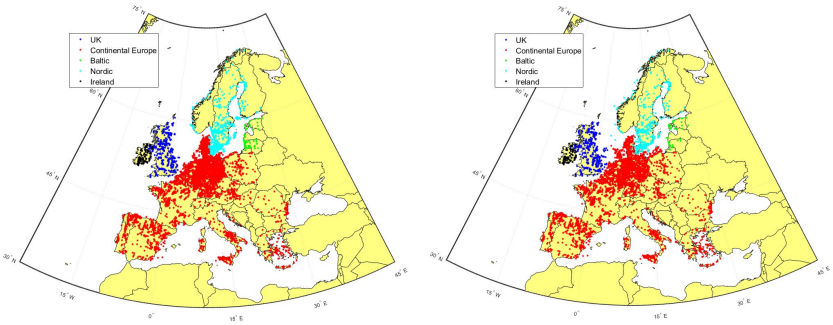

(a) 2020 (b) 2030

Figure 3-1: Wind Power Scenario for ENTSO-E Networks in 2020 and 2030

together.

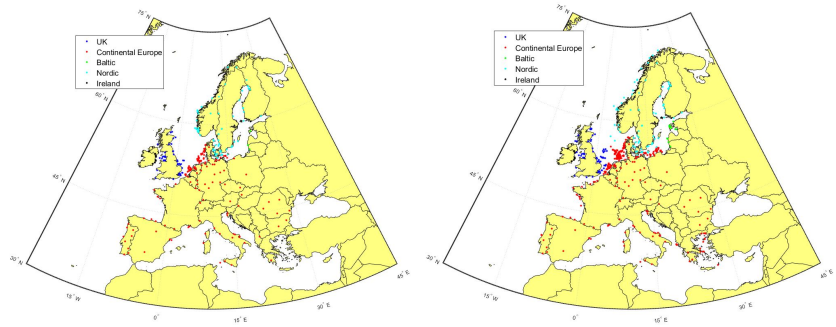

(a) 2020 (b) 2030

Figure 3-2: Simplified Wind Power Scenario for ENTSO-E Networks in 2020 and 2030

It should be mentioned that each country in the ENTSO-E synchronous network is assumed as a single TSO/control area. Denmark is divided into 2 control areas since East Denmark is connected to Nordic synchronous network, while West Denmark is connected to CE synchronous network.

CorWind is used to generate hour ahead forecast, online prognoses and real-time available power from the wind for each of the wind power scenarios for ENTSO-E networks depicted in Figure 3-2. These data are simulated for the wind data of 14 meteorological years.

3.3 Wind Power Forecast Error Challenges

A set of simulations has been performed for European wind power scenarios of 2020 and 2030 for 14 meteorological years. Online prognose, hour ahead prognose and real-time available power are simulated using CorWind. Hour-ahead prognose error $E_{Prognose\_HA,t,i}$ for any control area (TSO) is computed as the difference between real-time available power $P_{realtime,t,i}$ and hour-ahead power prognose $P_{HA,t,i}$ as given by Equation 3.1.

$$E_{Prognose\_HA,t,i} = P_{realtime,t,i} - P_{HA,t,i} \tag{3.1}$$

where,

- $E_{Prognose\_HA,t,i}$: Total hour ahead prognose error at t^{th} time instant for each control area i
- $P_{realtime,t,i}$: Total real-time available power at t^{th} time instant for each control area i
- $P_{HA,t,i}$: Total Hour-ahead power prognose at t^{th} time instant for each control area i

On analysing these simulated results, two different types of challenges from wind power forecast errors are observed. **One challenge is large error in meteorological forecast and another challenge is fast rate of change of power imbalances.** These challenges are discussed in details in following:

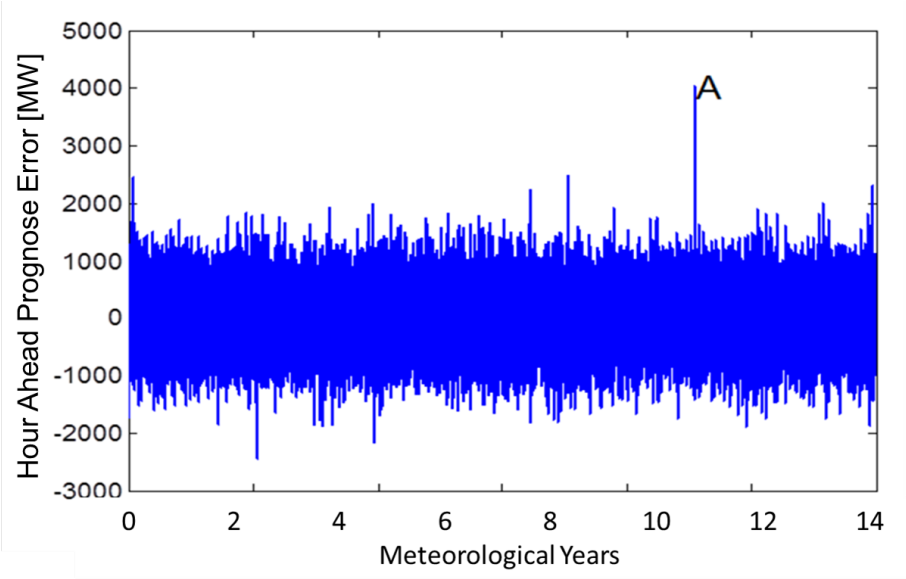

Figure 3-3: Power imbalance for Nordic Network in 2020 scenario

Hour-ahead prognosis depends on meteorological forecast. Meteorological forecast model generally generate forecasts every 6 hours [76]. Therefore, if there is large error in any meteorological run, then that error is transferred to short-term forecasts like hour-ahead prognosis. This forecast error persists for 6 hours. Large forecast error in meteorological forecasts can invoke large errors in hour ahead prognoses. In these situations, power imbalances from the wind power can be large especially if the penetration of wind power is high. Since the volume of FCR and FRR are limited and RR deployment is a slow process, the power imbalances provoked by possible forecast errors may invoke short term frequency instability. An example of such case is observed in the simulated Nordic network data as illustrated in Figure 3-3, where there is abnormally high power imbalance at point 'A'. It is important to mention the imbalance balancing practice at this point. In Nordic network, the Balance Responsible Parties (BRP) schedule and trade the generations to balance in the day-ahead market. They also trade balancing reserves in the intra-day market, 1 hour ahead of delivery. In the operational hour, balancing is performed by the TSOs through RR, automatic FRR and FCR. For example, Nordic TSOs have defined automatic reserves of 600 MW for normal operation and about 1000 MW to cover the dimensioning fault [76].

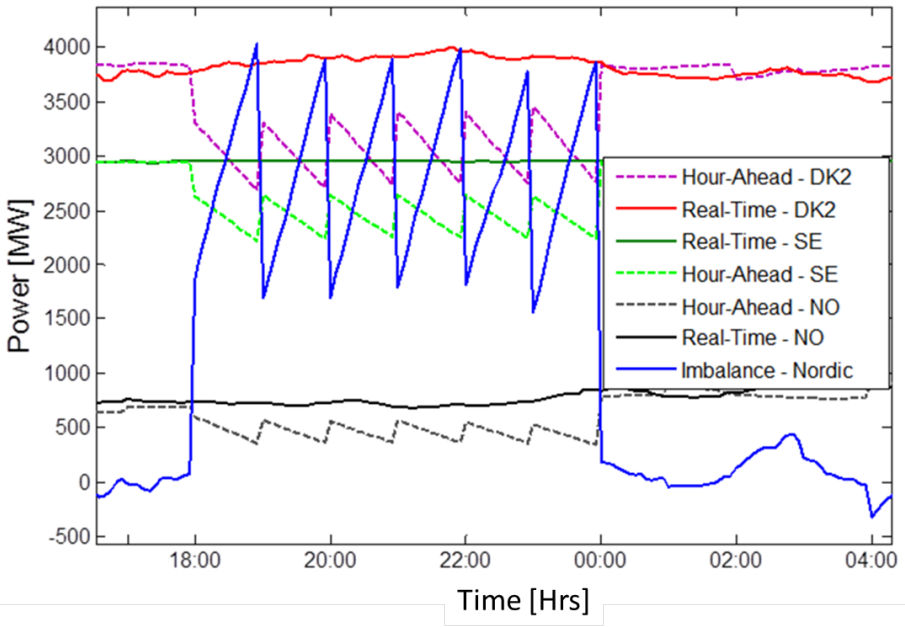

Figure 3-4: Hour-Ahead Prognoses, Real-Time Values and Imbalance for Nordic Network in 2020 scenario

Figure 3-4 illustrates the hour-ahead prognoses, real-time values and power imbalance for Nordic network as a zoom-in at point 'A' along with real-time production values and online prognoses for East Denmark (DK2), Sweden (SE) and Norway (NO).

Figure 3-4 demonstrates that there are large difference between hour-ahead prognoses and real-time available power for all the countries in Nordic network. Therefore, the total imbalance due to hour-ahead prognose error for Nordic network $E_{Prognose\_HA,t,Nordic}$ as given by Equation 3.2 is as large as 4000 MW.

$$E_{Prognose\_HA,t,Nordic} = \sum_{i=1}^{Number\_TSOs\_Nordic} E_{Prognose\_HA,t,i} \tag{3.2}$$

where,

- $E_{Prognose\_HA,t,Nordic}$: Total hour ahead prognose error at t^{th} time instant for Nordic network
- $Number\_TSOs\_Nordic$: Total number of control areas (TSOs) in Nordic network

The accuracies of the short term forecasts like online prognosis or hour-ahead prognosis are depended on the meteorological forecast. Meteorological forecast error is one of the main contributor to the wind power production forecast error. Meteorological forecast model are generally run every 6 hours [76]. This forecast error, therefore cannot be improved until new meteorological run occurs for the next 6 hours. Therefore, large imbalance due to hour ahead prognose error in Nordic network as shown in Figure 3-4 continues for exactly 6 hours where hour-ahead prognoses are not updated. The imbalance in this case is as high as 4000 MW for the Nordic network, whereas the available automatic reserves are much less for Nordic network as discussed previously.

One solution to this problem is to update the meteorological forecast at higher frequency than 6 hours. This may be computationally challenging and expensive. Another solution can be simulation of short term forecasts in different way with lesser weighage to the meteorological forecasts, such as persistence forecasts [77]. From the power system point of view, these types of situations can be handled with higher values of operating reserves. On the other hand, since the probability of these situations is low, allotting static reserves is neither an optimal nor an economical choice. Therefore, when these situations occur, reserves can be deployed dynamically on addition of designed static reserves. This example shows the absolute necessity to quantify the risk of imbalance due to wind power forecast error exceeding the designed FCR for future wind power scenarios.

Figure 3-5 shows another interesting and challenging situation. While example of Figure 3-3 and 3-4 show the requirements for higher volume of reserves for future networks, Figure 3-5 shows an example where faster deployment of reserves might be essential. Figure 3-5 shows hour ahead prognose error in the UK network for a short period of 45 minutes. It can be observed that the hour ahead prognose error changes from 347.9 MW at 6.55 to -1778 at 7.00, i.e. power imbalances change by 2125.9 MW in 5 minutes. This rate of change of power imbalance is very high compared to usual operation. Main reason for this high rate of change is sudden change in hour ahead prognoses to follow meteorological forecasts. Probability of occurrence of these situations is high. In situations like these, FRR may not be fast enough to be deployed completely within 5 minutes. **These types of situations require utilizing of FCR in**

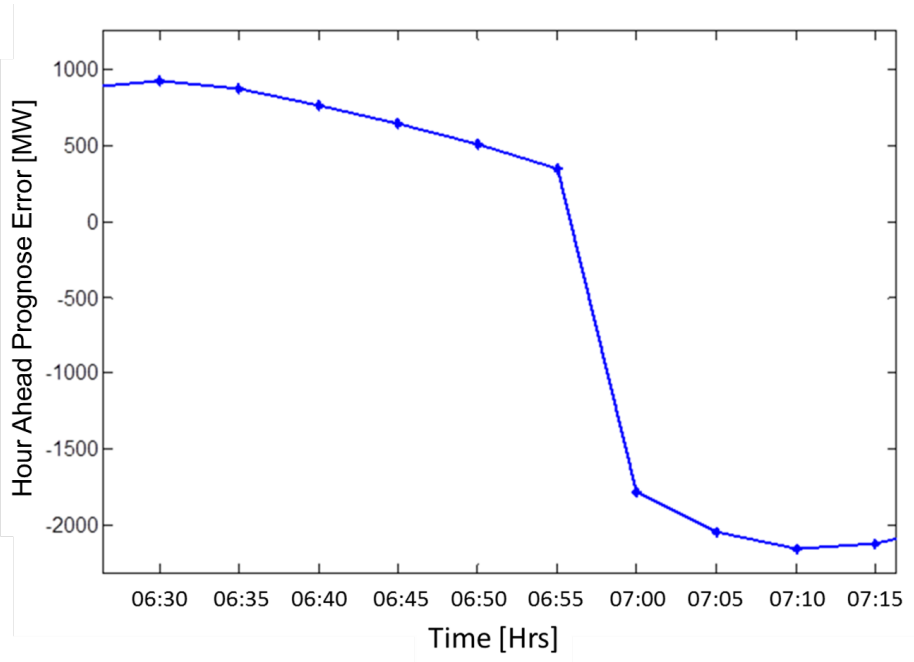

Figure 3-5: Imbalance for 45 minutes in UK network for 2020 scenario

order to handle the imbalance. One way to handle this challenge is by increasing the volume of FCR. This requirement for FCR will be additional to the system requirement to satisfy n-1 security constraint. Since the probabilities of these situations are high, the FCR allotted to handle these power imbalances might add to static reserves and not to dynamic reserves. This increases the cost of FCR. Another solution could be faster activation of FRR. Faster FRR activation from LFC needs to be studied to find out the requirement of FCR to deal with this kind of imbalance. FRR are also limited. **Therefore, the volumes of FRR should also be increased if faster FRR is to be deployed to handle these power imbalances.**

3.4 Probabilistic Risk Estimation Algorithm

In this PhD work, an algorithm to estimate the risk of imbalance due to wind power forecast error exceeding the designed FCR is proposed and developed. Generally, it is the responsibility of each TSO to maintain the frequency of their own control area within a predefined range as well as to honour the inter-area power transfer commitment. Therefore, whenever there is an imbalance in generation and load in own control area, the imbalance is handled using FRR. However, it should be noted that FRR activation can also be manual as it is in Nordic synchronous network. Whereas in some synchronous networks like CE, FRR activation is through automatic LFC. Nevertheless, the general activation time requirement for FRR activation is that it should be

fast enough to restore the frequency back to its nominal value ranging from seconds to minutes. Full frequency restoration reserve activation is required to be done within 15 minutes for CE and Nordic network and 10 minutes for UK network [22]. The maximum volume of FRR is limited based on agreements and decided based on maximum anticipated load in the specific control area. This requires replacement of activated FRR in order to handle further power imbalances in the system. This function is achieved through RR activation. Generally, RR are activated manually by the operators. Whenever there are imbalance prognoses in the system, the operators take decisions on RR activations. Based on these decisions, RR are activated. The rational for activating RR based on prognoses is to take time delays between decision and real-time activation process of these reserves into account. Since there is a delay of few minutes before FRR is fully deployed, power imbalances are handled instantaneously using FCR. Based on these above operating principles, reserve estimation methodology is modelled as shown in the flowchart of Figure 3-6.

In these studies, the methodology depicted in Figure 3-6 is modelled as according to the rules and regulations of CE. Although, it should be noted that the methodology discussed is generic and can be extended for other synchronous networks. Flowchart in Figure 3-6 illustrates that each control area takes decision on activation of RR whenever imbalance is prognosed. While in real-time, power imbalances are handled by FRP through LFC. However, power imbalances occurring before FRR and RR are deployed are to be handled using FCR. FCR is shared among all the control areas therefore power imbalances for all the control areas are added together based on which probabilistic risk estimation analysis is performed. The flowchart is explained in details as follows.

At the beginning of the operating hour, each control area is assumed to be balanced through hour-ahead power trading. Power trading and hence, unit commitment of all generators are based on the hour-ahead prognoses of the wind power generation. Error in forecast decreases as it approaches nearer to the operating time. Therefore, hour-ahead prognoses are generally expected to have higher error than online prognoses. When online prognoses of wind power generation are obtained 5 minutes ahead of the operation time, imbalance prognoses are computed for each control area as the difference between online prognoses and hour-ahead prognoses as given in Equation 3.3. These power imbalances will be handled by FCR and FRR in real-time. When FRR will be activated and deployed, they would have to replaced by RR.

$$I_{Prognose,t+5min,i} = P_{online,t+5min,i} - P_{HA,t+5min,i} - P_{RR_{signal},t+5min,i} \quad (3.3)$$

where,

- $I_{Prognose,t+5min,i}$: Total imbalance prognose at time instant $t + 5min$ for each control area i
- $P_{online,t+5min,i}$: Total online power prognose at time instant $t + 5min$ for each control area i
- $P_{HA,t+5min,i}$: Total Hour-ahead power prognose at time instant $t + 5min$ for each

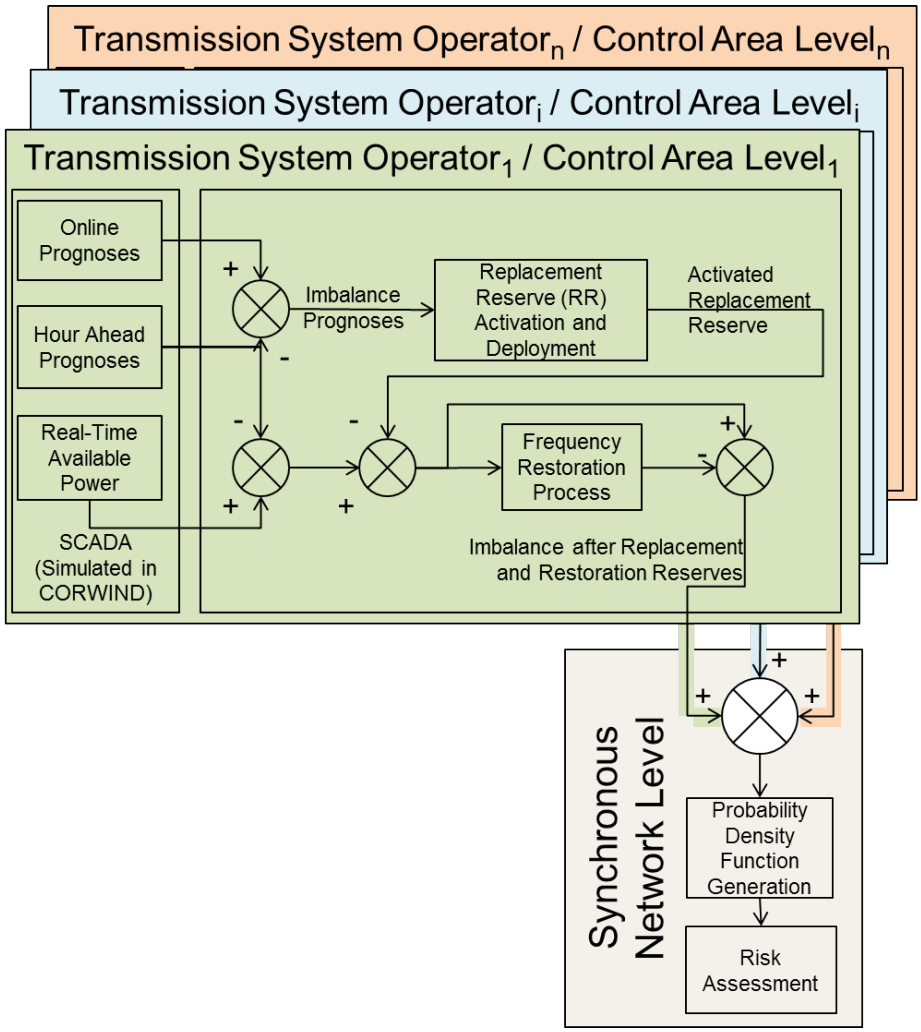

Figure 3-6: Flowchart of the system model

control area i

- $P_{RR_{signal},t+5min,i}$: Total already activated RR based on the previous activation signals sent by operators at time instant $t + 5min$ for each control area i

Based on these imbalance prognoses, operators need to take decisions on whether RR should be activated in advance taking into account that RR activation requires certain duration. Figure 3-7 depicts the RR activation and deployment process. Whenever power imbalances are prognosed, operators need to decide whether RR should be activated. If the decision is made to activate RR, future imbalance prognoses should be updated taking into consideration of the activation plan. The proposed RR activation decision algorithm is shown in Figure 3-8.

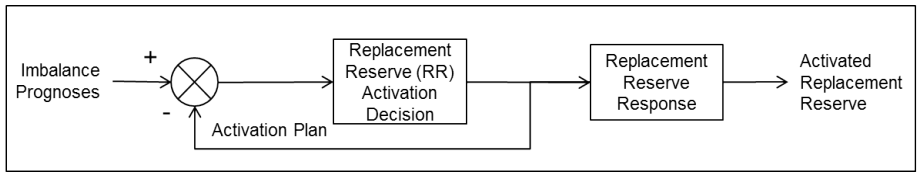

Figure 3-7: Replacement Reserve Activation and Deployment Process

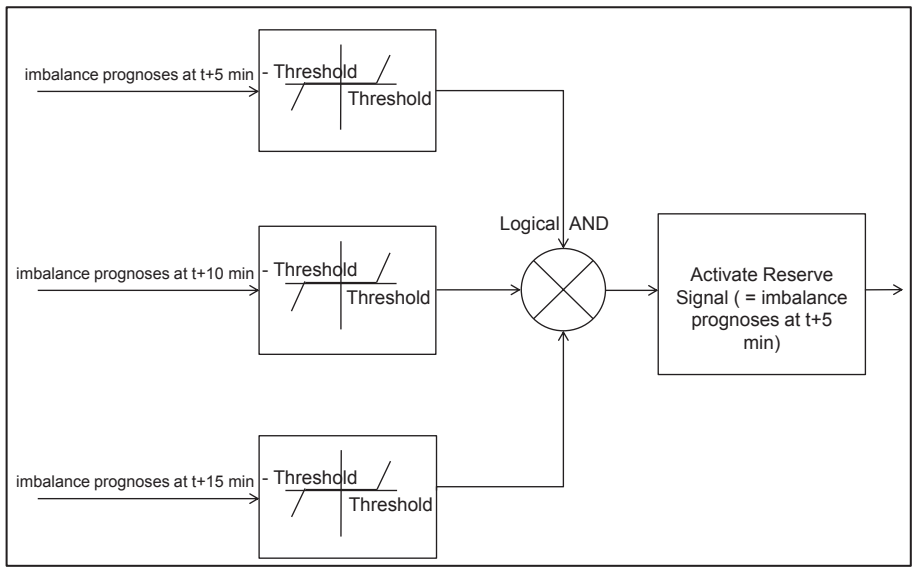

Figure 3-8: Replacement Reserve Activation Decision

The operators need to be certain that the imbalance prognoses are not random noises and therefore if imbalance prognoses are found to be greater than a threshold value for next 15 minutes, then RR is activated to mitigate the power imbalance as shown in Figure 3-8. Threshold can be decided based on experience of the operators.

Since, RR sources are activated manually and are generally slow therefore RR response is delayed from the activation plan. RR responses are modelled in this work with 5 minute delay and ramping rate of 10 minutes.

Real time operation is simulated in this work by computing power imbalance as the difference between real-time available wind power generations, hour-ahead prognoses and the RR already activated and deployed based on imbalance prognoses as given in Equation 3.4.

$$I_{realtime_{RR},t,i} = P_{realtime,t,i} - P_{HA,t,i} - P_{RR_{activated},t,i} \tag{3.4}$$

where,

- $I_{realtime_{RR},t,i}$: Total realtime imbalance with activation of RR only at time instant t

for each control area i

- $P_{realtime,t,i}$: Total realtime available wind power generated at time instant t for each control area i. It is assumed that all the wind power plants are operated at their maximum available wind power.
- $P_{HA,t,i}$: Total Hour-ahead power prognose at time instant t for each control area i
- $P_{RR_{activated},t,i}$: Total activated and deployed RR at time instant t for each control area i

The remaining real-time imbalance considering RR activation and deployment needs to be handled using FCR and FRR. FRR is assumed to be activated by automatic LFC in this methodology. LFC control is modelled with an anti-windup PI controller along with measurement filter as shown in Figure 3-9. Filter is modelled as a first order transfer function with time constant T_{filter}. Real-time imbalance input to the FRP is of

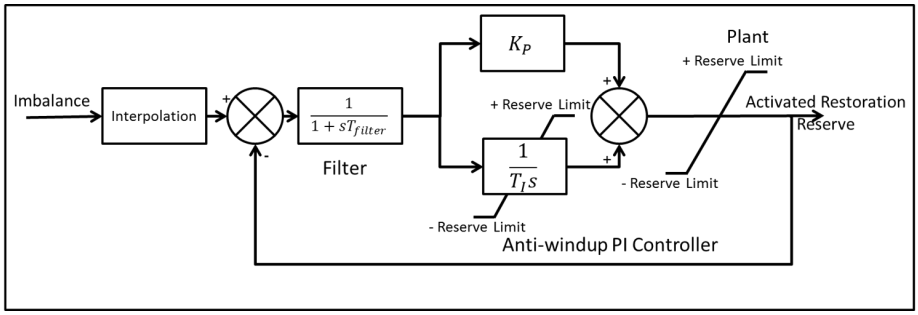

Figure 3-9: Frequency Restoration Process

5 minute resolution. Since, FRP has faster response, the imbalance is interpolated to 10 seconds resolution which is input to the anti-windup PI controller as shown in Figure 3-9.

Table 3.3: Parameters for Frequency Restoration Process

Parameters	Symbol	Values	Unit
Proportional Gain	K_p	0.1-1	p.u.
Integration Time Constant	T_I	30-140	s
Filter time constant	T_{filter}	16	s

Table 3.3 illustrates the typical values and ranges for LFC parameters for FRP of CE network [1]. Typical values for K_p and T_I for Danish network can be obtained in [61].

Different methodologies for dimensioning of FRR are defined in "P1–Policy 1: Load-Frequency Control and Performance [C]" of UCTE operation handbook [71] based on different operational needs in control areas of LFC, due to different characteristics

[1]These values are obtained in courtesy of Dr. Martin Høgdahl Zamastil, Energinet.Dk

and patterns of generation (including hydraulic, thermal and HVDC- link) and demand (including BRP and forecast qualities). The sizing of the FRR is done by reference to deterministic and / or probabilistic approaches as following:

- **Empiric Noise Management Sizing Approach** - The FRR for each control area is computed based on [21], [71]

$$R = \sqrt{a\ L_{max} + b^2} - b \tag{3.5}$$

  Where,

  – R: Recommendation for control Reserve in MW
  – L_{max}: Maximum anticipated load in MW for the control area

  The parameters, a and b are assumed as: a = 10 MW and b = 150 MW

- **Probabilistic Risk Management Sizing Approach** - For the probabilistic assessment the Network Code on Load Frequency Control and Reserve defines a minimum value for the sum of FRR Capacity and RR Capacity which is defined by the 99 % quantile of the LFC Block Imbalances (separate for positive and negative direction) [8].
- **Largest Generation Unit or Power Infeed** - The sizing is done based on largest possible generation incident for each control area.
- **Extra-ordinary Sizing of Reserves** - Other criteria e.g. consideration of large changes in exchanges, expected load variations, adverse climatic conditions, strikes etc. might influence the size of the reserve.

In this PhD work, Empiric Noise Management Deterministic Sizing Approach and Probabilistic Risk Management Sizing Approach is used for dimensioning of FRR. However, Equation 3.5 is modified to include a multiplying factor K_{wind} so that the imbalance caused by wind power generation can be handled statistically 99% of the time by FCR.

$$R = K_{wind}\ (\sqrt{a\ L_{max} + b^2} - b) \tag{3.6}$$

K_{wind} is defined as the ratio of future FRR dimension in p.u. to present FRR dimension taken as base value. It means, K_{wind} basically signifies amount of FRR required in future as compared to present value. For example, a value of 2 for K_{wind} means that in future FRR should be dimensioned double as compared to present value in order to handle imbalances due to wind power forecast error.

FRR dimension as estimated based on Equation 3.6 is used as Reserve Limit in the flowchart shown in Figure 3-6.

Remaining power imbalance is handled by FCR. This power imbalance can occur either if the LFC is yet to be activated or if FRR is exhausted but RR is not yet activated.

Since, FCR in a synchronous network are shared among all the control areas / TSOs, therefore the power imbalances for all the control areas in each synchronous area are added together as shown in Figure 3-6 and given by Equation 3.7.

$$I_{realtime_{FRR+RR},t,Network} = \sum_{i=1}^{Number\_TSOs\_Network} I_{realtime_{RR},t,i} - P_{FRR_{activated},t,i} \tag{3.7}$$

where,

- $I_{realtime_{FRR+RR},t,Network}$: Total realtime imbalance with activation of FRR and RR at time instant t for synchronous network
- $P_{FRR_{activated},t,i}$: Total activated FRR at time instant t for each control area i
- $Number\_TSOs\_Network$: Total number of TSOs or control areas in the concerned synchronous network

Probability density functions of the imbalance $I_{realtime_{FRR+RR},t,Network}$ provide the information about the risk of power imbalance exceeding designed FCR dimension $FCR_{dimension}$ (For example- FCR requirement designed based on dimensional fault for CE is 3000 MW). Probabilistic risk of exceeding the designed FCR dimension $FCR_{dimension}$ value of the synchronous network is given by Equation 3.8.

$$\begin{aligned} Risk &= Pr[|I_{realtime_{FRR+RR},t,Network}| > FCR_{dimension}] \\ &= 1 - Pr[-FCR_{dimension} < I_{realtime_{FRR+RR},t,Network} < FCR_{dimension}] \end{aligned} \tag{3.8}$$

where,

- $FCR_{dimension}$: Designed FCR dimension for concerned synchronous network

Equation 3.8 depicts that $Risk$ is calculated as the probability of total realtime imbalance with activation of FRR and RR exceeding designed FCR dimension for concerned synchronous network.

In order to be able to handle imbalance with the available $FCR_{dimension}$ for 99% of time, the risk estimated through Equation 3.8 should be less than 1% i.e 0.01. Therefore, the design criterion for dimensioning FRR for handling wind power imbalances with 1% risk is given by Equation 3.9.

$$\begin{aligned} Risk &= Pr[|I_{realtime_{FRR+RR},t,Network}| > FCR_{dimension}] \\ &= 1 - Pr[-FCR_{dimension} < I_{realtime_{FRR+RR},t,Network} < FCR_{dimension}] < 0.01 \end{aligned} \tag{3.9}$$

Equation 3.9 is the design criterion for probabilistic risk estimation algorithm. It is possible using proposed algorithm to estimate the volume and speed of FRR activation so that the probabilistic risk is less than 0.01.

3.5 Sensitivity Analysis

In order to test the sensitivity of dynamic capabilities of LFC for different values of integration time constant T_I, responses of the LFC to unit step function are generated and illustrated as shown in Figure 3-10. Proportional gain K_p and filter time constant T_{filter} for LFC for these sensitivity studies are assumed constant values of 0.2 and 16 s respectively.

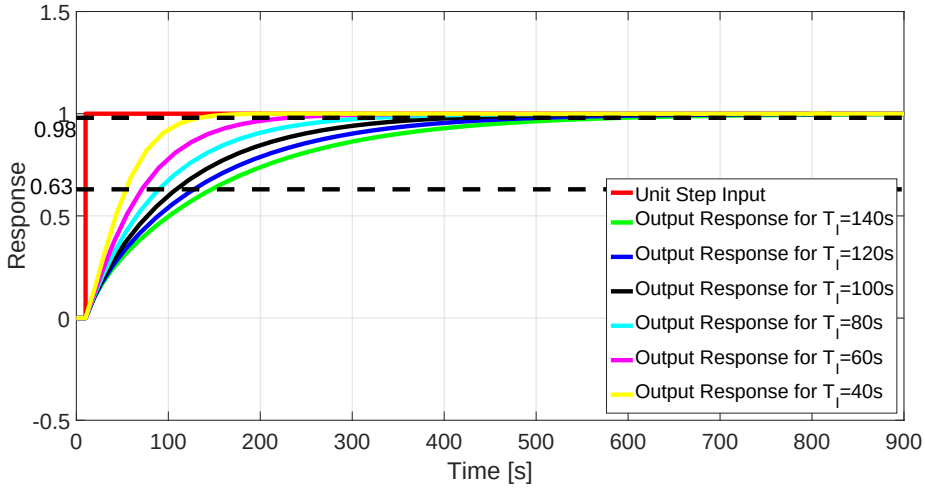

Figure 3-10: LFC response to unit step function

LFC Time Constant defined as the time taken for the step response to rise to 63% of its final value by the LFC for different values of integration time constant T_I are given in Table 3.4. LFC Settling Time defined as the time taken for the response to reach, and stay within, 2% of its final value by the LFC for different values of integration time constant T_I is also given in Table 3.4.

When LFC Time Constant and LFC Settling Time from Table 3.4 are plotted against Integration Time Constant T_I as shown in Figure 3-11, it is observed that LFC Time Constant and LFC Settling Time decrease nearly linearly with decrease in integration time constant T_I.

Therefore, it should be noted that the response speed of the LFC depends on the integration time constant of PI controller of LFC. However, the capability of LFC in terms of volume depends on the limited FRR available for each control area as denoted by $Reserve\ Limit$ in Figure 3-9.

Table 3.4: Behavior of step response of LFC for different values of T_I with K_P = 0.2 p.u. and T_{filter} = 16s

Integration Time Constant, T_I [s]	LFC Time Constant [s]	LFC Settling Time [s]
140	147.2	594.72
120	127.91	504.63
100	108.71	414.21
80	89.71	323.07
60	71.19	230.8
40	54.1	134.1

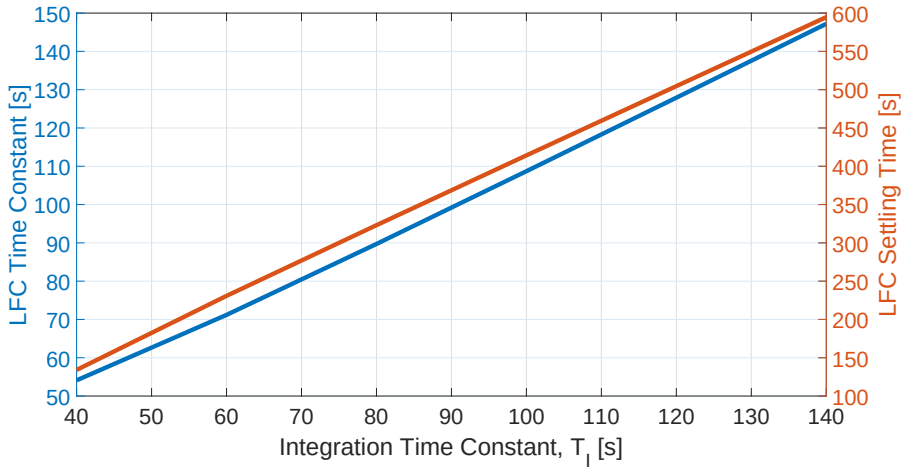

Figure 3-11: Time Constant and Settling Time of LFC response to unit step function for different values of T_I with K_P = 0.2 p.u. and T_{filter} = 16s

3.6 Study Cases

Anticipated wind power installation scenarios for CE network for 2020 and 2030 are developed as discussed in section 3.2. Wind power forecasts for hour-ahead, online prognoses and real-time available power from wind power generations are obtained trough Supervisory Control and Data Acquisition System (SCADA) in real time. These power prognoses and real-time available power are simulated using CorWind (Appendix A). These data are simulated for the wind data of 14 meteorological years. Online prognoses are obtained at the resolution of 5 minutes for next 15 minutes.

Following are the assumptions and considerations for probabilistic risk assessment algorithm for CE:

- Each country in CE network is assumed as a control area
- Threshold for RR activation for the studies is 30 MW

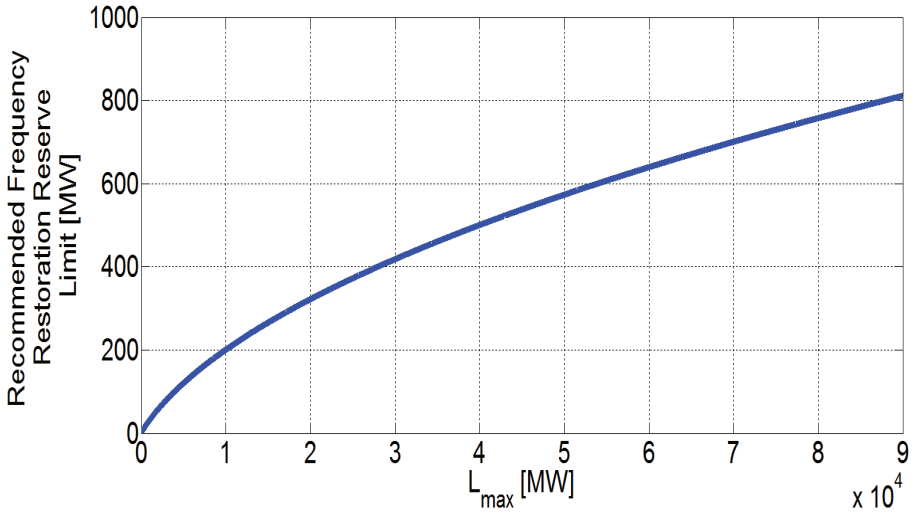

Figure 3-12: Frequency restoration reserve limit as a function of the maximum anticipated load

- RR responses are modelled with 5 minute delay and ramping rate of 10 minutes
- Proportional gain K_p for FRP is assumed 0.2 p.u.
- Filter time constant T_{filter} is assumed as 16 s.
- Generally, each TSO is responsible to handle power imbalances in its own control area, therefore it is assumed in these studies that that there is no contribution from neighboring control area to mitigate power imbalances in other control areas.
- The maximum anticipated loads for each control area for 2020 and 2030 scenarios are based on ENTSO-E adequacy forecast [9]. FRR limit as a function of maximum anticipated load derived using Equation 3.6 with $K_{wind} = 1$ is shown in Figure 3-12. Based on the maximum anticipated load for each control area, $Reserve\ Limit$ is obtained from Equation 3.6. This $Reserve\ Limit$ limits the volume of FRR deployment as shown in Figure 3-9.
- The total volume of FRR for CE is around 12000 MW [1].
- $FCR_{dimension}$ designed for CE network is 3000 MW

Simulations are performed for different FRR activation volumes and activation time. Studies are done for CE synchronous network.

3.6.1 Analysis of CE network for 2020 Scenario

The probability density functions for CE network for 2020 scenario is shown in Figure 3-13 for 2 cases- one without FRR+RR activation and one with FRR+RR activation.

It is observed that the probability density function curve for imbalance becomes much narrower after activation of FRR and RR. This implies that probabilities of power imbalances decrease with activation of FRR and RR.

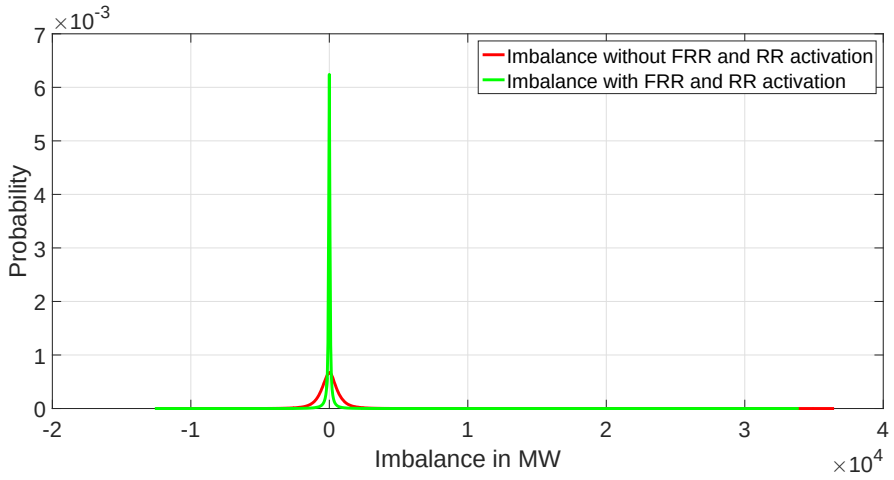

Figure 3-13: Probability density functions of imbalance for CE for 2020 scenario

The tail of the probability density function curve is quite long even after activation of reserves. This signifies that there is a very low probability of extreme high power imbalances. In order to handle such extreme situations, a very high amount of FCR are required. This advocates for dynamic deployment of FCR.

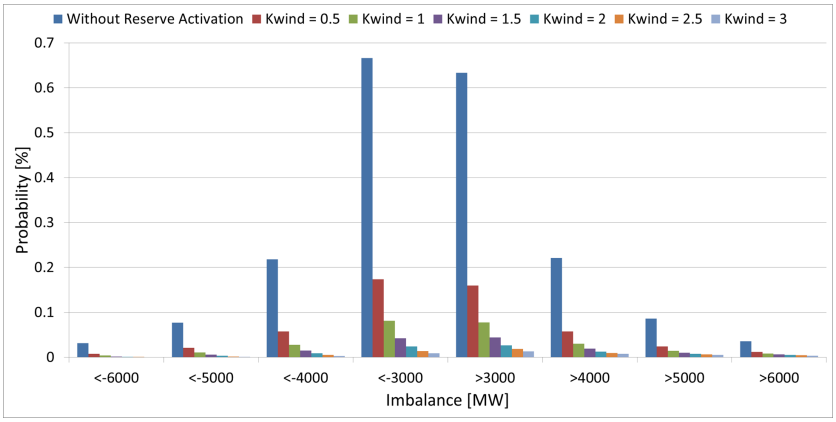

Figure 3-14: Probability of power imbalance exceeding reference incident for CE for 2020 scenario for different volumes of FRR activation

Figure 3-14 shows the probability of the imbalance exceeding FCR dimension (3000 MW) for CE for different volumes of FRR activation in 2020 scenario. As mentioned before, K_{wind} is the multiplier in Equation 3.6 incorporated to handle power imbalances due to wind power forecast error. It can be seen from Figure 3-14 that probability

of imbalance exceeding 3000 MW for 2020 scenario is quite low (less than 1%). Therefore, power imbalances can be handled more than 99% of the time. However, it is also noted from Figure 3-14 that higher the value of K_{wind} i.e. higher the volume of available FRR, lower is the probability of power imbalance beyond 3000 MW.

Another important point to be considered is the amount of time power imbalance is exceeding the standard range. Figure 3-15 shows occurrence of the power imbalance exceeding reference incident for CE for 2020 scenario. It can be observed from Figure 3-15 that occurrences are much less than 15000 min/yr. Higher the value of K_{wind}, lower is the occurrence of power imbalance beyond 3000 MW. Occurrence decreases substantially from 3350 min/yr for power imbalance without reserve activation to 35 min/yr for reserve activation with $K_{wind} = 3p.u.$ for positive power imbalance exceeding 3000 MW. Further, impact of faster activation of FRR is also studied. Figure

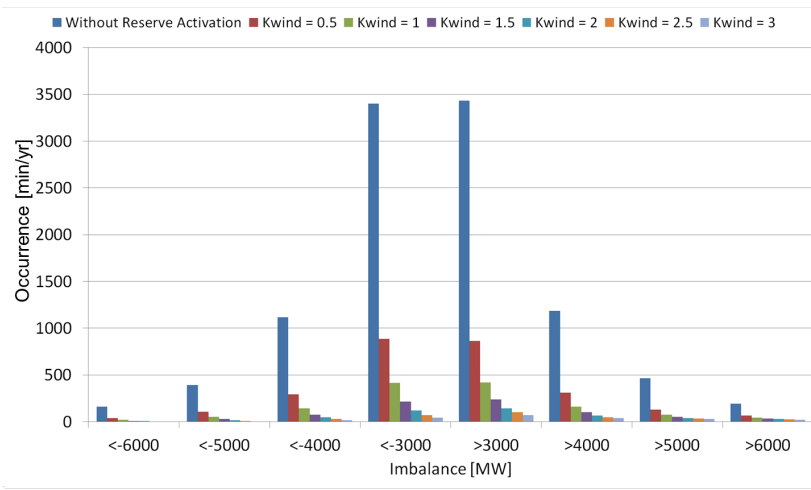

Figure 3-15: Occurrence of the power imbalance exceeding reference incident for CE for 2020 scenario

3-16 shows probability of the power imbalance exceeding reference incident for CE for 2020 scenario for different integration time constant of PI controller of LFC. Time response of LFC for different integration time constant is shown in Figure 3-11. It can be seen from Figure 3-16 that there is no improvement in reduction of imbalance with faster activation of FRR.

Finally, the probabilistic risk for different volumes and different integration time constants of FRR activation for negative and positive power imbalances are shown in Figure 3-17. Probabilistic risk is plotted against K_{wind} (volume of FRR) and T_I (speed of activation) simultaneously. Remark that risk of power imbalance exceeding 3000 MW is similar for both positive and negative imbalance as can be seen from Figure 3-17a and 3-17b respectively. It can be observed that risk of imbalances exceeding 3000 MW is much lower than 1%. However, T_I does not have impact in reducing power imbalance due to wind forecast error. Therefore, risk does not vary with T_I as depicted by straight line in Figure 3-14. While K_{wind} has significant impact in reducing risk.

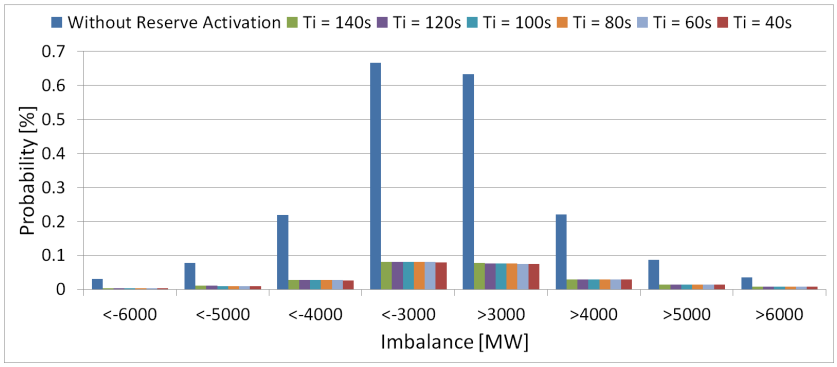

Figure 3-16: Probability of the imbalance exceeding reference incident for CE for 2020 scenario for different speed of FRR activation

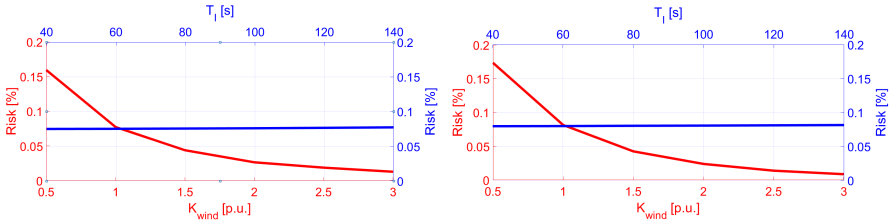

(a) Positive Imbalance

(b) Negative Imbalance

Figure 3-17: Risk of power imbalance exceeding reference incident for CE for 2020 scenario for different FRR activation

An important conclusion is that the risk reduces exponentially with increase in volume of FRR and remains almost unaffected by increase in integration time constant of FRR activation.

3.6.2 Analysis of CE network for 2030 Scenario

Figure 3-18 shows the probability of the power imbalance exceeding FCR dimension (3000 MW) for CE for different volumes of FRR activation for 2030 scenario. In contrast to 2020 scenario, probability of the power imbalance exceeding FCR dimension is almost 10 times higher. Power imbalance without reserve activation exceeding 3000 MW caused by error in wind power forecast is higher than 5%. This imbalance reduces substantially with activation of FRR and RR from 5% to 0.5% when $K_{wind} = 3$. If $K_{wind} = 0.5$ i.e. half of the FRR is already employed to handle other kinds of power imbalances from loads, contingencies, other generations etc., then the imbalance due to wind power can be as high as 3%. With 100% of the available FRR dimensioned (i.e. $K_{wind} = 1$) as it is in present system, imbalance comes down just below to 2%. **This implies that over-dimensioning of FRR is essentially required to handle wind**

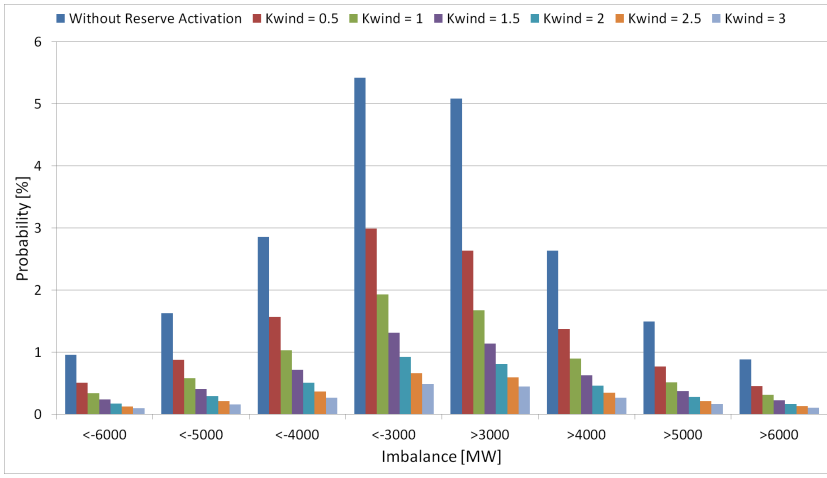

Figure 3-18: Probability of the imbalance exceeding reference incident for CE for 2030 scenario for different volumes of FRR activation

power imbalances in 2030 scenario. By dimensioning FRR double ($K_{wind} = 2$) as that of present volume, imbalance reduces down to less than 1%. However, in order to take consideration of power imbalances due to other sources, further over-dimensioning of FRR might be advisable. Increasing the FRR dimension to three times ($K_{wind} = 3$), the power imbalances due to wind reduces to less than 0.5%, which is equivalent to power imbalance in 2020 scenario.

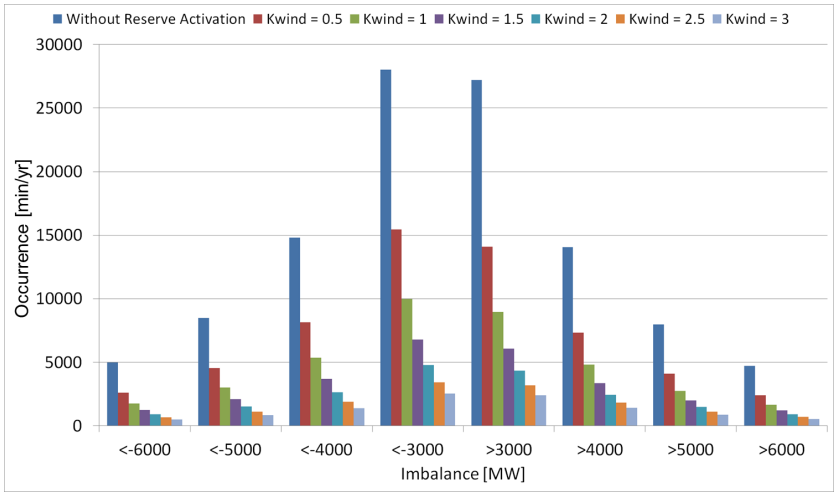

Figure 3-19: Occurrence of the imbalance exceeding reference incident for CE for 2030 scenario

Another point of consideration is that the power imbalances exceeding 3000 MW should not be more than 15000 min/yr. Figure 3-19 shows the occurrence of power imbalance due to wind power exceeding 3000 MW for CE for 2030 scenario. It can be seen that

power imbalances without FRR and RR activation occur much more frequently than 15000 min/yr. It does not came below 15000 min/yr with half ($K_{wind} = 0.5$) of the FRR activated to handle wind power imbalances. However, with 100% of the FRR utilised to handle power imbalances due to wind, occurrences of power imbalances become less than 15000 min/yr.

Remark that power imbalances can even be higher than 6000 MW. Figure 3-18 depicts probability of power imbalances exceeding 6000 MW is lower than 0.5%. However, Figure 3-19 illustrates that power imbalances exceeding 6000 MW still can be occurring for several hundred min/yr. These power imbalances can have high impact on frequency stability.

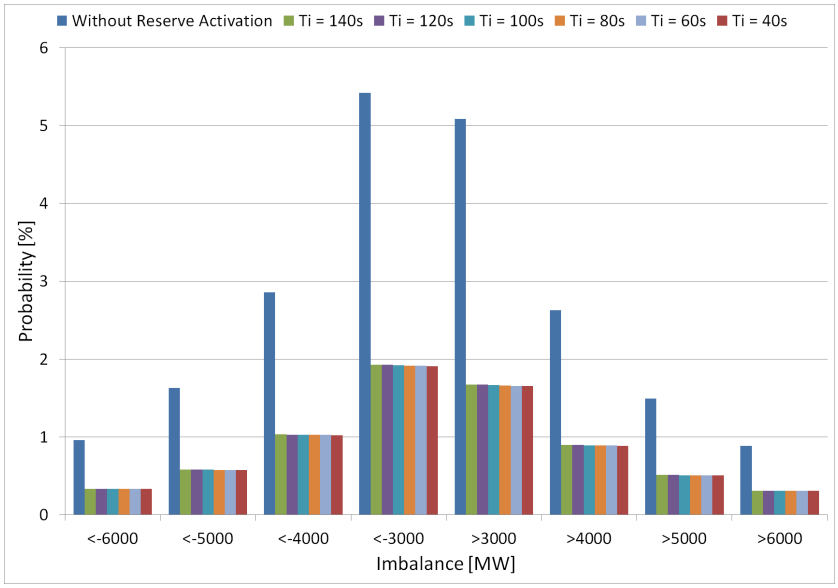

Figure 3-20: Probability of power imbalance exceeding reference incident for CE for 2030 scenario for different speed of FRR activation

Figure 3-20 illustrates probability of the imbalance exceeding reference incident for CE for 2020 scenario for different integration time constant of PI controller of LFC. Remark that there is no improvement in reduction of imbalance with faster activation of FRR.

Probabilistic risk of positive and negative power imbalances exceeding 3000 MW for different volumes and different speed of FRR activation as computed based on Equation 3.8 as shown in Figure 3-21. Probabilistic risk is plotted against K_{wind} (volume of FRR) and T_I (speed of activation) simultaneously. Remark that risk of power imbalance exceeding 3000 MW is similar for both positive and negative imbalance as can be seen from Figure 3-21a and 3-21b respectively. It can be concluded that FRR should at least be dimensioned to double the volume ($K_{wind} = 2$) as that of present volume in order to reduce the power imbalance down to less than 1%.

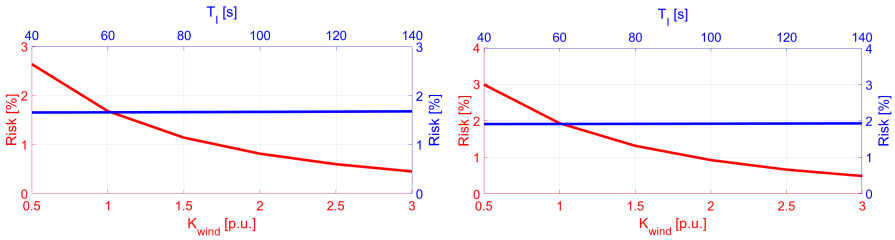

(a) Positive Imbalance

(b) Negative Imbalance

Figure 3-21: Risk of power imbalance exceeding reference incident for CE for 2030

Similar to observation of 2020 scenario, the risk reduces exponentially with increase in volume of FRR and remains almost unaffected by increase in integration time constant of FRR activation for 2030 scenario.

3.7 Summary and Recommendations

- The studies presented in this chapter only considers imbalance caused by wind power forecasts. Therefore, the imbalances caused from other sources like load, other stochastic generations like solar PV, contingencies etc. are not considered in this work.
- Power imbalances can originate due to uncertainties in wind power forecast. These imbalances can be high in future power systems when penetration of wind power is high.
- Two major challenges from wind power forecast error are observed. One challenge is large error in meteorological forecast and another challenge is fast rate of change of power imbalances.
  - Large errors in meteorological forecast is observed to be a low probable event. Imbalances caused by these errors may be handled using dynamic reserve deployment.
  - Fast rate of change of power imbalances can be handled faster activation of reserves.
- The imbalance simulated in this study is only considering imbalance caused by wind power forecasts. It should be noted that although the method presented in this study is general, but the output imbalance depends largely on the input forecast error. If a better wind power forecast model is available, then the imbalance is expected to be reduced.
- A methodology is proposed and developed to estimate adequacy of reserves for wind power scenarios in ENTSO-E networks.

- Probabilistic risk assessment of power imbalances exceeding designed frequency containment reserves with activation of frequency restoration and replacement reserves is computed using this methodology.
- It is observed that probabilistic risk for wind scenarios for CE reduces exponentially with increase in volume of FRR and remains almost unaffected by increase in integration time constant of FRR activation.
- Probability of power imbalance due to wind forecast error exceeding 3000 MW for CE in 2020 scenario is low and can be handled with reserves dimensioned as it is in present system.
- Frequency restoration reserves for countries with high wind power penetration of 2030 scenario should have additional volume (at least 2 times higher than reserve volume in present scenario) in order to handle power imbalances from wind power forecast error.

Chapter 4

Sensitivity Studies for Frequency Containment Process

This chapter is concerned with frequency containment process (FCP). A mathematical analytical approach for FCP is proposed and discussed. Capabilities of different types of generation sources, namely, fossil fuel steam generation, hydro steam generation, nuclear steam generation, cross-compound steam generation and wind turbines in providing FCP are analysed through this mathematical analytical approach. A set of simulations have been performed in a power system consisting of either generic governor model or generic wind turbine model. The impacts of droop settings and system inertia on peak frequency value or frequency nadir (for overfrequency and underfrequency respectively) are analysed following a major disturbance in the system. Whether the maximum/minimum frequency value can be controlled with the help of FCP through frequency containment reserves (FCR) supplied from conventional generators is investigated. The success of the control is measured by its ability to prevent the frequency reaching beyond permissible range. Comparative studies between cases when FCR are supplied from conventional generators and where FCR are supplied from wind turbines are carried out. Observations from these simulations are analyzed and explained with the help of analytical model which provide the feasible range of droop settings for different values of system inertia.

In previous chapter, the requirement for FCR in order to handle imbalances caused by wind power generation has been discussed and investigated. In this chapter, the attention is drawn to the speed of deployment of FCR as this is of high importance in situations when power systems are operating with penetration of converter connected renewable generations.

Renewable generations like large controllable variable speed wind turbines are connected to the power system through power electronic converters. Therefore the rotational mass of these generators are physically isolated from the network, and as result, they do not contribute with inertia in the power system. Consequently, higher the pen-

etration of wind power replacing conventional generations, lower is the inertia of the power system. A power system with low inertia as i.e. an island power system, may experience high frequency fluctuations following a large disturbance in the power system like disconnection of a generator. However this effect can also happen in an interconnected system like CE network, as it was the case for the disturbance of 4^{th} November, 2006. Tripping of a 380 kV line due to overload and other cascading tripping led to the final separation of the entire UCTE grid in three island areas. Frequency in the North-Eastern area of the UCTE network got very high following the system split. North-Eastern region had lost export of 10 GW (around 17% of the total generation) due to the separation. Wind power generation of this region was around 17% of the total generation, thereby system inertia fortunately was not too low otherwise the condition could get even worse.

As stated in [11], fast change of frequency following a large disturbance can cause short term frequency instability. Different types of frequency control processes, viz. FCP, FRP and Replacement Process (RP) are employed to restrict the frequency change and stabilize the frequency. FCP is employed to limit the frequency from going too high (or low) and exceeding the acceptable limits (50 $\pm$ 0.050 Hz for CE) following a large disturbance FCP is completely deployed within 30 s after the disturbance and utilizes reserved power (for underfrequency situations) from dedicated generators referred as frequency containment reserves. In case FCP is either inadequate or not fast enough to contain the frequency, defence plans like underfrequency load shedding or overfrequency generation disconnections are employed to prevent frequency instability [12]. However, these defence plans are only considered as last resorts since they cause economic losses and discomfort to consumers. Therefore, all the available resources in the power system should be employed before activating these defence plans. Generally, underfrequency load shedding starts at 49 Hz and overfrequency generation disconnection happens at 51.5 Hz for CE network [6],[56].

4.1 Mathematical Model of FCP

A mathematical per unit (p.u.) model for FCP loop is proposed in the following having as starting point the block diagram model for FCP provided by a FCP controller. FCP controller can be either a turbine-governor controlled power generator or a converter connected wind turbine. The block diagram for the FCP provided is shown in Figure 4-1. $\Delta\omega$ represents the change in angular speed (change in frequency f).

The FCP controller is further modelled for mathematical analytical approach as droop control with slope of $\frac{-1}{R}$ and a turbine technology represented by a zero(z)-pole(p)-gain(k) transfer function model as depicted in Figure 4-2. The power system is represented with respect to system angular momentum M and system damping D. ΔP_{ref} represents the change in load reference point for the generator and ΔP_d represents the power imbalance seen by the power system due to a disturbance. The disturbance can be disconnection of large generator/load or system separation in the case of large interconnected system. In case of system separation into smaller areas, ΔP_d denotes the loss of import/export to other areas.

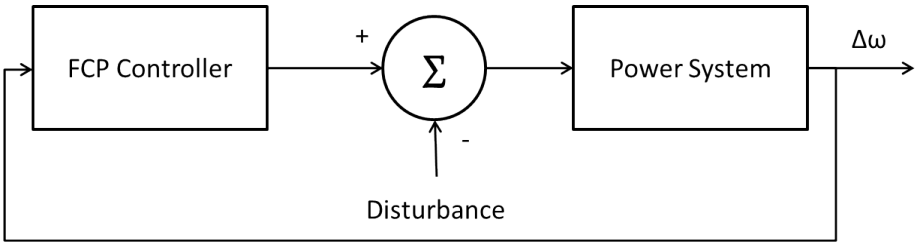

Figure 4-1: Block Diagram for FCP Loop

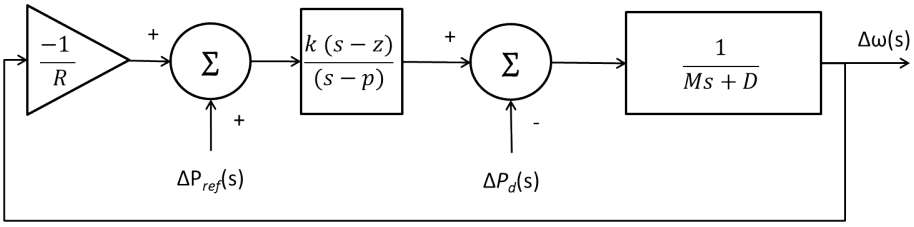

Figure 4-2: FCP block diagram for mathematical analytical approach

The time frame of FCP of few seconds following a large disturbance. During the period, FRP is not activated and therefore, the set-points P_{ref} for the generators are not changed by LFC, therefore, ΔP_{ref} in Figure 4-2 can be neglected.

The mathematical formulation for the model in Figure 4-2 is given in Equation

$$\left(-\frac{\Delta\omega(s)}{R} \times \frac{k(s-z)}{(s-p)} - \Delta P_d(s) \right) \frac{1}{Ms+D} = \Delta\omega(s) \tag{4.1}$$

or,

$$\frac{\Delta\omega(s)}{\Delta P_d(s)} = \frac{\frac{-1}{M}s + \frac{p}{M}}{s^2 + (\frac{k+DR-pMR}{RM})s + (\frac{-pDR-kZ}{RM})} \tag{4.2}$$

Damping of the system, D does not have large and fast impact on FCP due to the short time frame of FCP, therefore D can be safely assumed zero henceforth.

$$\frac{\Delta\omega(s)}{\Delta P_d(s)} = \frac{\frac{-1}{M}s + \frac{p}{M}}{s^2 + \left(\frac{k-pMR}{RM}\right)s + \left(\frac{-kZ}{RM}\right)} \tag{4.3}$$

It can be observed from Equation 4.3 that the closed loop transfer has a zero and 2 poles. The denominator of Equation 4.3 can be compared with the denominator of the standard second order transfer function given by $s^2 + 2\zeta\Omega_n s + \Omega_n^2$.

Therefore, Equation 4.3 can be further rewritten as

$$\frac{\Delta\omega(s)}{\Delta P_d(s)} = \frac{\frac{-1}{M}s + \frac{p}{M}}{s^2 + 2\zeta\Omega_n s + \Omega_n^2} \tag{4.4}$$

where,

$${\Omega_n}^2 = \frac{-kz}{RM} \tag{4.5}$$

namely, natural frequency Ω_n is given by:

$$\Omega_n = \sqrt{\frac{-kz}{RM}} \tag{4.6}$$

while attenuation $\zeta\Omega_n$ is given by:

$$\zeta\Omega_n = \frac{k - pMR}{2RM} \tag{4.7}$$

namely damping ratio ζ is given by:

$$\zeta = \frac{k - pMR}{2RM\Omega_n} \tag{4.8}$$

Generally, a disturbance occurs instantly, therefore, ΔP_d can be modelled as step response with magnitude A_d. Equation 4.4 can be thus further written as,

$$\Delta\omega(s) = \frac{-\frac{1}{M}s + \frac{p}{M}}{s^2 + 2\zeta\Omega_n s + {\Omega_n}^2} \times \frac{A_d}{s} \tag{4.9}$$

which can be rewritten as following:

$$\Delta\omega(s) = \frac{pA_d}{M{\Omega_n}^2}\left[\frac{1}{s} - \frac{s + \frac{\Omega_n}{p}(\Omega_n + 2p\zeta)}{s^2 + 2\zeta\Omega_n s + {\Omega_n}^2}\right] \tag{4.10}$$

By adding and subtracting $\zeta^2{\Omega_n}^2$ to the denominator, the Equation 4.10 can be written as

$$\Delta\omega(s) = \frac{pA_d}{M{\Omega_n}^2}\left[\frac{1}{s} - \frac{s + \frac{\Omega_n}{p}(\Omega_n + 2p\zeta)}{s^2 + 2\zeta\Omega_n s + \zeta^2{\Omega_n}^2 + {\Omega_n}^2 - \zeta^2{\Omega_n}^2}\right] \tag{4.11}$$

or,

$$\Delta\omega(s) = \frac{pA_d}{M{\Omega_n}^2}\left[\frac{1}{s} - \frac{s + \frac{\Omega_n}{p}(\Omega_n + 2p\zeta)}{(s + \zeta\Omega_n)^2 + {\Omega_n}^2 - \zeta^2{\Omega_n}^2}\right] \tag{4.12}$$

or,

$$\Delta\omega(s) = \frac{pA_d}{M{\Omega_n}^2}\left[\frac{1}{s} - \frac{s + \frac{\Omega_n}{p}(\Omega_n + 2p\zeta)}{(s + \zeta\Omega_n)^2 + {\Omega_d}^2}\right] \tag{4.13}$$

or,

$$\Delta\omega(s) = \frac{pA_d}{M{\Omega_n}^2}\left[\frac{1}{s} - \frac{1}{\Omega_d}\frac{(s + \frac{\Omega_n}{p}(\Omega_n + 2p\zeta))\Omega_d}{(s+\zeta\Omega_n)^2 + {\Omega_d}^2}\right] \tag{4.14}$$

where, damped frequency can be written as,

$$\Omega_d = \Omega_n\sqrt{1-\zeta^2} = \frac{\sqrt{-(k-pMR)^2 - 4kz}}{2RM} \tag{4.15}$$

Taking inverse Laplace of Equation 4.14, gives Equation 4.16

$$\Delta\omega(t) = \frac{pA_d}{M{\Omega_n}^2}\left[1 - e^{-\zeta\Omega_n t}\left(\cosh(j\Omega_d t) - \frac{j(\frac{{\Omega_n}^2 + 2p\zeta\Omega_n}{p} - \zeta\Omega_n)\sinh(j\Omega_d t)}{\Omega_d}\right)\right] \tag{4.16}$$

$\cosh(j\Omega_d t)$ can be written as,

$$\begin{aligned}\cosh(j\Omega_d t) &= \frac{e^{j\Omega_d t} + e^{-j\Omega_d t}}{2} \\ &= \frac{\cos(\Omega_d t) + j\sin(\Omega_d t) + \cos(\Omega_d t) - j\sin(\Omega_d t)}{2} \\ &= \cos(\Omega_d t)\end{aligned} \tag{4.17}$$

Similarly,

$$\sinh(j\Omega_d t) = \frac{e^{j\Omega_d t} - e^{j\Omega_d t}}{2} = j\sin(\Omega_d t) \tag{4.18}$$

Therefore, Equation 4.16 gets modified to Equation 4.19

$$\Delta\omega(t) = \frac{pA_d}{M{\Omega_n}^2}\left[1 - e^{-\zeta\Omega_n t}\left(\cos(\Omega_d t) + \frac{\sin(\Omega_d t)}{\Omega_d}\left(\frac{{\Omega_n}^2 + 2p\zeta\Omega_n}{p} - \zeta\Omega_n\right)\right)\right] \tag{4.19}$$

or,

$$\Delta\omega(t) = \frac{pA_d}{M{\Omega_n}^2}\left[1 - e^{-\zeta\Omega_n t}\left(\cos(\Omega_d t) + \frac{{\Omega_n}^2 + p\zeta\Omega_n}{p\Omega_d}\sin(\Omega_d t)\right)\right] \tag{4.20}$$

Equation 4.20 shows that $\Delta\omega(t)$ **oscillates sinusoidally with an exponential decay, which depends on attenuation** $\zeta\Omega_n$, which is given by Equation 4.7.

Since the main responsibility of the FCP is to limit (or contain) the frequency within a

short time frame, the peak (or nadir in case of underfrequency) value of $\Delta\omega(t)$ and the time to reach this peak value (t_p) are of primal interest.

In order to find the peak of $\Delta\omega(t)$ given by $\Delta\omega_{peak}$, the derivative of $\Delta\omega(t)$ should be zero, i.e.,

$$\left.\frac{d\Delta\omega(t)}{dt}\right|_{t=t_{peak}} = 0 \tag{4.21}$$

or,

$$\zeta\Omega_n e^{-\zeta\Omega_n t_{peak}}\left[\cos(\Omega_d t_{peak}) + \frac{{\Omega_n}^2 + p\zeta\Omega_n}{p\Omega_d}\sin(\Omega_d t_{peak})\right] \tag{4.22}$$

$$- e^{-\zeta\Omega_n t_{peak}}\left[-\Omega_d \sin(\Omega_d t_{peak}) + \frac{{\Omega_n}^2 + p\zeta\Omega_n}{p}\cos(\Omega_d t_{peak})\right] = 0$$

or,

$$\tan(\Omega_d t_{peak}) = \frac{\Omega_d}{p + \zeta\Omega_n} \tag{4.23}$$

or,

$$t_{peak} = \frac{\tan^{-1}\left(\frac{\Omega_d}{p+\zeta\Omega_n}\right)}{\Omega_d} \tag{4.24}$$

It can be observed from Equation 4.24, that time t_{peak} to reach peak value is independent of disturbance ΔP_d and depends on characteristics of technology (k, p, z), droop settings (R) and inertia of the power system (M).

From Equation 4.23, $\sin(\Omega_d t_{peak})$ and $\cos(\Omega_d t_{peak})$ can be written as;

$$\sin(\Omega_d t_{peak}) = \frac{\Omega_d}{\sqrt{p^2 + 2p\zeta\Omega_n + {\Omega_n}^2}} \tag{4.25}$$

$$\cos(\Omega_d t_{peak}) = \frac{p + \zeta\Omega_n}{\sqrt{p^2 + 2p\zeta\Omega_n + {\Omega_n}^2}} \tag{4.26}$$

such that,

$$\sin^2(\Omega_d t_{peak}) + \cos^2(\Omega_d t_{peak}) = 1 \tag{4.27}$$

Replacing values of Equations 4.25 and 4.26 in Equation 4.20, we get

$$\begin{aligned}\Delta\omega_{peak} &= \Delta\omega(t_{peak}) \\ &= \frac{pA_d}{M{\Omega_n}^2}\left[1 - e^{-\zeta\Omega_n t_{peak}}\left(\frac{p+\zeta\Omega_n}{\sqrt{p^2+2p\zeta\Omega_n+{\Omega_n}^2}}\right.\right. \\ &\quad \left.\left. + \frac{{\Omega_n}^2+p\zeta\Omega_n}{p\Omega_d}\frac{\Omega_d}{\sqrt{p^2+2p\zeta\Omega_n+{\Omega_n}^2}}\right)\right]\end{aligned} \tag{4.28}$$

or,

$$\Delta\omega_{peak} = \frac{pA_d}{M{\Omega_n}^2}\left[1 - e^{-\zeta\Omega_n t_{peak}}\left(\frac{\sqrt{p^2+2p\zeta\Omega_n+{\Omega_n}^2}}{p}\right)\right] \tag{4.29}$$

$p^2 + 2p\zeta\Omega_n + {\Omega_n}^2$ can be calculated from Equation 4.5 and 4.7 and given as

$$p^2 + 2p\zeta\Omega_n + {\Omega_n}^2 = \frac{k(p-z)}{MR} \tag{4.30}$$

Substituting the values from Equation 4.30 into Equation 4.29, we get

$$\Delta\omega_{peak} = -\frac{pA_dR}{kz}\left[1 - \frac{e^{-\zeta\Omega_n t_{peak}}}{p}\sqrt{\frac{k(p-z)}{MR}}\right] \tag{4.31}$$

Note that in these studies, the peak frequency considered is the first peak value of the frequency. However, there can be many subsequent peaks if the attenuation $\zeta\Omega_n$ is low. If the attenuation is negative, subsequent peaks become even higher than the first peak. The focus in this work is on the first peak along with the attenuation $\zeta\Omega_n$ / damping ratio ζ are studied together. It can be observed that peak value of $\Delta\omega_{peak}$ is directly proportional to the magnitude of the disturbance, A_d and droop, R. Moreover, it is dependent on generation technology, as $\Delta\omega_{peak}$ is directly proportional to the ratio of pole to gain and zero i.e., $\frac{p}{zk}$.

Angular momentum of the system M in p.u. is twice the inertia constant H as given by Equation 4.32,

$$M = 2H \tag{4.32}$$

Since $\Delta f = \Delta\omega_{peak}$, hence the frequency and peak frequency (or nadir) are given by $f = f_{nom}(1 + \Delta\omega)$, where f_{nom} is the nominal frequency of the system (50 Hz in Europe).

The summary of the formulae derived from mathematical model expressed based on inertia constant H are given as Equation 4.33

$$
\begin{aligned}
f &= f_{nom}\left(1 + \frac{pA_d}{2H{\Omega_n}^2}\left[1 - e^{-\zeta\Omega_n t}\left(\cos(\Omega_d t) + \frac{{\Omega_n}^2 + p\zeta\Omega_n}{p\Omega_d}\sin(\Omega_d t)\right)\right]\right) \\
f_{peak} &= f_{nom}\left(1 - \frac{pA_d R}{kz}\left[1 - \frac{e^{-\zeta\Omega_n t_{peak}}}{p}\sqrt{\frac{k(p-z)}{2HR}}\right]\right) \\
t_{peak} &= \frac{\tan^{-1}\left(\frac{\Omega_d}{p+\zeta\Omega_n}\right)}{\Omega_d} \\
\Omega_n &= \sqrt{\frac{-kz}{2RH}} \\
\zeta\Omega_n &= \frac{k - 2pHR}{4RH} \\
\Omega_d &= \Omega_n\sqrt{1-\zeta^2} = \frac{\sqrt{-(k-2pHR)^2 - 4kz}}{4RH}
\end{aligned}
\tag{4.33}
$$

Following observations can be summarized from Equation 4.33:

- Frequency fluctuates sinusoidally with an exponential damping dependent on attenuation $\zeta\Omega_n$
- Peak frequency f_{peak} mainly depends on droop, disturbance, generation technology $\frac{pA_dR}{kz}$
- Peak time t_{peak} is independent of disturbance and dependent on attenuation $\zeta\Omega_n$ and damped frequency Ω_d
- Attenuation $\zeta\Omega_n$ depends on generation technology, droop, system inertia and independent of disturbance
- Damped frequency Ω_d depends on generation technology, droop, system inertia and independent of disturbance

This set of formulae is used in the following to perform sensitivity studies.

When the inertia of the system is low, RoCoF following a large disturbance can be high. Response of the generation technology should be fast in such system. This can be obtained by reducing the droop (faster droop). $\Delta\omega_{peak}$ is also directly proportional to droop R as can be seen by Equation 4.33. Therefore, reducing droop reduces $\Delta\omega_{peak}$. However, capabilities to respond to faster droop depend on type of generation technology. Faster droop can cause reduction in attenuation and damping ratio. This in turn can cause undamped response resulting in oscillatory instability.

4.2 Sensitivity Studies

The capabilities of different generation technologies differ by large extent. The impact of 1) System inertia and 2) faster droop are investigated on different parameters of generation technologies.

In the following, sensitivities of different generation technologies towards FCP are studied. Impacts of system inertia and droop on frequency maximum/minimum during a frequency event are also analyzed.

In order to study different technologies of generation technologies, general purpose governor block for conventional generators proposed by Anderson and Fouad [78] as shown in Figure 4-3 is used. This general purpose governor model basically represents "FCP Controller" of Figure 4-1. Different parameters of model of Figure 4-3 are as following:

- $\Delta\omega$: change in frequency in p.u.
- $T1$ - $T5, F$: parameters for the transfer functions.
- R: droop of the governor.
- P_{m0}: mechanical power set-point of the generator.
- P_m: mechanical power output of the generator.
- P_e: electrical power output of the generator.
- P_a: accelerating power output of the generator.
- P_{max}: Maximum power output of generator.

The parameters F and $T1-T5$ vary for different types of generator affecting the output response for change in frequency.

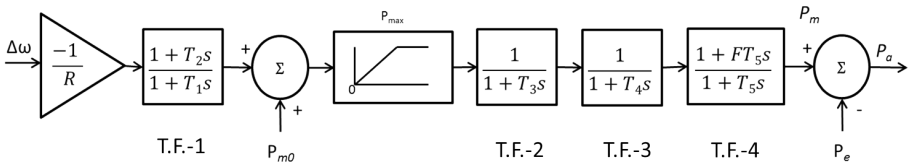

Figure 4-3: General Purpose Governor Block Diagram

The values for different parameters of general purpose governor (as shown in Figure 4-3) for different types of generators are given in Table 4.1. These values are obtained from Appendix D of [78].

Table 4.1 depicts parameters for a high capacity (820 MW) fossil fuel steam generator, a lower capacity (347 MW) fossil fuel steam generator, a hydro generator, a cross-compound steam generator, a nuclear steam generator. It can be observed that droop

Table 4.1: Parameters for General Purpose Governor Model for different types of Generators

Type of Generator	Maximum Power P_{max} [MW]	R [%]	T1[s]	T2[s]	T3[s]	T4[s]	T5[s]	F
Fossil Steam	820	2-6	0.1	0	0.2	0.1	8.72	0.3
Fossil Steam	347	2-6	0.1	0	0.4	0.05	8	0.25
Hydro	603.3	2-6	36	6	0	0	0.9	-2
Cross-Compound	436	2-6	0.1	0	0.3	0.05	14	0.58
Nuclear Steam	1216	2-6	0.15	0	0.2	0.814	2.46	0.34

values are varied from 2% to 6% in order to study the effects of different droop values on frequency. Another interesting point to be observed from Table 4.1 that hydro generator has a zero in right-half plane for the transfer function T.F.-4 in Figure 4-3 since F has negative value. This implies that the response of this transfer function will be in opposite direction as that of the input which is not desirable. This peculiar response is due to water inertia. A change in gate position produces an initial turbine power change in opposite direction. In order to mitigate this issue, generally a large transient droop with long resetting time is introduced [79]. However, in the studies presented in this chapter, hydro governors without transient droop are considered for simplicity. Table 4.1 also depicts that $T5$ is the main time constant for all the generators except hydro generator. Therefore, T.F.-4 plays the most important role in dictating the output response from these generators.

It should be emphasised again that the work presented in this chapter is mainly concerned with the fast response capabilities of generators for power system for FCP assuming that volume of FCR is sufficient. This work is not concerned with FRP therefore set-point of generators are kept constant. These assumptions allow for further simplification of the model shown in Figure 4-3. P_{max} is relaxed since volume of FCR is assumed sufficient to handle the disturbance.

Considering these assumptions and combining the models presented in Figure 4-1 and Figure 4-3, a simplified generic model for FCP is obtained as shown in Figure 4-4.

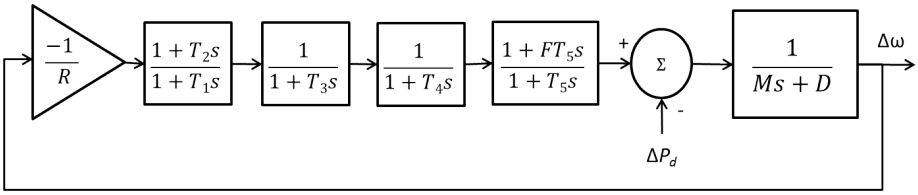

Figure 4-4: Generic delta model for FCP from conventional Governor-Turbine system

ΔP_d is assumed as large as 0.17 p.u. for the underfrequency studies and -0.17 p.u. for overfrequency studies, i.e., A_d in Equation 4.33 is ± 0.17 p.u. based on the UCTE 4^{th} November, 2006 system separation event when North-Eastern island area had 17% excess generation following the split.

However it should be mentioned that the generic model of Figure 4-4 is applicable only

for conventional generators. IEC 61400-27 generic wind turbine models [80] are used to study the FCP from wind turbines. FCP model for wind turbines is shown in Figure 4-5, while details of IEC 61400-27 generic dynamic wind turbine model type 4A are given in Appendix E.

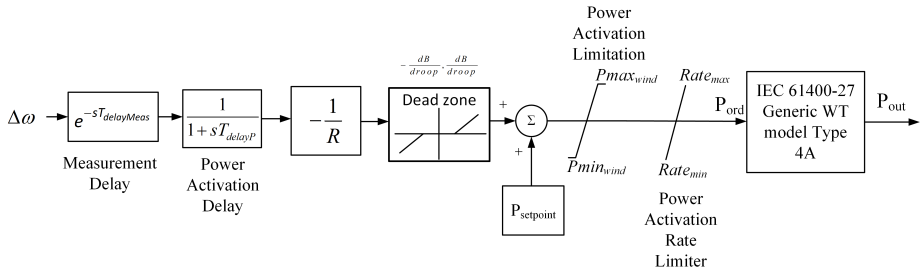

Figure 4-5: Frequency control model for FCP from wind turbine

Measurement delay ($T_{delayMeas}$) is assumed as 100 ms. Measurement delay is assumed comprising the communication delays, delays caused by sampling and computation of frequency and measurement delay. Power activation delay (T_{delayP}) is assumed as 50 ms. Maximum and minimum ramp rate ($Rate_{max}, Rate_{min}$) is assumed ± 0.5 p.u./s. It should be noted that the response capability from wind turbine depend largely on ramping rate limiter and delays of wind turbine control. Impacts of delay and ramping rate on wind turbine response are studied in details in next chapter.

In order to understand the behaviour of the generic FCP controller models, equivalent analytical pole-zero-gain model of Figure 4-2 is identified. This equivalent pole-zero-gain model is useful to compute attenuation and damping ratio of the frequency response. Comparisons of generic and analytical model for conventional governor-turbine system and generic wind turbine are shown in Figure 4-6.

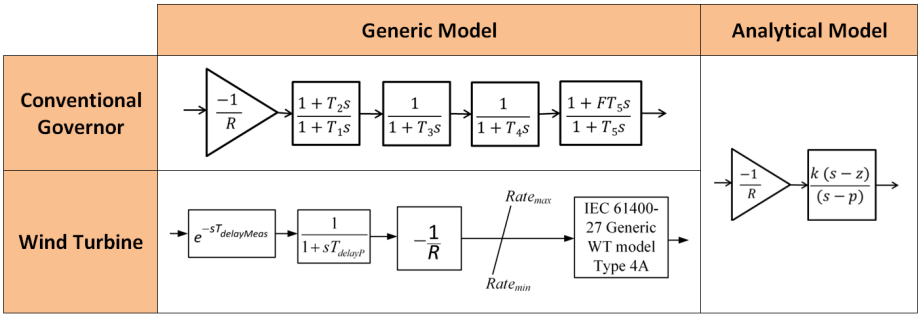

Figure 4-6: Comparisons of generic and analytical model of FCP for a conventional governor-turbine system and generic wind turbine

In order to investigate the sensitivities of different technologies of generators following studies are performed:

- Constant droop, constant inertia

- Constant droop, varying inertia
- Varying droop, varying inertia

For the following studies, only one technology of generator is considered at a time in the FCP model of Figure 4-1. Therefore, the results obtained considering a specific technology of generator is independent of other technologies of generators. Disturbance is modelled as step response with magnitude 0.17 p.u. after 1 second.

4.2.1 Constant Droop, Constant Inertia

In this section, control capabilities of different technologies of generators are studied and compared for constant droop and constant inertia. The droop and inertia constant values are chosen as 4% and 5 s respectively. The goal of this study is to understand the individual capabilities of different types of governors and wind turbine to contain frequency and prevent frequency instabilities.

Figure 4-7 depicts the frequency response and output of different technologies of generators.

The following observations can be made from Figure 4-7:

- **Fossil fuel steam generator** is capable in containing the frequency within 51 Hz. Larger fossil steam generator has better capability for FCP as compared to smaller fossil steam, since peak frequency with 820 MW fossil steam generator is 50.82 Hz while peak frequency with 347 MW fossil steam generator is 50.96 Hz. Further, it is observed from generator outputs that the large fossil steam provides faster response and therefore needs to provide lesser response than the small fossil steam generator. Therefore, it can be recommended to deploy FCR from larger fossil steam generators.
- **Hydro generators** in its basic form without transient droop characteristics are not suitable sources to provide FCP. The frequency increases beyond 53 Hz. The control of hydro generation is very slow pertaining to the time constant, T_1 of transfer function, T.F.-1 in Figure 4-3 which has a value of 36 s as seen from Table 4.1. The transfer function T.F.-4 has a zero in right half plane resulting in initial response from the hydro generator in opposite direction following the disturbance. As depicted in Figure 4-7, hydro generator increases its generation for around 2.5 s before reducing its generation. Notice also that the damping is very poor resulting in the frequency dropping down to less than 49 Hz. All these reasons make hydro generators unsuitable for FCP.
- **Cross-compound steam generators** contain the frequency within 50.6 Hz, as depicted in Figure 4-7.
- **Nuclear steam generators** are capable of containing the frequency within 51 Hz. However, their performance is poor pertaining to poor damping of the frequency. It can be seen that frequency while oscillation even go to underfrequency zone up to 49.5 Hz. This make nuclear generators also unsuitable for providing FCP.

(a) Fossil Steam Generator

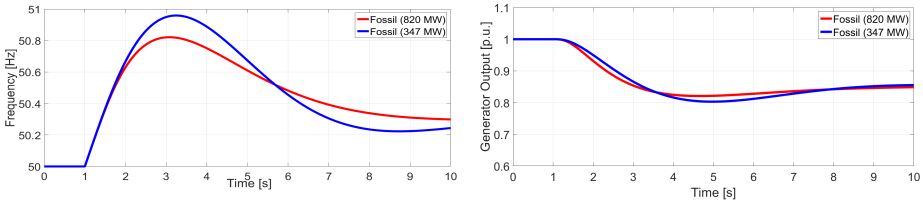

(b) Hydro Generator

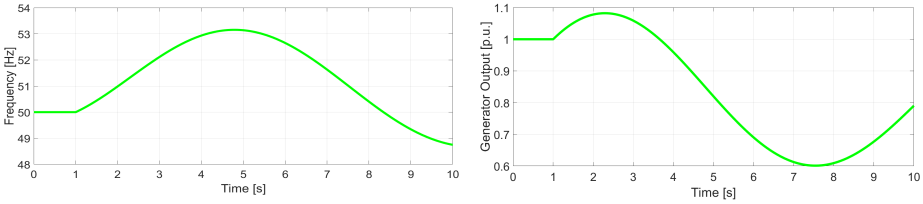

(c) Cross-Compound Fossil Steam Generator

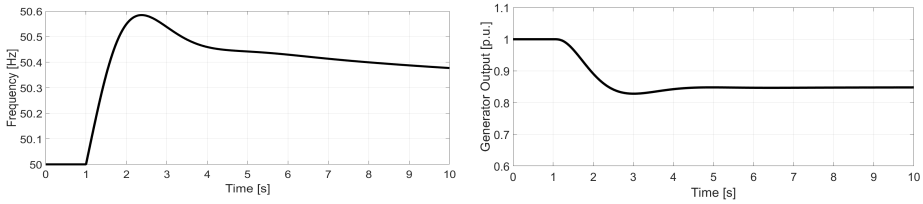

(d) Nuclear Steam Generator

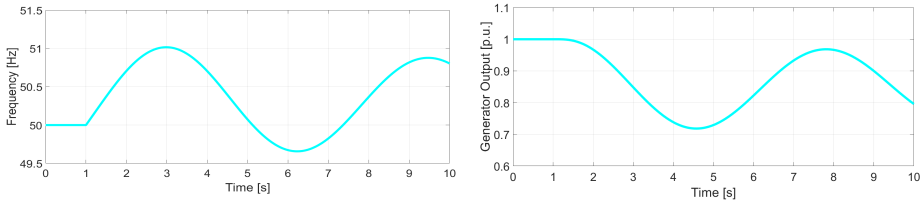

(e) Wind Turbine

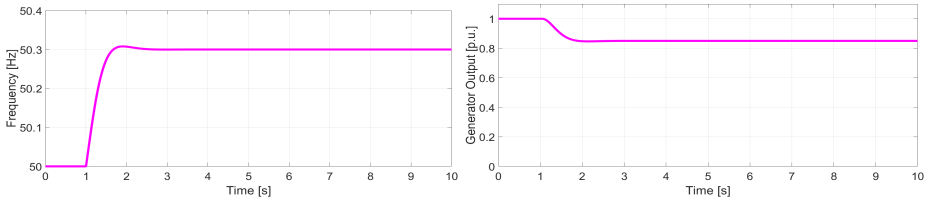

Figure 4-7: Frequency Response and Generator Output for different types of Generators

- **Wind turbines** perform quite well compared with other generators, as they are capable to contain the frequency within 50.35 Hz.

In order to understand peak frequency and damping of the frequency response from different generators, it is important to find equivalent pole-zero-gain of the analytical model depicted in Figure 4-6. The parameters of the analytical model for each generator for the response for given $R = 4\%$ and $H = 5s$ is given in Table 4.2. The parameters are obtained through Matlab "System Identification" tool. Fitness of the frequency response for this analytical model with the simulated generic model is also given in Table 4.2.

Table 4.2: Open loop pole-zero-gain for analytical model

Type of Generator	k	p	z	Fitness [%]
Fossil (820 MW)	5.5349e-04	-1.2553	-1.05E+03	97.6395
Fossil (347 MW)	-0.0043	-0.766	86.69	98.7696
Hydro	-0.3046	-0.7908	0.5469	99.3332
Cross-Compound	-0.1530	-2.4096	9.8666	99.3584
Nuclear	-0.0851	-0.261	3.9825	99.1686
Wind	-0.4335	-7.9687	18.4136	99.0736

Although it is hard to infer any information from the open loop pole-zero-gain presented in Table 4.2, however it is very useful in determining derived quantities based on formulae derived before. The parameters of interests are of closed loop poles in order to assess absolute and relative stability of the system. Closed loop poles are obtained by solving the characteristic equations of $s^2 + 2\zeta\Omega_n s + {\Omega_n}^2$ of Equation 4.4. Another important quantity is attenuation given by $\zeta\Omega_n$. Attenuation $\zeta\Omega_n$ provides the exponential decay of the sinusoidal oscillation as given by Equation 4.33. The derived quantities from Equation 4.33 are shown in Table 4.3.

Table 4.3: Derived Quantities from Analytical Model

Type of Generator	Closed loop poles Real	Closed loop poles Imaginary	Natural Freq. Ω_n	Attenuation $\zeta\Omega_n$	Damping Ratio ζ
Fossil (820 MW)	-0.6283	$\pm$0.9002	1.2051	0.6283	0.5214
Fossil (347 MW)	-0.3777	$\pm$0.9053	0.9622	0.3776	0.3924
Hydro	-0.0146	$\pm$0.8032	0.6453	0.0145	0.0225
Cross-Compound	-1.0136	$\pm$0.9567	1.9425	1.0135	0.5218
Nuclear	-0.0242	$\pm$0.9590	0.9203	0.0241	0.0262
Wind Turbine	-6.1596 -0.7252	0 0	4.4672	3.4424	0.7706

Table 4.3 depicts following observations:

- Closed loop poles give information about stability of the power system. The power system is stable for all type of generators since real parts of the poles are negatives.

However, their distances from origin (i.e. their absolute values) provide relative stabilities. It can be observed that poles are much closer to origin for hydro and nuclear generators. This means that they are closer to instability as compared to wind turbine, fossil and cross-compound fossil steam generators. Wind turbines are most stable since the poles are farthest from origin. Furthermore, wind turbine poles have no imaginary component inferring and therefore there is no oscillatory component in the output response from wind turbine.

- Attenuation $\zeta\Omega_n$ and damping ratio ζ of hydro and nuclear steam generators are much smaller as compared to wind turbine, fossil and cross-compound steam generators. This affects the damping of the frequency response. This fact matches the response illustrated in Figure 4-7 which depicts that damping is very poor for hydro and nuclear generators. Damping is very high for wind turbine as can also be seen from the response in Figure 4-7. Generally, damping ratio for the controller is chosen between $0.4 - 0.7$ in order to limit peak overshoot [81].

Based on the values of pole-zero-gain for different types of generators, peak frequency f_{peak} and peak time t_p values have been computed. These values are compared with the simulated results (Figure 4-7) with generic governor and generic wind turbine models and given in Table 4.4.

Table 4.4: Comparison of peak frequency and peak time for analytical and generic model

Type of Generator	Peak Time				Peak Frequency			
	Calc. [s]	Obs. [s]	Error		Calc. [Hz]	Obs. [Hz]	Error	
			Abs. [s]	Rel. [%]			Abs. [Hz]	Rel. [%]
Fossil (820 MW)	2.059	2.08	0.020	0.971	50.819	50.821	0.002	0.005
Fossil (347 MW)	2.242	2.247	0.005	0.227	50.956	50.959	0.003	0.006
Hydro	3.794	3.79	0.004	0.111	53.144	53.155	0.011	0.021
Cross-Compound	1.370	1.377	0.007	0.487	50.586	50.585	0.002	0.003
Nuclear	1.981	1.987	0.006	0.287	51.033	51.0161	0.017	0.033
Wind	0.9062	0.907	8e-04	0.088	50.3	50.3084	0.0084	0.017

Table 4.4 depicts that error between calculated and observed values is less than 1%. Thus, the confidence on the derived results and inferences discussed above is high.

4.2.2 Constant Droop, Varying Inertia

Further studies are done by varying the inertia while keeping the droop constant. This kind of studies are important since in real systems droops are kept constant during operating periods, while inertia can vary with varying penetration of converter connected generations. In the following studies, it is considered that inertia constant H is decreased from 6 to 1.5 s while droop R is kept constant at 4%. Equivalent analytical model is estimated from generic model for different inertia constants. Average fitness values for fossil steam (820 MW) generator, hydro generator, cross-compound fossil steam generator, nuclear steam generator and wind turbine are 98.16%, 99.01%,

98.96%, 99.03% and 97.14% respectively. Based on pole-zero-gain values, closed loop poles are computed. Trajectories for closed loop pole values for decreasing inertia constants for different types of generators are shown in Figure 4-8. Arrows in the trajectories in Figure 4-8 signify the directions in which closed loop poles move with decreasing inertia constant. It implies that starting point of the trajectory represents closed loop pole for inertia constant = 6s while the ending point represents closed loop pole for inertia constant = 1.5s.

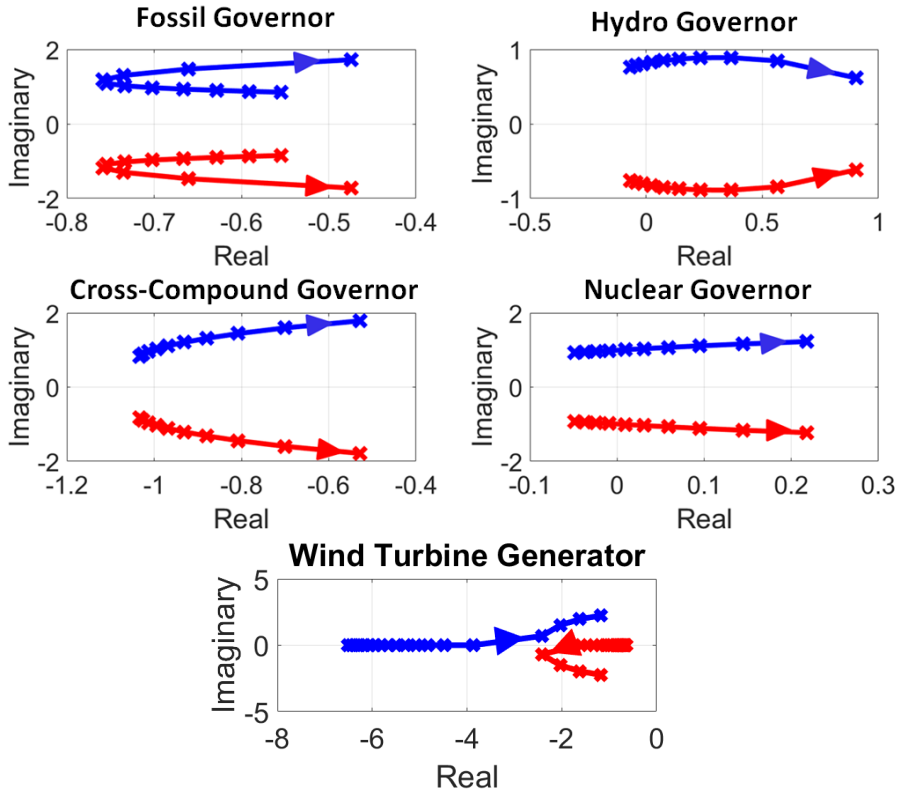

Figure 4-8: Impact of inertia on closed loop poles for different technologies of generators

Figure 4-8 shows that power system becomes unstable for hydro and nuclear generators since poles move to right-half plane. Fossil and cross-compound governor systems are quite stable since the real part of the poles is far from origin even with low inertia constant i.e. the ending point of the trajectory. Wind turbine also depicts interesting behaviour. For wind turbines, poles lie on real axis for high inertia. These real poles are quite further from imaginary axis implying fast output response. Since these poles have no imaginary component, there is no oscillation in the output response. However, as inertia is decreased, oscillations begin to appear in the output response as there are imaginary components in the complex poles for lower values of inertia. The values of these complex roots are quite far away from the real axis implying high oscillations in the transient response. This might make wind turbines incapable of providing FCP for

low values of inertia. However, in such situations it might be required to change the droop settings of wind turbines. This issue is investigated in the next section.

Notice that the pole trajectory plots provide information on power system stability, but not information on peak frequency and attenuation. As peak frequency and attenuation depend both on inertia constant and droop, they should be studied together and not independently. This is especially relevant when system inertia is low and faster responses from generators are required. This can be obtained by reducing the droop. Therefore, impacts on frequency with varying inertia and droop are studied in the following.

4.2.3 Varying Droop and Varying Inertia

In this study, system inertia constant H is varied from 1.5 s to 6 s while the droop R is varied from 2% to 6%. Impacts of droop and inertia constant on maximum and minimum frequency are studied for disturbance of -0.17 p.u. and 0.17 p.u. respectively. The success criteria for the FCP is considered as containment of frequency to less than 51 Hz for overfrequency and greater than 49 Hz for underfrequency events.

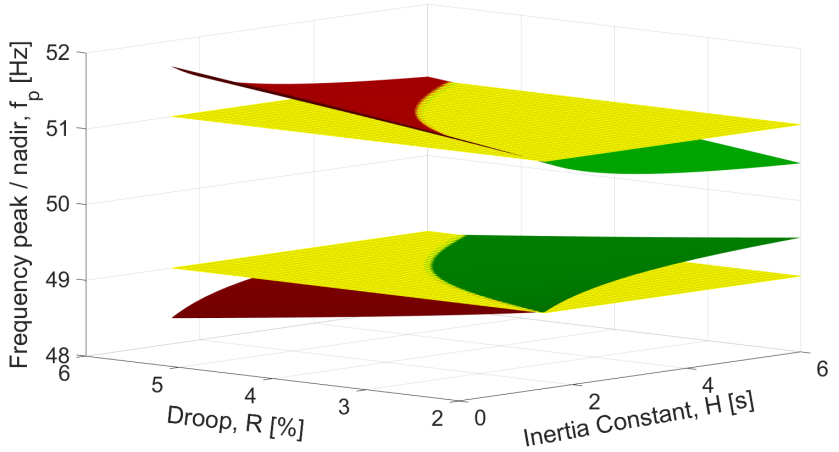

Figure 4-9: Impacts of droop and inertia constant on maximum/minimum frequency for fossil steam generator (820 MW)

The focus in the following is on 3 technologies of generations - fossil steam generator, cross-compound steam generator and wind turbine, while hydro and nuclear generator are not considered because they are not suitable for FCP. Impacts of droop and inertia constant on maximum/minimum frequency (based on first peak) for fossil steam generator (820 MW) is shown in Figure 4-9. The yellow planes in Figure 4-9 are the planes of 51 Hz and 49 Hz. Therefore, FCP is successful when the peak frequency (or nadir) is between these yellow planes. These points are marked with green color while the points outside these planes are marked in red color in Figure 4-9. Figure 4-9 shows that when inertia of the system is high (i.e. H=6s), droop of around 5% is enough for successful FCP. Decreasing inertia need to be handled with decreasing droop. However, when the

inertia is too low (i.e., H<2s) decreasing droop may not be enough to prevent frequency going outside the range of 49-51 Hz.

Similar studies are performed for for cross-compound steam generator and the result is shown in Figure 4-10. Figure 4-10 shows that for droop of 4% or lower, frequency always stays within 49-51 Hz for the studied disturbance of $\pm 0.17 p.u.$

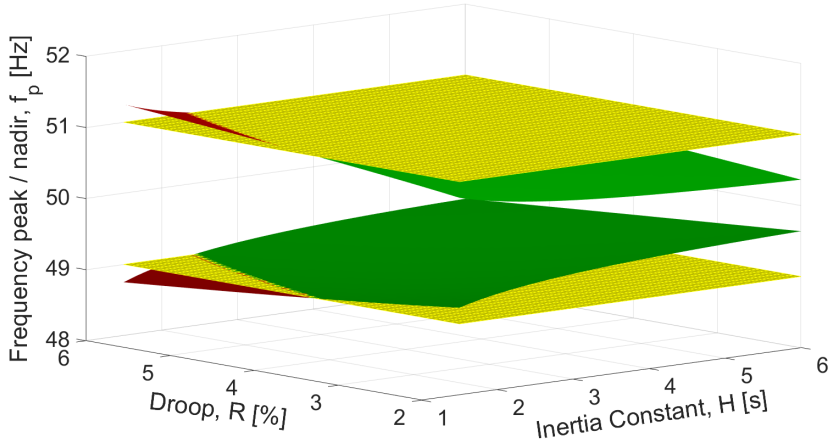

Figure 4-10: Impacts of droop and inertia constant on maximum/minimum frequency with cross-compound fossil steam generator

Figure 4-11 shows the impact of droop and inertia for wind turbine. It can be seen from Figure 4-11 that frequency always remains within 49-51 Hz.

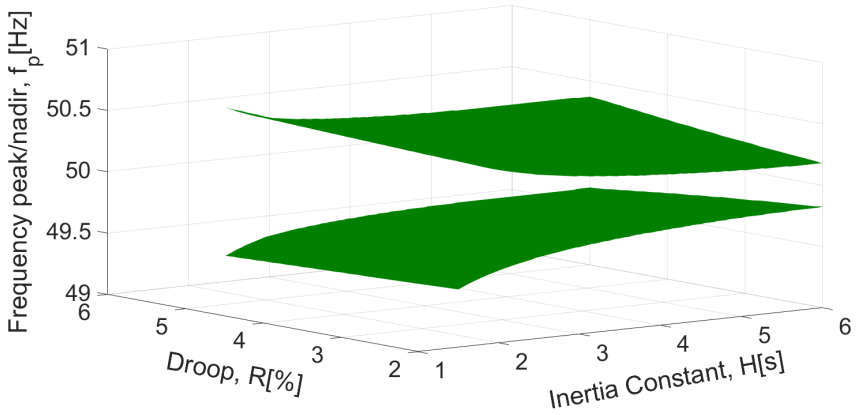

Figure 4-11: Impacts of droop and inertia constant on maximum/minimum frequency with wind turbine

It should be noted that in these studies only the first peak is considered. However, if the damping is inadequate then attenuation is low resulting in oscillation in frequency.

Attenuation can even be negative. In such case, the frequency increases in subsequent swings resulting in frequency instability.

In order to study the attenuation, impacts of droop and inertia constant on attenuation for cross-compound (yellow surface) and fossil (blue surface) steam generators are studied as shown in Figure 4-12. Figure 4-12 shows that attenuations of cross-compound generator are higher than fossil steam generator for higher droop and higher inertia. While for lower droop and lower inertia attenuations of cross-compound generator are lower than fossil steam generator. It can be seen that attenuation for cross-compound even can be negative when droop and inertia are lower than 3% and 2s respectively as denoted by gray region in Figure 4-12.

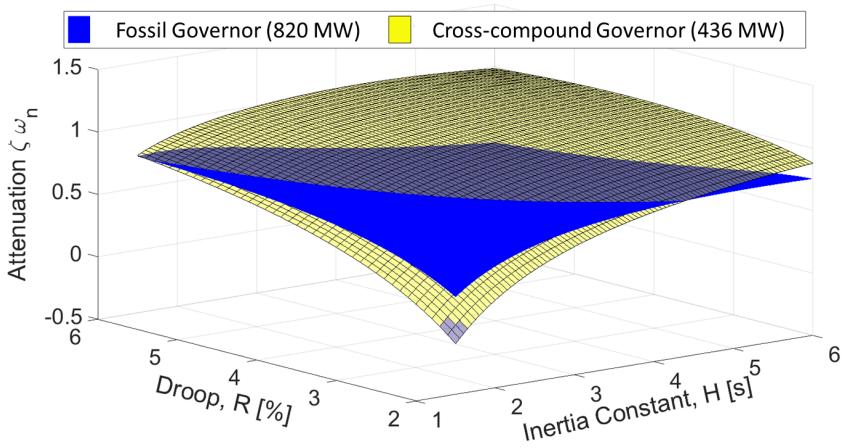

Figure 4-12: Impacts of droop and inertia constant on attenuation with cross-compound and fossil (820 MW) steam generators

The poor attenuation in the gray region is further exemplified in Figure 4-13, where the frequency response with cross-compound and fossil (820 MW) steam generators for R=2% and H=1.5s is depicted. Attenuation for fossil steam generator and cross-compound generator are computed as 0.28 and -0.09 respectively. Notice that, since attenuation for fossil steam generator is very small and positive there are large frequency excursions. Figure 4-13 also shows that system becomes unstable with cross-compound generator since attenuation is negative.

Figure 4-14 shows impacts of droop and inertia constant on attenuation for wind turbine. Notice that lower the droop and lower the inertia, attenuation is lower. Attenuation even becomes negative (black region) for very low value of inertia (H<3s) and low droop (R<4%). As illustrated in Figure 4-11, for wind turbine first peak is contained within 49-51 Hz. This means that attenuation becomes limiting criteria for deciding droop for different value of inertia for wind turbines.

From the previous results, it can be understood that peak frequency and attenuation both play crucial role in deciding droop values for different inertia constants. Therefore, feasibility of reducing droop with decreasing inertia constant is defined as limiting the first

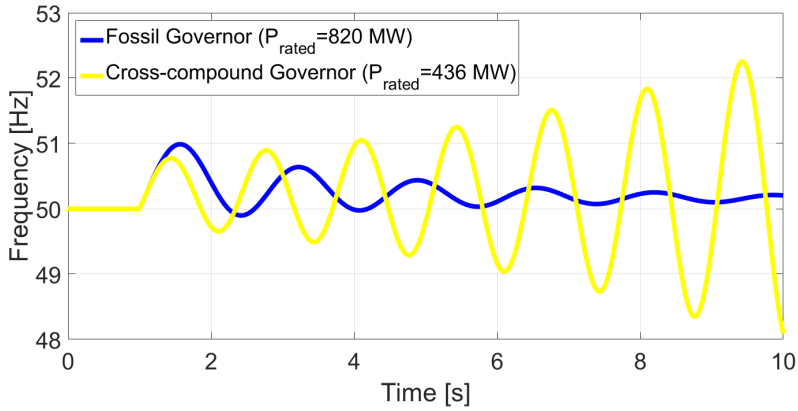

Figure 4-13: Frequency response with cross-compound and fossil (820 MW) steam generator for R=2% and H=1.5s

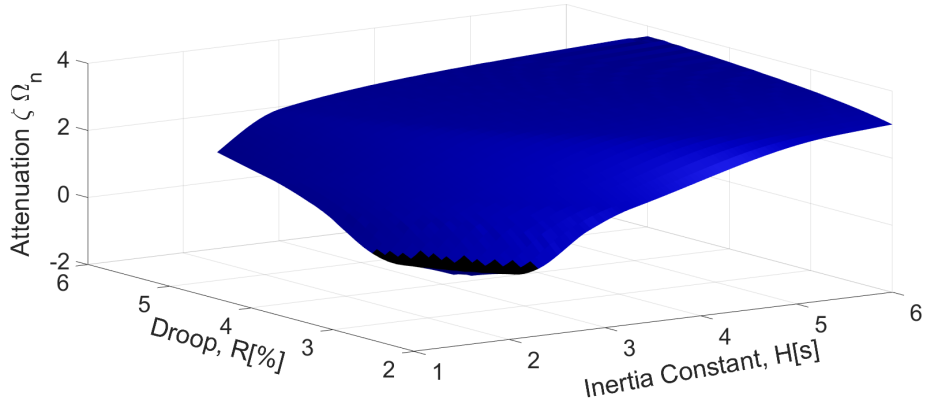

Figure 4-14: Impacts of droop and inertia constant on attenuation with wind turbine

peak frequency f_{peak} within 49-51 Hz as well as limiting the damping ratio ζ higher than 0.4. Figure 4-15 shows the feasibility of different droops for different inertia for fossil, cross-compound steam generator and wind turbine. This study is very important because it gives counter-intuitive result that for lower inertia values the droop should be higher in order to prevent oscillatory instability. Further, it can be observed that if droop is fixed at 4%, wind turbine can allow for operation with lower inertia than the other generators. Operating at 4% droop, minimum inertia constant possible for fossil steam generator is 2.75s, while for cross-compound steam generator it is 3.5s. Wind turbine allows to operate with inertia constant down to 2.35s for 4% droop. This shows that wind turbine should be attractive choice for providing FCP in future system with low inertia.

(a) Fossil Steam Generator

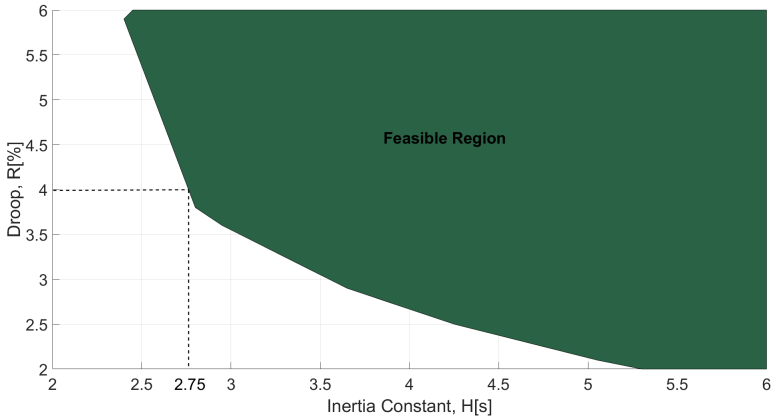

(b) Cross-Compound Fossil Steam Generator

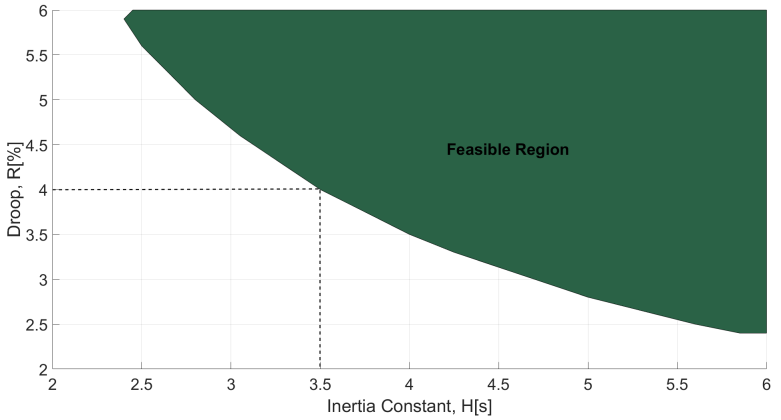

(c) Wind Turbine

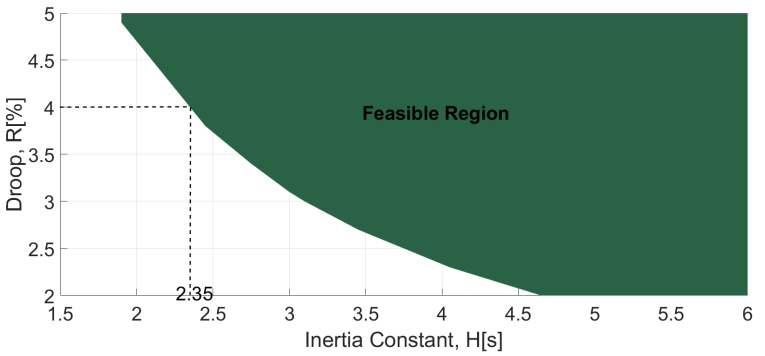

Figure 4-15: Feasibility of different droop for different inertia for fossil, cross-compound steam generator and wind turbine

4.3 Summary

The studies presented in this chapter have shown that providing FCP can become challenging in low inertia system for large disturbances. The conclusions from the chapter can be listed as following:

- Availability of adequate volume of FCR is necessary but not sufficient condition for frequency stability.
- The proposed mathematical analytical approach for FCP shows that the droop, inertia and technology providing FCP are all important in deciding the frequency response following a large disturbance in order to contain frequency. It has been observed that
  - Time to reach peak response is independent of the size of the disturbance.
  - Frequency oscillates sinusoidally with an exponential decay following a large disturbance. The exponential decay depends on attenuation and damping ratio.
  - Attenuation and damping ratio are independent of size of disturbance and dependent on inertia constant and droop.
- Different technologies have different capabilities for providing FCP as follows:
  - Hydro and nuclear generators are unsuitable for providing FCP in their inherent forms. They are too slow to provide fast response specially in low inertia scenarios.
  - Both peak frequency/frequency nadir and attenuation play crucial role for decision on droop settings for different inertia values.
  - For low inertia systems, droop should be high in order to prevent oscillatory instability.
  - Wind turbine is capable of providing better response in terms of FCP than conventional generators.

In the next chapter the focus is on investigating the capability of wind turbine to provide support in combination with other conventional generation units for overfrequency situations. Similar studies for underfrequency on a Danish (DK2) equivalent system have also been performed. The results are not included in this thesis as they are represented in details in [82].

Chapter 5

Wind Power Support during Overfrequency Emergency

This chapter is concerned with protection and control settings of converter connected wind turbines in order to support the grid during overfrequency emergency situations. Overfrequency event on North-Eastern area of UCTE at 4^{th} November, 2006 [1] is used as base study case in this chapter. Importance of correct protection settings for this simulated system is investigated first and then the design and recommendations for frequency control settings of WTs are proposed. Overfrequency responses from WTs depend on power activation delays, ramping rate capabilities and droop settings. These settings are recommended in this chapter for WTs for different degrees of wind power penetration. The success of frequency control from WTs with recommended settings are validated at the end using large scale simulated Pan-European EHV model [83].

During overfrequency situations conventional generations decrease their power outputs based on their governor characteristics as described in Chapter 4. However, in high wind power generation scenarios, conventional generators may be operated closer to their minimum power set-points and therefore have limited ramping down capabilities. Beside this aspect some of conventional generators might be de-commissioned or be out of operation. In such situations the inertia of the system can even get drastically low and this can be a challenge for the system following a large disturbance when the rate of change of frequency (RoCoF) is high, resulting in high peak frequency during overfrequency events. This in turn can trigger overfrequency protection systems of the generators resulting in frequency instability as more and more generations trip out. This phenomenon can be critical especially in island power systems. However, these situations can also arise in interconnected systems, as it was the case experienced in 4^{th} November, 2006 when UCTE system was split into 3 areas with North-Eastern area experiencing overfrequency [1]. This real situation happened in the North-Eastern area of UCTE formed during the disturbance of 4^{th} November, 2006 is investigated in order

to study the impacts and opportunities of WTs during overfrequency.

5.1 Power System Model

North-Eastern area of UCTE power system disturbance on 4^{th} November, 2006 has been implemented in order to simulate overfrequency event.

5.1.1 Description of the UCTE Disturbance at 4^{th} November, 2006

According to [1], UCTE system was split into 3 areas during the disturbance occurred at $22:10$ on 4^{th} November, 2006.

Pre-disturbance Condition
Generation in the whole UCTE system on the day at $22:09$ is estimated at around 274 100 MW including approximately 15 000 MW of wind generation (mostly in Northern Europe and Spain). Figure 5-1 shows the estimated generation (G), the sum of power flows on the lines which tripped during the incident (blue arrows) and exchanges over HVDC cables (orange arrows) in the three "virtual" areas distributed after the split of the system.

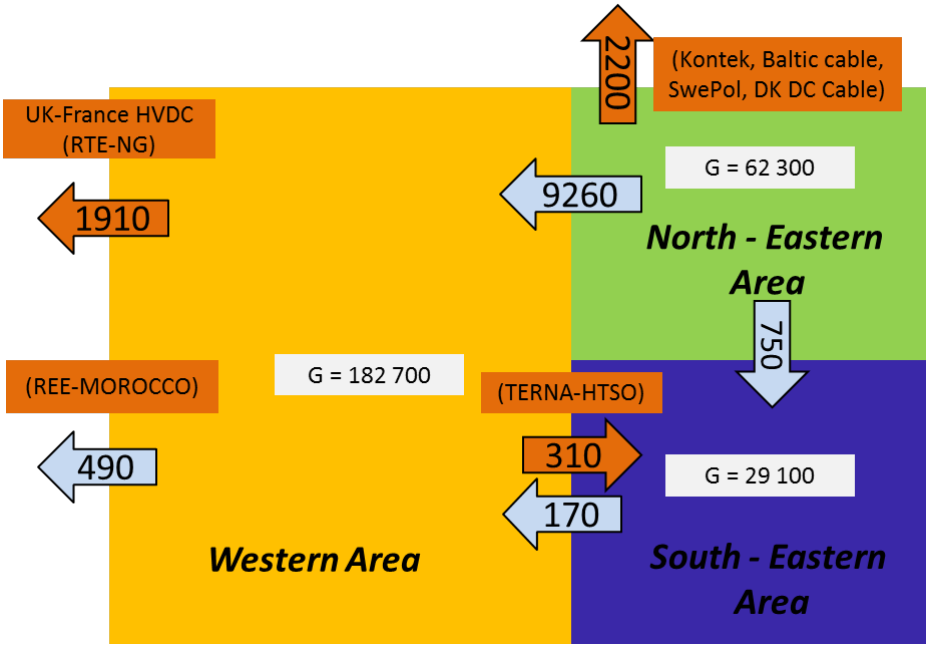

Figure 5-1: Generation and power flows between the three areas just before splitting

- Western area: 182700 MW including 6500 MW of wind generation
- North-Eastern area: 62300 MW including 8600 MW of wind generation
- South-Eastern area: 29100 MW

Sequence of events
A set of domino reactions has been created which triggered the split of UCTE network into 3 areas. The summary of sequence of events are as following:

- At 21:38, E.ON Netz (DE) manually switched off first circuit of the 380 kV line Conneforde-Diele, so called Conneforde-Diele red.
- At 21:39 E.ON Netz switched off second circuit of the 380 kV line Conneforde-Diele, so called Conneforde-Diele white.
- The manual switching of the Conneforde-Diele line at 21:38 resulted in a significant increase (over 600 MW) in the power flow on another line called Landesbergen-Wehrendorf line, and thus its loading exceeded 1 200 MW close to the secure limit for RWE TSO.

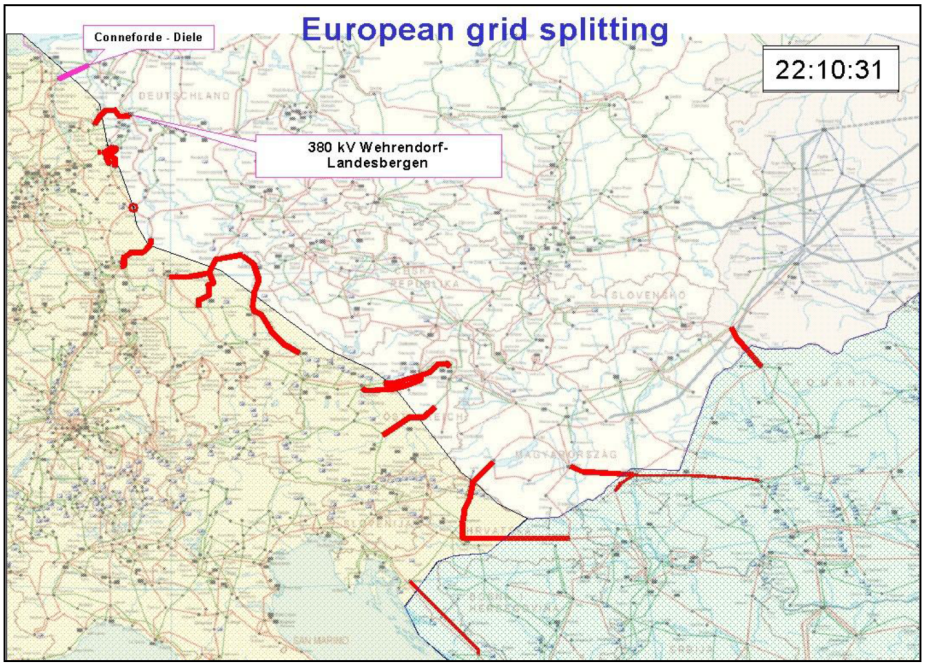

Figure 5-2: Cascading trippings of overhead lines to split UCTE into three areas [6]

- E.ON Netz expected that coupling of the busbars in the substation of Landesbergen would end in a reduction of the current by about 80 A. This maneuver was done at 22:10 without any further coordination with RWE TSO due to necessary rush. The

ex-post simulations made in the course of investigations showed that this action led to a result which was contrary to what dispatchers expected; the current on the line increased by 67 A (instead of decreasing) and the line was automatically tripped by the distance relays in the Wehrendorf substation (RWE TSO) due to overloading. This tripping led to cascading line trippings throughout the UCTE area. Figure 5-2 shows the cascading tripping of lines which caused the split in UCTE system.

More details of cascaded trippings can be found in Appendix 3 of Final report on system disturbance on 4 November 2006 [1].

Schematic map of UCTE area after split into three areas is shown in Figure 5-3 and frequency recordings for 3 areas after the split is shown in Figure 5-4 [1].

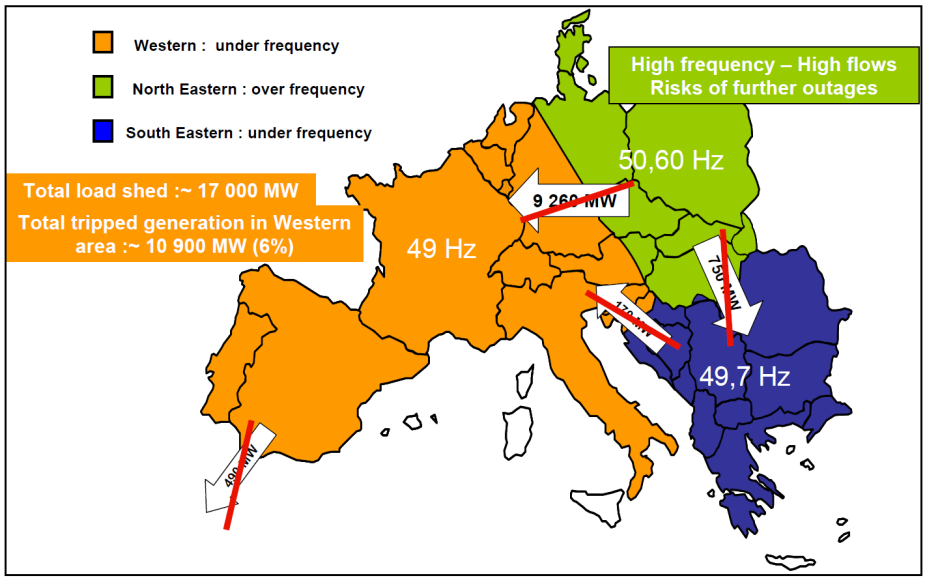

Figure 5-3: Schematic map of UCTE area after split into three areas [6]

Following cascading, the UCTE system was split into 3 island areas. The power balance in each area was no longer ensured at the moment of system splitting. About 9500 MW power flow from the East area to the Western area was cut. Therefore the frequency sharply dropped to about 49 Hz in the Western area due to the sudden lack of power. On the contrary, the North East area faced a surplus of generating power of the same magnitude which induced a high overfrequency. Just after the splitting, the South East area was also missing an amount of power of around 800 MW which induced a slight underfrequency to about 49.7 Hz.

The work presented in this chapter is concerned with the overfrequency situation experienced in North-Eastern part of the UCTE system. After the split this region had a surplus of more than 10 GW (i.e. around 17% of the total generation in this area). This system had wind power generation of more than 6 GW (10% of total generation) which started disconnecting at around 51 Hz according to [1]. The maximum frequency ex-

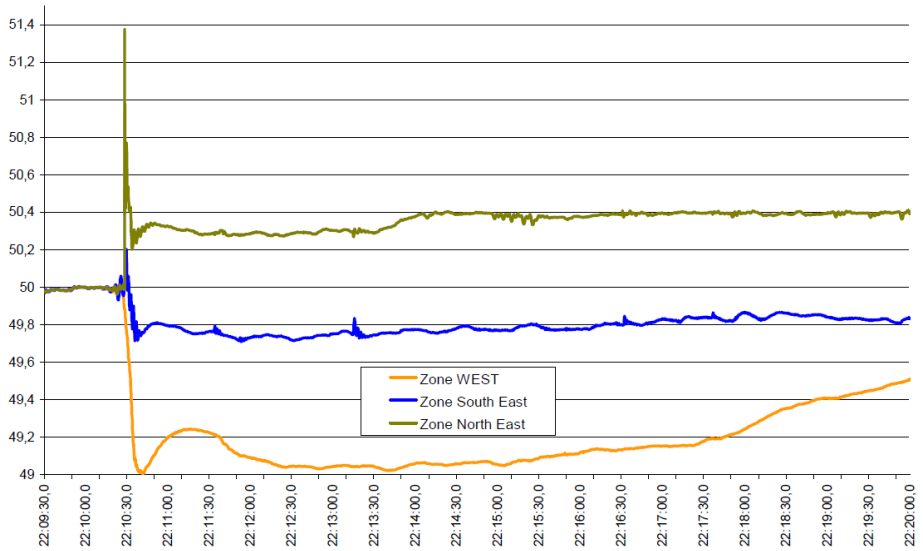

Figure 5-4: Frequency recordings after the split [1]

perienced by the system went as high as 51.4 Hz. However, frequency was controlled mainly by the primary control of the generators and brought down to 50.3 Hz. At this point, wind power plants started reconnecting resulting in further increase in frequency. This situation was particularly vulnerable, since many of the conventional generators were operating at their minimum at this point and were unable to provide further support. Through co-ordinated manual control from all the TSOs (complex controls, generator rescheduling etc.), frequency was stabilized and it was possible to reconnect all the sub-systems further.

In this work, overfrequency situation experienced in North-Eastern part of the UCTE system is simulated as a single bus model. The simulated result from the single bus model is compared with the data from UCTE report.

5.1.2 Single Bus model

Figure 5-5 depicts the single bus model of the simulated power system. Description of different components of this model are as following:

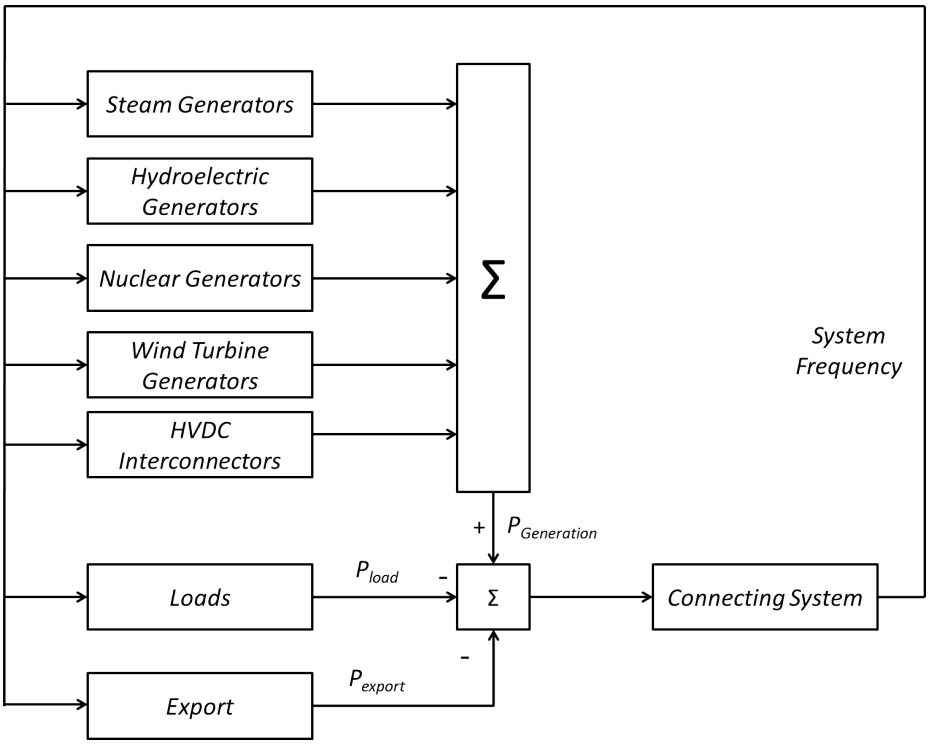

Figure 5-5: Single bus power system model

Generation

Table 5.1: Generation Scenario

Type	Capacity [MW]	Generation [MW]	Inertia Constant [MWs/MVA]
Steam	46000	39100	5
Hydro	6000	6000	3
Nuclear	10000	10000	4
Wind	6900	6900	0

Load

52000 MW

Export

10000 MW

Contingency

Simulation of system split by disconnection of Export of 10000 MW

Protection

Disconnection of Loads

Load shedding settings are given in Table 5.2.

Table 5.2: Load Shedding Settings

Frequency[Hz]	Amount of load Shed [%]
49	5
48.8	10
48.6	10
48.4	10
48.2	10
48	5

Disconnection of Generators

Disconnection of 2000 MW of steam generation at 50.78 Hz. Rest of the conventional generators are designed to disconnect at 51.5 Hz.
Several disconnections and reconnections of WTs have been simulated in this model resulting in net disconnection of 2250 MW of wind power generation.

System Components

Steam governor model, hydro governor model, nuclear governor model and IEC type 4 WT model are simulated in this work and are described in Appendices B, C, D and E respectively.

Emergency control from HVDC interconnections

Activation Frequency: 50.6 Hz
Deactivation Frequency: 50 Hz
Available Capacity: 200 MW
Ramp Rate: 1 p.u./s
Activation Delay: 100 ms

Simulated Result of the Event

Figure 5-6 shows the comparison between simulated event result and the data from UCTE Report [1].

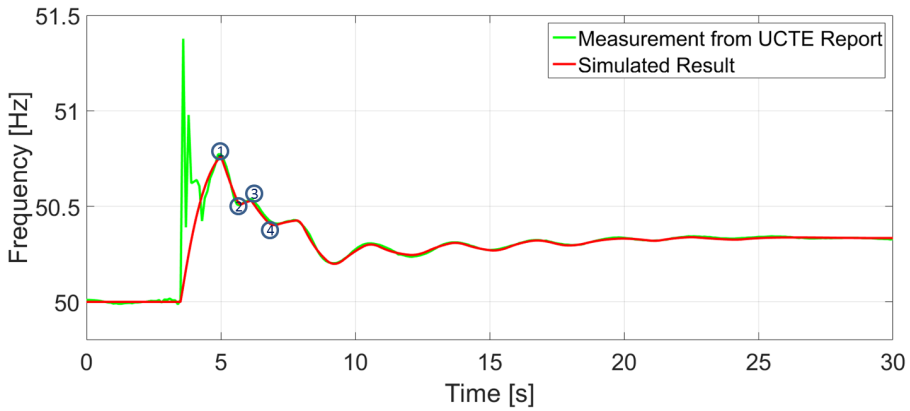

Figure 5-6: The measured and simulated frequency response during overfrequency situation experienced in North-Eastern part of the UCTE

Notice that frequency increases upto 50.78 Hz neglecting initial transients, which can be due to measurement errors. After 50.78 Hz there are several generation disconnection (①,③,...) and reconnections (②,④,...) happening as characterised by sharp changes in frequency as seen in Figure 5-6. It is worth noticing that simulated result closely matches with that of report [1]. This gives confidence on the single bus model which is

used in this work to design the recommendations for frequency control settings of WTs.

5.1.3 Impacts of Increasing Wind Power Penetration

Wind power penetration of 10% in the simulations presented in section 5.1.1 is considered as the base case. However, if the wind power penetration is increased without proper control and protection settings for WTs, the system might experience frequency instability. The requirement of proper control and protection settings for WTs for different degrees of wind power penetration is investigated in this section.

Remark that different wind power penetration definitions can exist. Wind power penetration of the system in terms of capacity is defined in this work as Equation 5.1

$$Wind\ Power\ Penetration = \frac{Wind\ Power\ Generation\ Capacity}{Total\ Power\ Generation\ Capacity} \tag{5.1}$$

Different wind power penetrations are considered as indicated in Table 5.3. For each wind power penetration, the capacity and the set points of each generation technology are indicated along with the inertia of the system.

In order to increase the wind power penetration while keeping the loading of the system constant, other generations can be reduced until their lowest set-points are reached. However, facilitation of further increase in wind power penetration requires disconnection of the conventional generations. It can be seen from Table 5.3 that until 40% wind power penetration capacity of conventional generators remain unchanged while their set points are reduced. However, when wind power penetration get higher than 40%, capacities of conventional generations need to be reduced thereby reducing the inertia of the system. Inertia constant for different degrees of wind power penetration is shown in Figure 5-7.

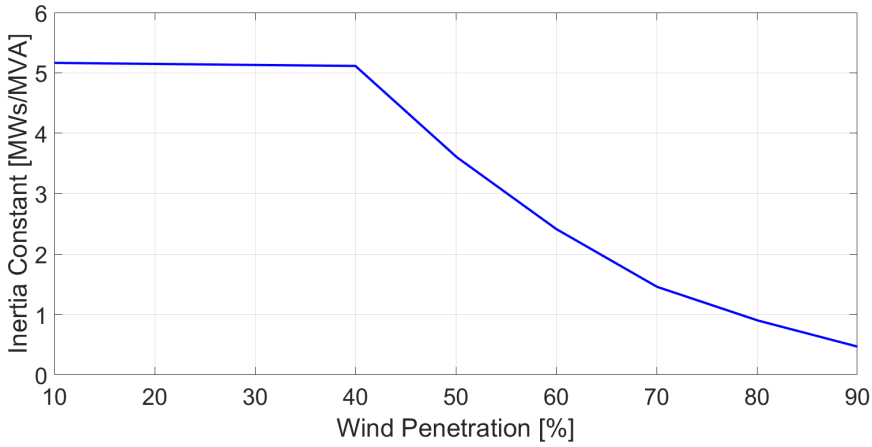

Figure 5-7: Wind Power Penetration vs. Inertia Constant

Table 5.3: Generation Scenarios for different degrees of wind power penetration

Wind Power Penetration[%]	Type	Capacity [MW]	Set point [MW]	Inertia Constant [MWs/MVA]
10	Steam	46000	39100	5.17
	Hydro	6000	6000	
	Nuclear	10000	10000	
	Wind	6900	6900	
20	Steam	46000	30500	5.15
	Hydro	6000	6000	
	Nuclear	10000	10000	
	Wind	15500	15500	
30	Steam	46000	19430	5.14
	Hydro	6000	6000	
	Nuclear	10000	10000	
	Wind	26570	26570	
40	Steam	46000	10800	5.12
	Hydro	6000	1870	
	Nuclear	10000	8000	
	Wind	41330	41330	
50	Steam	29200	7440	3.61
	Hydro	6000	1200	
	Nuclear	10000	8000	
	Wind	45360	45360	
60	Steam	16000	4800	2.41
	Hydro	6000	1200	
	Nuclear	10000	8000	
	Wind	48000	48000	
70	Steam	5420	2690	1.46
	Hydro	6000	1200	
	Nuclear	10000	8000	
	Wind	50110	50110	
80	Steam	3650	3000	0.9
	Hydro	2000	1200	
	Nuclear	7000	7000	
	Wind	50800	50800	
90	Steam	3000	3000	0.47
	Hydro	1200	1200	
	Nuclear	2000	2000	
	Wind	55800	55800	

Notice that when penetration becomes higher than 40%, inertia constant of the system keeps on decreasing and becomes lower than 1.5s when penetration is higher than 70%.

Retaining same protection settings as on 4^{th} November, 2006:
A set of simulations are carried out for the system with same protection settings as on 4^{th} November, 2006 while increasing the degrees of wind power penetration. Remark that several uncontrolled and unplanned disconnections and reconnections of WTs were

observed in the 4^{th} November, 2006 overfrequency scenario. Same percentage of WTs (with respect to total WT capacity) are designed to be disconnected and reconnected at various frequencies similar to 4^{th} November, 2006 case (base case) in these studies.

Figure 5-8 depicts frequency response for different degrees of wind power penetration with the same simulated event as in the base case.

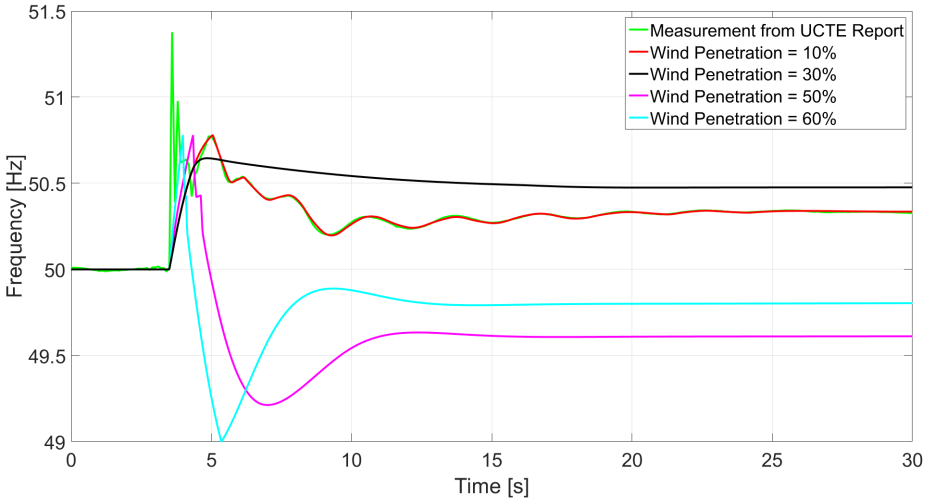

Figure 5-8: Frequency response for different wind power penetration without modification of protection settings

Figure 5-8 shows that unplanned and uncontrolled disconnection of wind generations is not recommendable. It is observed that when wind power penetrations are 10% and 30%, disconnection of WTs are capable of mitigating overfrequency. However, when wind power penetration is 50%, the system inertia has decreased to 3.61s as compared to 5.17s for 10% wind power penetration. Sudden disconnection of large volume of WTs in low inertia system, reduces the frequency to 49.26 Hz. Although the system is stabilised at 49.63 Hz but the frequency response is poor and verge of instability. When wind power penetration is 60%, system inertia is as low as 2.41s. Sudden disconnection of large volume of WTs let the frequency reach down to 49 Hz thereby starting load shedding and highlighting the ineffectiveness of protection settings. **Therefore, it becomes clear that protection settings need to be modified in order to handle high penetration of wind generation.**

Protection settings modified according to present grid code requirements:
In the present network code requirements, all generators are required to be remain connected for overfrequency up to 51.5 Hz [32]. A set of simulations are now carried out where the protection settings of WTs are modified requiring them to remain connected up to 51.5 Hz. Frequency responses while increasing wind power penetration levels with the modified protection settings are shown in Figure 5-9. Figure 5-9 depicts that with increasing wind power penetration the peak frequency keeps on increasing.

When the wind power penetration becomes 60%, the peak frequency reaches 51.5 Hz thereby disconnecting all the generations rendering the system unstable. **This implies that modification of protection settings alone can't prevent frequency instability specially when wind power penetration is high.** Another interesting point to note is that when wind power penetrations are 10% and 30%, initial RoCoF is similar while for increasing wind power penetration of 50% and 60% RoCoF is higher. This is because of the decrease in inertia with increasing wind power penetration as already indicated.

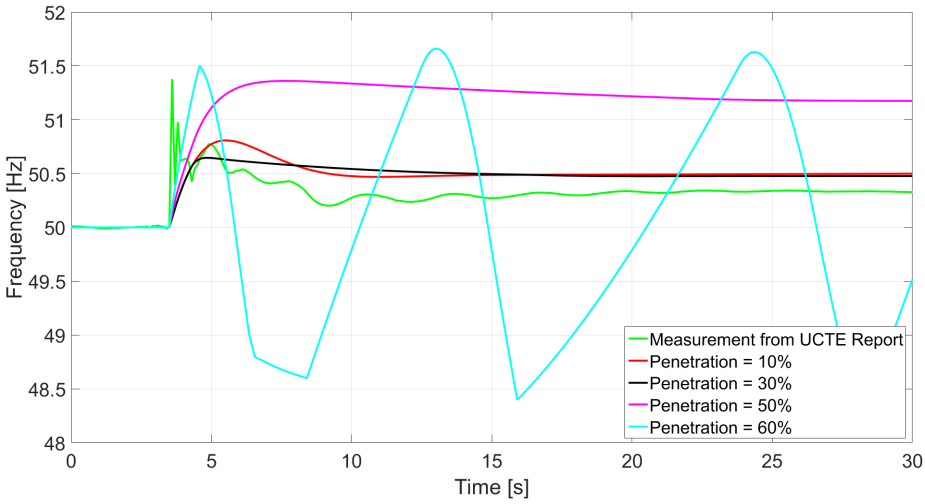

Figure 5-9: Frequency for different wind power penetration with modified protection settings

Since modification of protection settings is not sufficient to prevent frequency instability, overfrequency control from WTs becomes an obvious option especially when the wind power penetration is high.

In the context of overfrequency frequency containment control process, network code on requirements of grid connection of generators [32] defines 'limited frequency sensitive mode - overfrequency' (denoted by 'LFSM-O'). 'LFSM-O' means that a power generating module should reduce its active power output generation in response to a change in system frequency above a certain value.

The following rules with regard to the LFSM-O are defined in the network code [32]:

1. Power generating module shall be capable of activating frequency response above a frequency threshold with a droop settings specified by the relevant TSO.
2. Instead of the above mentioned capability, the relevant TSO may choose to allow within its control area automatic disconnection and reconnection of power generating modules of Type A at randomised frequencies, ideally uniformly distributed.
3. Frequency threshold shall be between 50.2 Hz and 50.5 Hz.
4. Droop settings shall be between 2% and 12%.

5. Power generating module shall be capable of activating frequency response with an initial delay less than 2 seconds.

6. Relevant TSO may require that upon reaching minimum regulating level, power generating module should either be capable of continuing operation at minimum level or decreasing active power output further.

7. Power generating module shall operate stably during LFSM-O operation. When LFSM-O is active, the LFSM-O setpoint will prevail over any other active power setpoints.

While inspecting these rules, it should be emphasised that the results presented in this section already show that automatic disconnection and reconnection of WT generators fail to stabilise the frequency when the wind power penetration is as high as 60%. Therefore, the next focus of this work is to study the capability of WT generators and recommend the overfrequency control settings of WT generators based on these rules.

5.2 Frequency Control Capabilities of Wind Turbine

Overfrequency responses from converter connected WT generators mainly depend on ramping rate, droop settings and delay. Frequency controller for WT is developed as shown in Figure 5-10 where,

- $\Delta\omega$: change in frequency in p.u. with respect to reference frequency (50 Hz)
- $T_{delayMeas}$: frequency measurement delay
- T_{delayP}: power activation delay
- $droop_{WT}$: droop settings in %
- $RampRate$: ramp rate in p.u./s
- $Pmax_{WT}$: maximum power output from WT in p.u.
- $Pmin_{WT}$: minimum power output from WT in p.u.

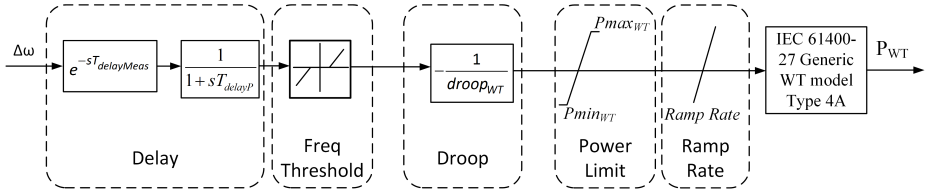

Figure 5-10: Frequency control from WT

Total delay is decomposed of 2 parts a) measurement delay $T_{delayMeas}$ and b) power activation delay T_{delayP}. In these studies, $T_{delayMeas}$ is assumed as 100 ms, while

T_{delayP} is varied from 100 ms to 1 s. Droop settings $droop_{WT}$ for WT is varied from 2% to 10%. $RampRate$ is varied between 0.1-0.5 p.u./s. $Pmax_{WT}$ is assumed as 1 p.u. $Pmin_{WT}$ is chosen as 0.1 p.u. based on the recommended value of Energinet's Technical Regulation 3.2.5 [84]. Frequency thresholds are chosen as 49.8 Hz and 50.2 Hz.

In order to study the frequency control capabilities of WT, a set of open loop studies are performed. Frequency illustrated Figure 5-6 is fed as input to the model depicted in Figure 5-10. In the following, the impacts on the frequency response of different parameter settings are analysed.

5.2.1 Impact of delay

In order to study the impact of different power activation delays, the droop and the maximum ramp rate limits are kept constant.

Figure 5-11 illustrates the active power of WTs for different activation delays. Two different ramp rates (0.1 p.u./s and 0,5 p.u./s) are considered while the droop of the WT is kept constant. It can be observed from Figure 5-11 that when ramp rate limit is 0.1

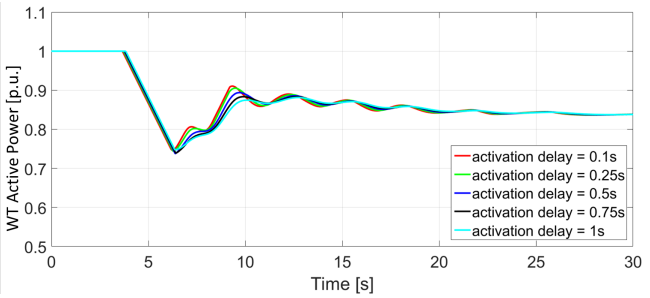

(a) ramp rate = 0.1 p.u./s, $droop_{WT}$=4%

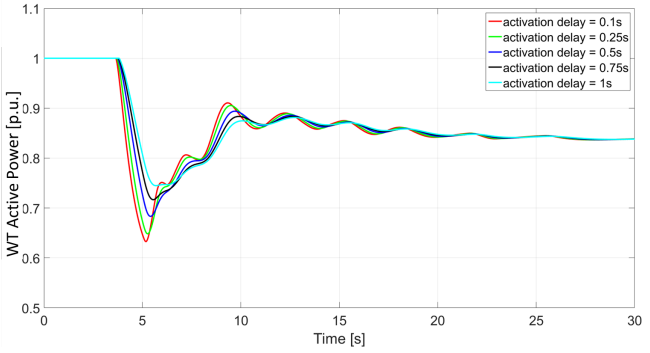

(b) ramp rate = 0.5 p.u./s, $droop_{WT}$=4%

Figure 5-11: Frequency response for different activation delays

p.u./s, the activation delay doesn't have large impact in frequency response. The reason

for this is when ramp rate in 0.1 p.u./s, the response is slower than when ramp rate is 0.5 p.u./s. As indicated in Figure 5-11b, when ramp rate is 0.5 p.u./s, there is large impact with respect to activation delay. For an activation delay of 0.1 s, active power from WT reduces from 1 p.u. to 0.63 p.u., while for an activation delay of 1 s, the active power reduction is much less, decreasing from 1 p.u. to 0.75 p.u. only. Therefore, it should be recommended to have minimum delay when ramping rate is as high as 0.5 p.u./s.

5.2.2 Impact of ramp rate

Figure 5-12 shows the active power from WT for different ramp rate limitations for constant values of droop and activation delays.

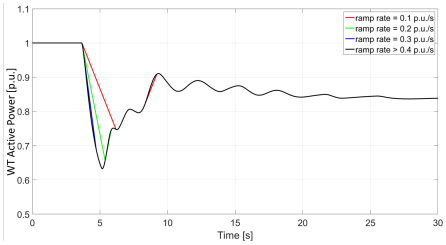

(a) activation delay = 0.1 s, $droop_{WT}$=4%

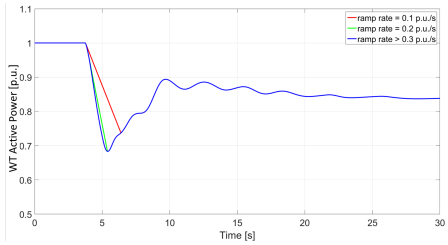

(b) activation delay = 0.5 s, $droop_{WT}$=4%

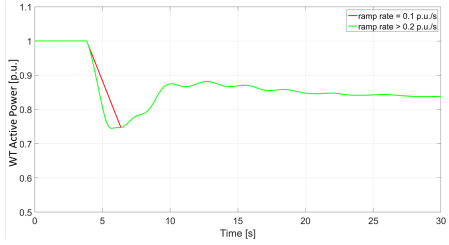

(c) activation delay = 1 s, $droop_{WT}$=4%

Figure 5-12: Frequency response for different ramp rate limitations

Studies are done for $droop_{WT}$ = 4% and activation delays = 0.1, 0.5 and 1 s respectively. It can be observed from Figure 5-12 that when activation delay is as low as 0.1 s, ramp rate should be higher than 0.4 p.u./s in order to have maximum power output support from WT generator. When activation delay is 0.5 s, ramp rate should be higher than 0.3 p.u./s. When activation delay is as high as 1 s, ramp rate should be higher than 0.2 p.u./s in order to have most power output support from WT. It is clear from these results that WT response is dependent on ramp rate and activation delay simultaneously and should not be treated separately.

5.2.3 Impact of droop

Figure 5-13 shows WT output for different $droop_{WT}$ settings for two sets of ramp rate and delay. Input frequency is also plotted in Figure 5-13 in order to differentiate the WT response for different droop settings during peak frequency.

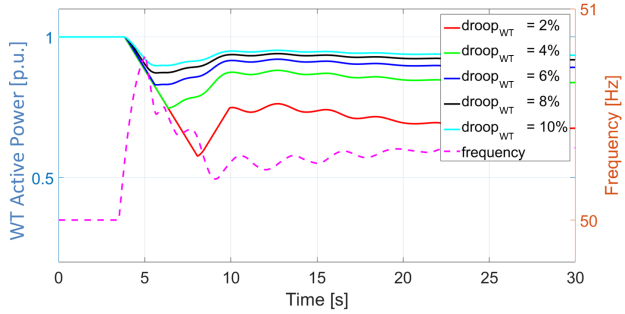

(a) ramp rate = 0.1 p.u./s, activation delay=1 s

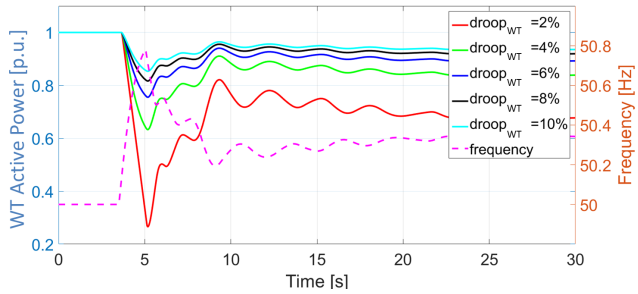

(b) ramp rate = 0.5 p.u./s, activation delay=0.1 s

Figure 5-13: Frequency response for different $droop_{WT}$

In first case, activation delay is large (1s) and ramp rate is low (0.1 p.u./s). WT responses in this case are slow. Consequently reduction in active powers when input frequency reaches peak value are low and doesn't depend on droop settings. $droop_{WT}$ for this case can be recommended as 10% since lower droop values are unable to help in reducing peak frequency. In second case, activation delay is small (0.1s) and ramp rate is high (0.5 p.u./s). The response in this case is fast. Consequently, lower the $droop_{WT}$ value, more the reduction in WT active power output. The recommended $droop_{WT}$ in this case is 2%. Therefore it is evident that $droop_{WT}$ settings are dependent on ramp rate and activation delay.

Similar investigations have been done for different sets of activation delays and ramp rates. The recommended $droop_{WT}$ settings for different activation delay and ramp rate limitation is shown in Table 5.4.

Table 5.4 depicts that ramp rate plays more important role than activation delay in deciding the droop settings. It is clear from Table 5.4 that ramp rate limitation should

Table 5.4: Recommended droop settings for different activation delays and ramp rates

activation delay [s]	ramp rate [p.u./s]	$droop_{WT}$ [%]
0.1	0.1	10
	0.2	4
	0.3	2
	0.4	2
	0.5	2
0.25	0.1	10
	0.2	4
	0.3	2
	0.4	2
	0.5	2
0.5	0.1	10
	0.2	4
	0.3	2
	0.4	2
	0.5	2
0.75	0.1	8
	0.2	4
	0.3	2
	0.4	2
	0.5	2
1	0.1	6
	0.2	4
	0.3	2
	0.4	2
	0.5	2

be at least 0.3 p.u./s or more in order to obtain maximum power output support from WTs. When ramp rate is 0.3 p.u./s or greater, recommended $droop_{WT}$ value is 2% irrespective of activation delay.

However, impact of inertia is not evident from these studies. The impact of inertia on the frequency response is investigated in the following section by increasing the wind power penetration level.

5.3 Recommendations for different degrees of wind power penetration

In order to study the impacts of different degrees of wind power penetration, the WT frequency control depicted in Figure 5-10 is incorporated in the single bus power system model. In these studies ramp rate is considered as 0.3 p.u./s as per the recommendation of previous section. Activation delay is assumed as 0.5 s.

Figure 5-14 depicts frequency response for 10% wind power penetration for different $droop_{WT}$ values. It is noticeable that for a low wind power penetration there is not a considerable improvement in frequency response from WT as compared to frequency output without any support from WT.

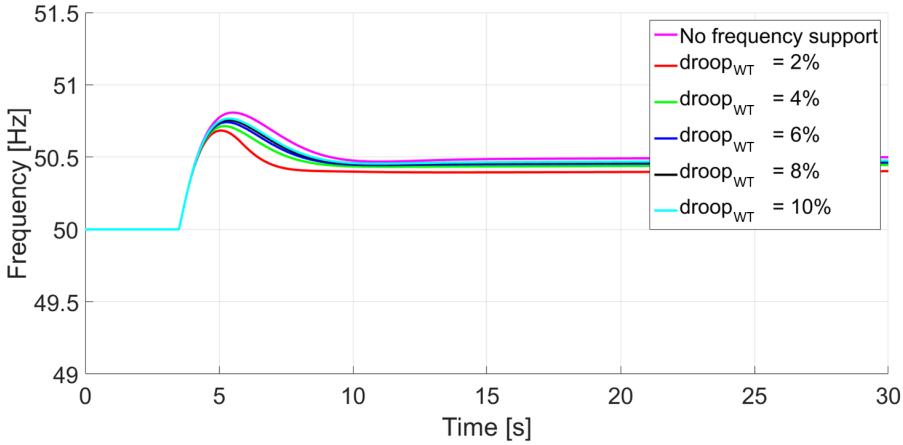

Figure 5-14: Frequency Response with 10% Wind Power Penetration

However, an increased wind power penetration of 40% has considerable impact, namely an improvement in the frequency response with frequency support from WT as shown in Figure 5-15. Notice that lower the $droop_{WT}$, better the frequency response is. Thus the recommended $droop_{WT}$ settings is 2%.

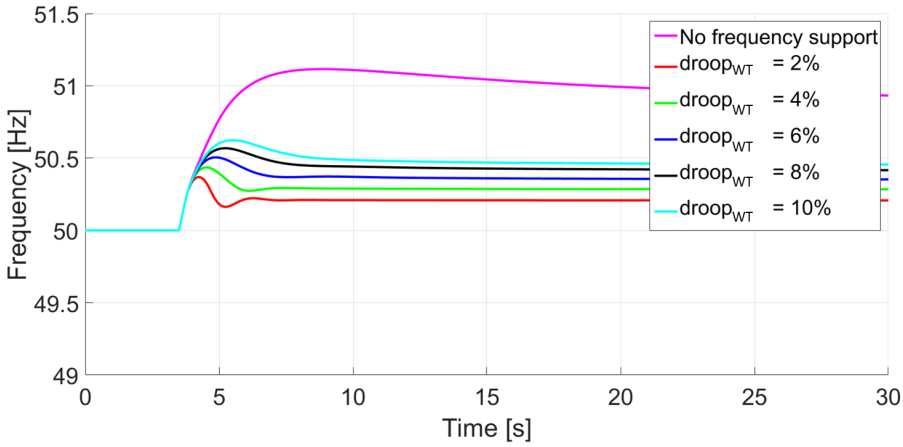

Figure 5-15: Frequency Response with 40% Wind Power Penetration

However, when wind power penetration is increased beyond 40%, inertia of the system starts decreasing drastically as already indicated in 5-7. Figure 5-16 depicts the frequency response with wind power penetration increased to 60%.

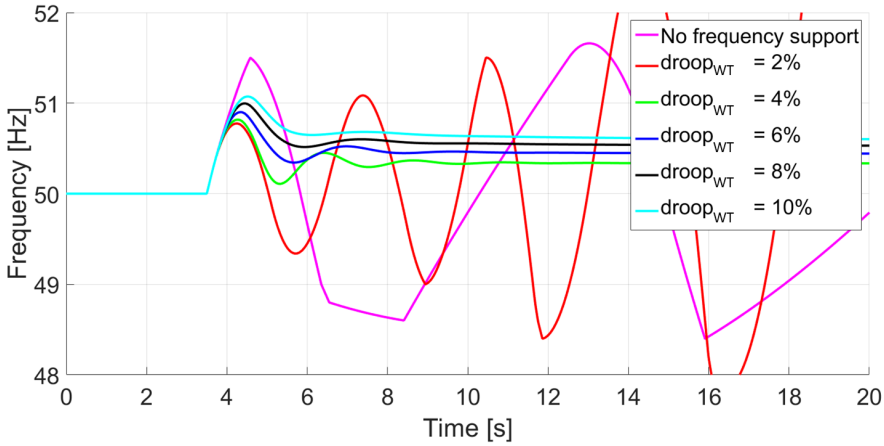

Figure 5-16: Frequency Response with 60% Wind Power Penetration

Remark that system becomes unstable when there is no frequency support from WTs and for low value of $droop_{WT}$. System becomes stable for frequency support from WT generator with droop settings 4-10%. The response is best when $droop_{WT}$ settings is 4%. The system becomes unstable with $droop_{WT} = 2\%$ because of reduced damping and attenuation for this $droop_{WT}$ and inertia values. This was mathematically analysed and depicted in Chapter 4. Therefore, the recommended droop settings is 4%.

Figure 5-17 indicates the frequency response for 80% wind power penetration. In this case the inertia of the system is so low that frequency support from WT generators with any $droop_{WT}$ settings is not sufficient enough to prevent frequency instability.

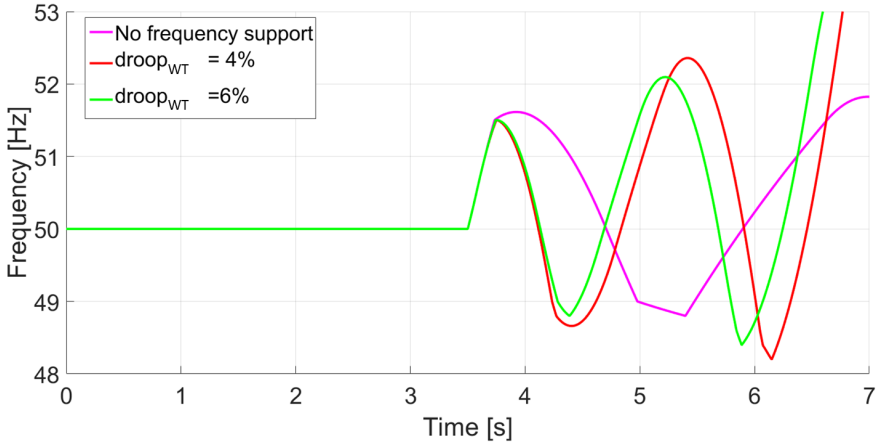

Figure 5-17: Frequency Response with 80% Wind Power Penetration

Virtual inertia support from WT is clearly needed when the system inertia is low and wind power penetration is high. Virtual inertia support from WTs is modelled in this PhD work as described in Zeni et. al. [57]. The virtual inertia support is incorporated

to the droop based frequency support model of WT generator is shown in Figure 5-18, where,

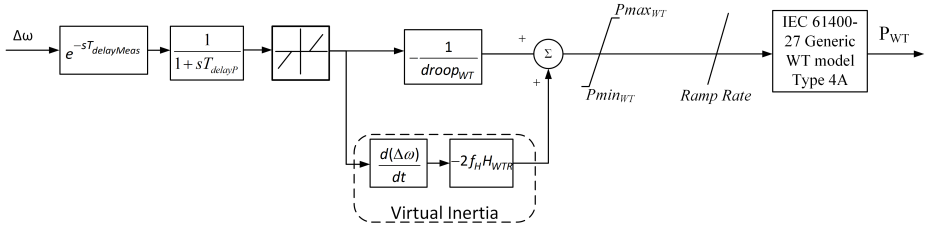

Figure 5-18: Virtual inertia support is incorporated in frequency control from WT generator

- f_H: virtual inertia gain
- H_{WTR}: wind turbine rotor inertia
- $\frac{d(\Delta\omega)}{dt}$: rate of change of frequency

In these studies, f_H is chosen as 1 and H_{WTR} is assumed as 4.225s.

Figure 5-19 illustrates the frequency response for a 80% wind power penetration for different droops and when WT is also equipped with a virtual inertia controller.

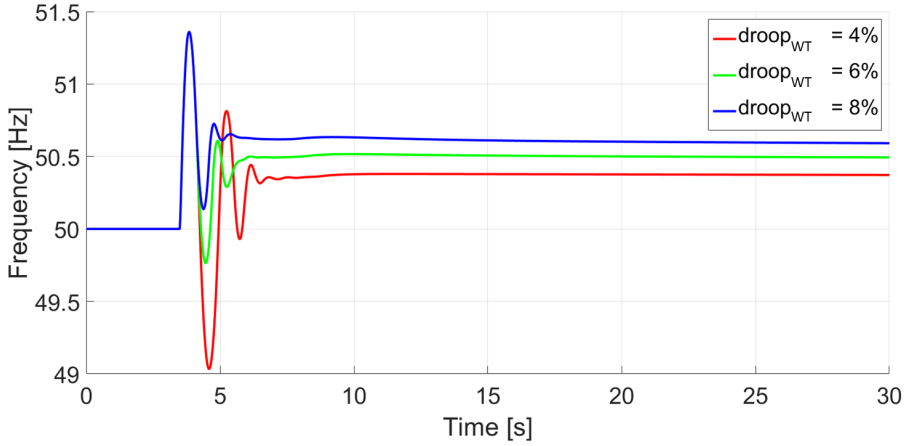

Figure 5-19: Frequency Response with 80% Wind Power Penetration considering Virtual Inertia

Notice that system becomes stabilised with 80% wind power penetration when virtual inertia support is obtained from WT. Figure 5-19 depicts that systems goes to the limit of instability with droop settings of 4% due to high frequency oscillation. Frequency

goes very close to 49 Hz where load shedding is designed to start. However, system is stabilised with droop settings of 6 and 8%. Since the steady state frequency is better with 6% droop settings therefore recommended droop settings for WT generator for 80% wind power penetration is 6%.

From the above studies, it is clear that improper settings for WT control can invoke frequency instability. This issue becomes more prominent with increasing wind power penetration. **Low $droop_{WT}$ settings for WT generators are advisable in low wind power penetrated high inertia system, while high $droop_{WT}$ settings are recommended for high wind power penetrated low inertia system.**

5.4 Validation of recommendations using PEGASE Pan European EHV Network

In the above studies, network constraints such as system voltage, line limits, network protections etc. were relaxed. However, it is imperative to validate these recommendations on WT control on a detailed power system network model. Therefore, a representative model of European Transmission Network called PEGASE EHV network [83] has been used in this PhD work for validation of the recommendations. This model is representative of the Continental Europe system. The system has 16578 buses, 3240 generators, 14044 lines, 9654 transformers, and total load of 400 GW [83]. These simulations are performed in Eurostag.

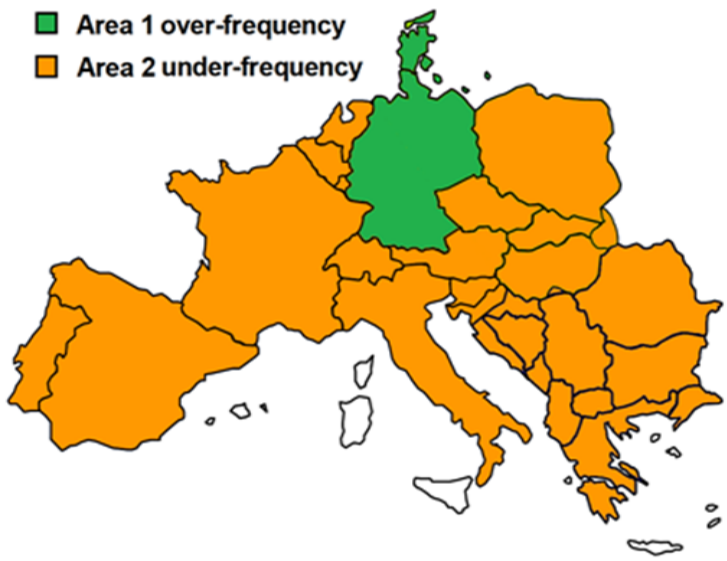

Figure 5-20: Simulated Scenario in PEGASE network

In order to simulate overfrequency event in the PEGASE network, system split is simulated. Figure 5-20 indicates the split of Denmark + Germany network from the rest of

the CE network. Area 1 consisting of Danish and German networks experience overfrequency while Area 2 consisting of rest of the network experiences underfrequency.

Wind power penetration in Area 1 is varied to validate the recommendations. Figure 5-21 depicts the frequency response when wind power penetration is 20%.

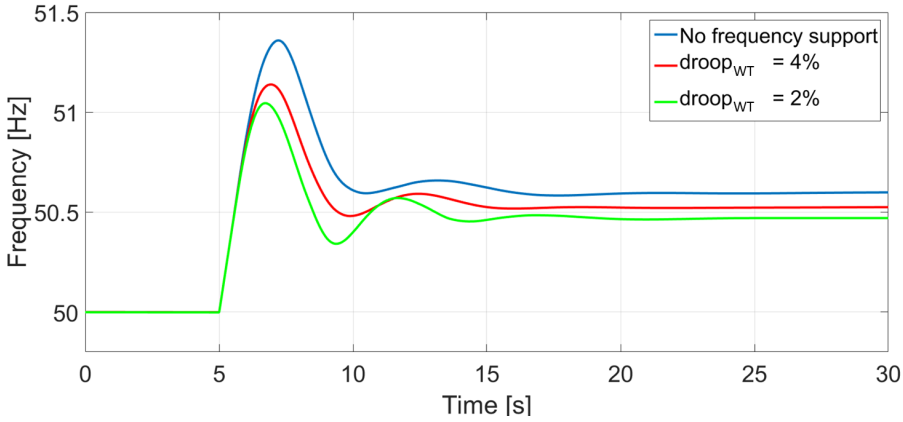

Figure 5-21: Frequency Response with 20% Wind Power Penetration in Area 1 in PEGASE network

It can be seen that there is considerable improvement with frequency control from WT generators. $droop_{WT}$ setting of 2% as per recommendation performs best.

Figure 5-22 depicts the frequency response when wind power penetration is 40% in Area 1 of the PEGASE network.

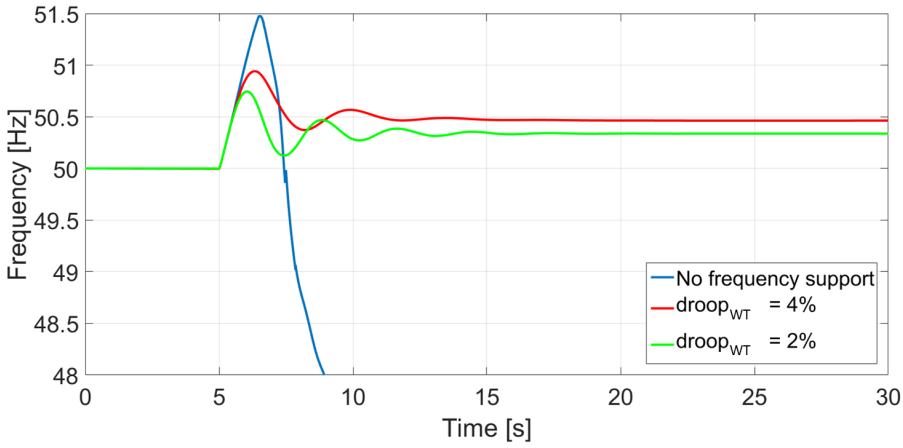

Figure 5-22: Frequency with 40% Wind Power Penetration in Area 1 in PEGASE network

It can be seen that without any frequency support from WT generators system becomes unstable. However, system becomes stable with frequency support from WT generators. $droop_{WT}$ setting of 2% as per recommendation performs best and peak frequency is constricted to less than 50.75 Hz.

Frequency support from WT is crucial in future power system with high wind power penetration.

5.5 Summary

- Uncontrolled and unplanned disconnections and reconnections of WTs can cause frequency instability. This advocates for designing of proper protection settings for WTs.
- Adequate protection settings alone can not prevent frequency instability, especially when wind power penetration is high. This calls for proper overfrequency emergency control from WTs.
- Overfrequency control from WTs are dependent on droop settings, activation delays and ramp rate capabilities. Droop settings, activation delays and ramp rate capabilities are dependent on each other and should not be treated independently.
- Studies shows that ramp rate should be 0.3 p.u./s or greater in order to obtain maximum support from WTs irrespective of droop and activation delay.
- Low droop settings for WTs are advisable in low wind power penetrated high inertia system, while high droop settings are recommended for high wind power penetrated low inertia system. It is observed that for wind power penetration less than 40%, droop settings for WTs should be 2%. For wind power penetration between 40% and 60%, droop settings for WTs should be 4%. While for wind power penetration beyond 60%, droop based frequency control may not be sufficient to prevent frequency instability.
- If wind power penetration is as high as 80%, inertia of the system may be too low to prevent frequency instability. In such cases, a virtual inertia support from WT generator is essentially required. Droop settings for WT generators should be 6% in such cases.
- The recommendations of this PhD work have been validated in the large scale Pan-European EHV network model.

This page would be intentionally left blank if we would not wish to inform about that.

Chapter 6

Underfrequency Load Shedding considering Distributed Generation

---

This chapter proposes new Underfrequency Load Shedding (UFLS) schemes considering the amount of Distributed Generations (DGs) connected to the feeders in real-time and compares them with traditional UFLS scheme. The UFLS schemes proposed and discussed are - i) traditional method using static relay ii) directional relay based UFLS using power flow direction in the feeders, iii) UFLS scheme using power flow magnitude and direction, iv) UFLS scheme using power flow and DG data respectively. In order to use DG data, amount of DG connected to each feeder are estimated in real-time. Based on the real-time estimation of the amount of DG connected, each feeder is prioritized for UFLS. Following prioritization, feeders are selected for load shedding using mathematical optimization technique. These methods are studied and compared on a simulated transmission system developed by Energinet.Dk in which distribution networks are incorporated. In order to test the results over large WT and PV generation scenarios, multiple simulations are run for 400 randomly selected WT and PV scenarios over a span of 1 meteorological year.

6.1 Introduction

The penetration of renewable generation in the power systems has been increasing significantly all over the world. High proportion of these generation units are connected to the distribution systems and are referred to as Distributed Generations (DGs). However, high penetration of DG imposes certain challenges for UFLS.

In order to have stable operation of a power system, it is essential to keep the frequency within the nominal operating ranges. However, a severe disturbance can cause fast decline of frequency which can result in frequency instability. In order to limit the

frequency from going too low, frequency containment reserves are deployed from dedicated generators. If these reserves are exhausted or unable to contain the frequency, the system enters in an emergency state. Special defence strategies employing system protection schemes (SyPS) are employed to defend against instabilities in emergency state. Underfrequency load shedding is one such SyPS which is considered as last resort to prevent frequency instability. ENTSO-E recommendation for UFLS for European networks is shown in Figure 6-1 [6]. It can be observed from Figure 6-1 that minimum load shedding is recommended to start at 49 Hz and multiple stages of load shedding are continued until 48.1 Hz as represented by the red region. However, load shedding from 49.2 until 48.6 (as represented by the green region) is desirable. Since UFLS causes

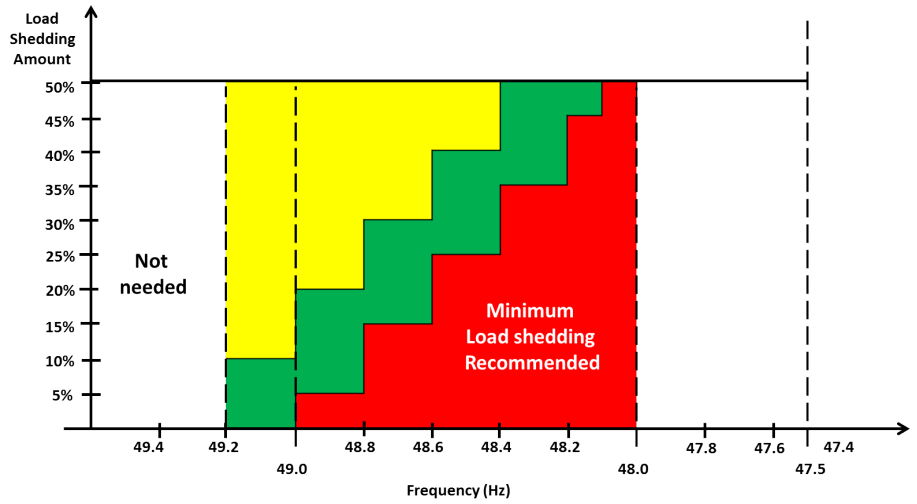

Figure 6-1: ENTSO-E Recommendation for UFLS[6]

economic loss and consumer discomfort, it is considered as last resort to contain frequency decline. UFLS is generally performed by automatically disconnecting the feeders at distribution substations. Disconnecting feeders with large penetration of DG may disconnect substantial amount of generation. Consequently, the required amount of load disconnection as per design requirements (e.g. Figure 6-1) is not achieved. Traditional load shedding relays do not consider this effect. "IEEE Guide for the Application of Protective Relays Used for Abnormal Frequency Load Shedding and Restoration" [39] has clearly mentioned that tripping feeders that have active DG certainly diminishes the beneficial affect of load shedding, and can even have negative impact by eliminating sources of generation that supports system inertia. Thus high penetration of DG advocates for advanced UFLS approach which would take DG into account [39]. Therefore, in this work, novel load shedding schemes are developed which try to minimize the amount of DG disconnection while disconnecting the required amount of consumption.

6.2 Power System Model

The transmission network model [7] as shown in Figure 6-2 is developed by Energinet.Dk and is used for the studies presented here. Total generation capacity of this synthetic transmission system is 7080 MW whereas demand of the system is 6060 MW.

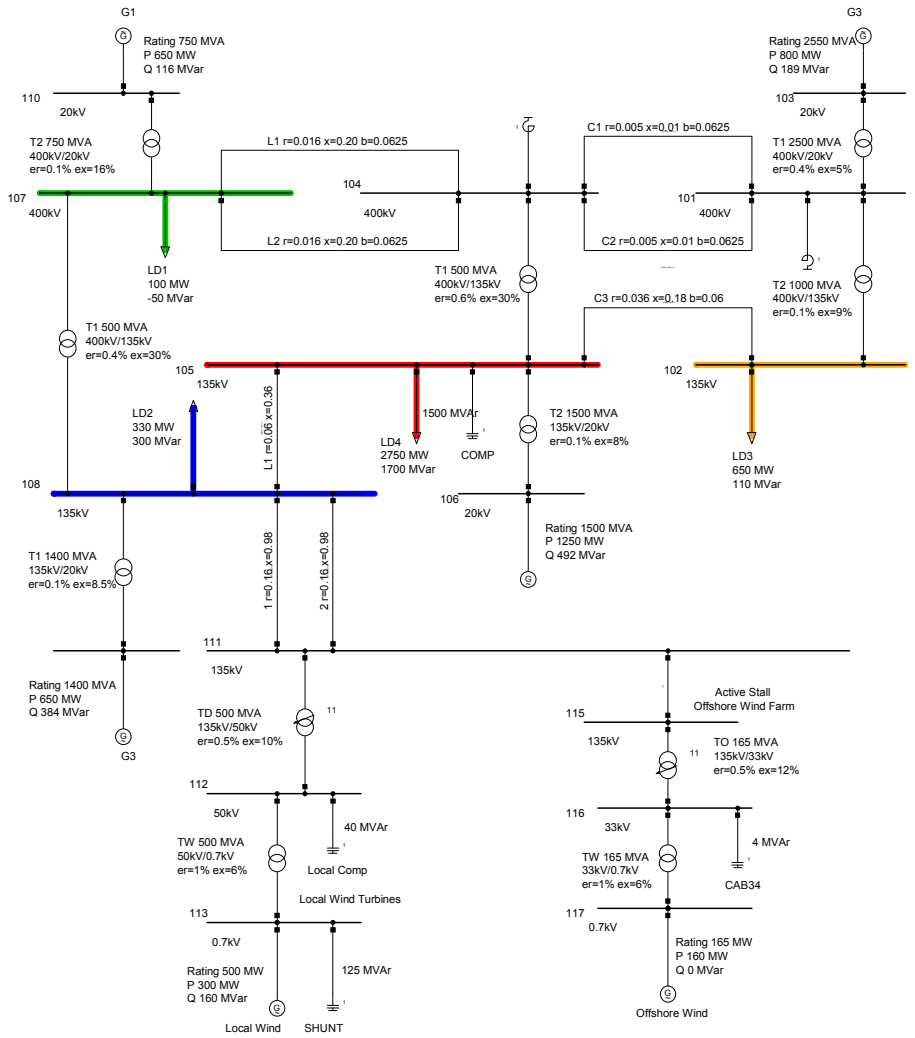

Figure 6-2: Transmission System Model [7]

In order to study the effects of load shedding on this transmission system, 4 different loads (LD1, LD2, LD3 and LD4) as shown in Figure 6-2 at 4 different locations in the network are replaced with distribution networks. Distribution networks are modelled as combination of feeders with aggregated loads, PV generation and WT generation in each feeders as shown in Figure 6-3. The distribution system is modelled as a 110

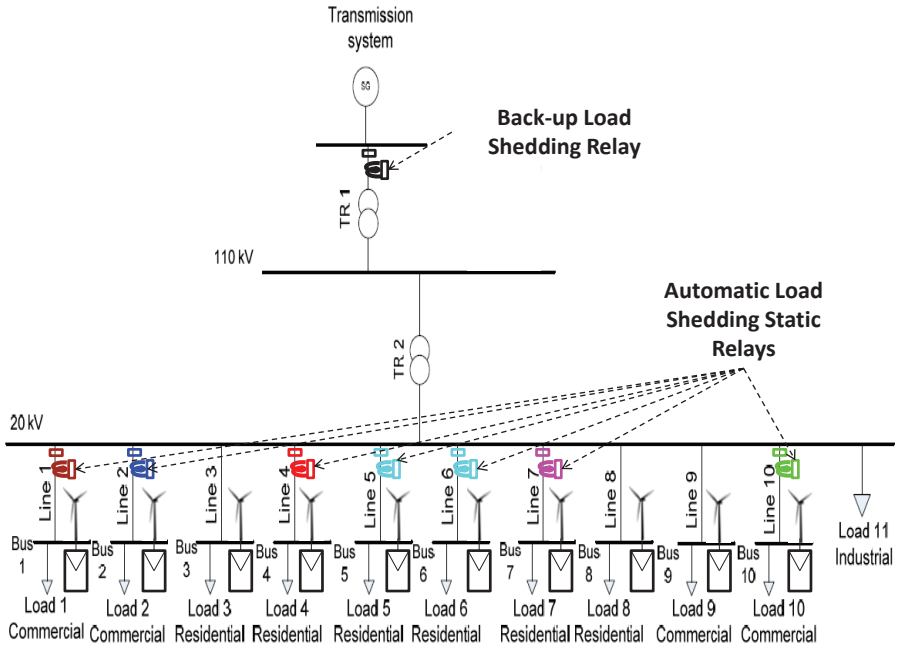

Figure 6-3: Distribution System Model

kV substation where loads are modelled as aggregated loads connected to 11×20 kV feeders. 6 of these feeders are connected to residential loads, 4 feeders are connected to commercial loads and 1 feeder has industrial loads connected to it.

WT generations are modelled as IEC 61400-27 Type 1 generic wind turbine [85] and PV generations are modelled using standard models provided by DigSilent PowerFactory [86]. However, it should be noted that the model as well as the developed UFLS scheme is generic for any distribution network. Frequency dependencies of active and reactive power of different types of loads are designed as:

$$P = P_0[1 + K_{pf}(\Delta freq)] \tag{6.1}$$

$$Q = Q_0[1 + K_{qf}(\Delta freq)] \tag{6.2}$$

where,

- $\Delta freq$: frequency deviation in Hz
- P: active power consumption of the load in MW
- Q: reactive power consumption of the load in MW
- P_0: active power consumption of the load in MW when $freq = 50Hz$
- Q_0: reactive power consumption of the load in MW when $freq = 50Hz$
- K_{pf}: frequency sensitivity parameter with respect to P

- K_{qf}: frequency sensitivity parameter with respect to Q

Frequency parameters, K_{pf} and K_{qf} for different types of loads are given in Table 6.1.

Table 6.1: Typical Load frequency parameters

Load Type	Frequency Parameters K_{pf}	K_{qf}
Residential		
Electrical Heating	1	-1.7
Non Electrical Heating	0.8	-1.7
Commercial		
Electrical Heating	1.5	-1.1
Non Electrical Heating	1.7	-0.9
Industrial	2.6	1.6

Four different distribution system networks are connected at four different locations as shown in Figure 6-2. Wind speed and hence available wind power generation for these 4 different locations are modelled using CorWind model (Appendix A). Whereas, PV generation are modelled based on the data provided by Belgian TSO, ELIA for different locations in Belgium network [87]. Underfrequency disconnection settings of the DG is set on 47.5 Hz according to the European Commission's Network Code Requirements for Connection [32]; the grid code connection requirements for small generators in Denmark (current rating 16 A or lower) [88] and the grid code connection requirements for Wind and PV plants above 11 kW in Denmark [89], [90].

Disconnection of a large generator in the transmission network is simulated in order to simulate large frequency drop in the system.

The UFLS scheme is designed based on the minimum load shedding recommendations as shown in Figure 6-1. The applied settings are given in Table 6.2. Frequency and Rate

Table 6.2: Recommendation for Underfrequency Load Shedding

Stage(k)	Frequency [Hz]	Minimum Load Shedding Amount(A_k)
1	49	5%
2	48.8	10%
3	48.6	10%
4	48.4	10%
5	48.2	10%
6	48.1	5%

of Change of Frequency (RoCoF) measurements are computed using a moving average filter as described in IEC 61400-27-1 standard [85].

6.3 Different Load Shedding Schemes

4 load shedding schemes are discussed in the following:

6.3.1 Load Shedding Algorithm using Static Relay (LSA-Static)

Traditionally static relays are installed in selected feeders based on amount of installed loads in these feeders [39], [91]. A certain number of feeders are selected based on the historical measured load data of these feeders such that their disconnection should disconnect the required amount of load. For example, among the regional reliability councils of North American Electric Reliability Council (NERC), SERC Reliability Corporation requires that these load shedding strategies should have the capability of shedding certain percent of demand at the time coincident with the previous year actual peak demand [92], whereas Southwest Power Pool (SPP) requires to shed certain percentage of the forecasted peak load [93]. Generally these feeders are chosen based on types of loads connected to the feeders, network topology, equal distribution of loads to be shed etc. [94].

Although this scheme is simple, robust and inexpensive to implement, it is sub-optimal. In case there is substantial amount of DG connected to these selected feeders, it may not disconnect required amount of consumption. Consequently, frequency decline is not restricted resulting in activation of larger number of load shedding stages. Therefore, at the end it may disconnect larger amount of consumption than required. Another major drawback of this scheme is that it may disconnect substantial amount of DG which is particularly undesirable during an underfrequency emergency. In case of disconnection of feeders with higher generation than consumption, UFLS will have negative impact. Consequently, the frequency may keep falling down making the system vulnerable to underfrequency instability.

Table 6.3: Load Shedding Settings for Static Relays

Stage(k)	Frequency [Hz]	Amount(A_k)	Locations
1	49	5%	Line 4
2	48.8	10%	Line 2
3	48.6	10%	Line 10
4	48.4	10%	Line 5,6
5	48.2	10%	Line 1
6	48.1	5%	Line 7

Table 6.3 depicts the UFLS settings for static relays. The locations of these UFLS relays are shown in Figure 6-3. The feeders in the system are expected to be disconnected to remove a predefined amount of demand, e.g. 10% of the demand should be disconnected at a frequency of 48.8 Hz [6]. This particular scheme is considered as the baseline scheme to which the performance of other load shedding schemes are compared. In this scheme, feeder with industrial load is considered as a high priority

feeder and is exempted from load shedding. Basically, the feeder with industrial load represents all the high priority feeders in a practical distribution networks which are excluded from load shedding such as traction loads, hospitals etc. All the other feeders are assumed of equal priorities.

6.3.2 Load Shedding Algorithm using Static Relay with Directional element (LSA-Directional)

One of the major drawback of the load shedding scheme using static relay is that it may disconnect substantial amount of DG while disconnecting specific feeders. It is possible that at certain time of the day, generations from DG can be higher than consumption for any of these feeders. As a result, the feeder acts as a generator instead of load. Disconnecting any such feeder can have negative impacts on system frequency. In order to prevent such scenarios, a directional power relay element can be incorporated along with the static relays. This relay checks whether the power flow in the feeder is from distribution network to transmission network. If power is flowing from distribution network to transmission network then the relay is blocked from activation and the corresponding feeder is not disconnected.

Although this scheme is expected to perform better than LSA-Static scheme, it is not optimal, as it still can disconnect substantial amount of DG and not disconnect required amount of consumption. Further, there may be no load shedding for a particular stage since all the pre-selected feeders may have generation more than consumption. In such scenario, frequency may decline further activating further load shedding stages which is undesirable.

6.3.3 Load Shedding Algorithm using Power Flow (LSA-PF)

A major issue with the previous two schemes is that required amount of load that needs to disconnected for a certain UFLS stage is not achieved. A new load shedding algorithm is proposed which disconnects the required amount of load for each stage. This scheme considers the actual value of power that flows in each feeder along with the direction of the power flow. The inputs of LSA-PF are the measured frequency, the RoCoF and the measured active power flows of all the distribution feeders. It is assumed that the total consumption forecast in the concerned distribution network is available from TSO.

The flowchart for the scheme is shown in Figure 6-4.

The parameters of the flowchart are described as following:

- $P_{m,i,t}$: Power flow measurements of feeder i at time t in MW
- $freq_k$: Load shedding activation frequency for stage k in Hz
- $freq_{m,t}$: Frequency measurement at time t in Hz

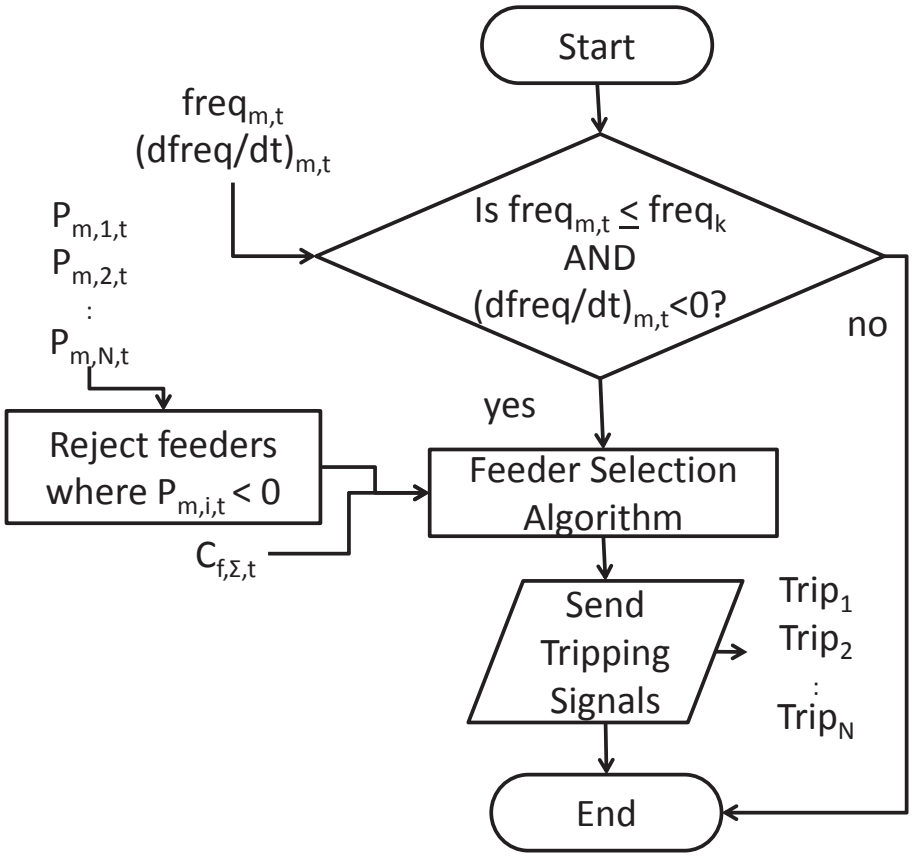

Figure 6-4: Flowchart for Load Shedding using Power Flow

- $(dfreq/dt)_{m,t}$: Rate of Change of Frequency measurement at time t in Hz
- $C_{f,\Sigma,t}$: Total consumption forecast for the distribution network at time t in MW
- $Trip_i$: Trip signal for feeder i

Power flow measurements for the feeders, $P_{m,i,t}$ are used to select the feeders for disconnection. It can be observed from Figure 6-4 that if any feeder produces more active power than what it consumes i.e. power flow is negative, it is not considered for load shedding. Frequency measurements, $freq_{m,t}$ are used to find out if frequency is less than load shedding activation frequency, $freq_k$ (Table 6.2) and RoCoF ($(dfreq/dt)_{m,t}$) is negative then "Feeder Selection Algorithm" (discussed below) is run. RoCoF is basically used to identify whether the frequency is going down or going up. Filtering of the RoCoF signal is necessary due to the noise generated by differentiating frequency. Moving Average filter is applied for filtering noise as given in [85].

Feeder Selection Algorithm:
As depicted in Table 6.2, the required amount of load to shed is different, depending on

the load shedding stage. Therefore, the algorithm finds the feeder or the combination of feeders that have the minimum amount of active power flow greater than 5% or 10% (denoted by A_k) of the total consumption, depending on the load shedding stage.

The amount of consumption needed to be disconnected for load shedding stage k is given by Equation (6.3):

$$C_{\Sigma,k,t,shed} = C_{f,\Sigma,t} * A_k \tag{6.3}$$

where,

- $C_{\Sigma,k,t,shed}$: Consumption needed to be disconnected for stage k in MW
- $C_{f,\Sigma,t}$: Total consumption forecast for the distribution network at time t in MW
- A_k: Amount of consumption required to be shed for stage k in %

The total consumption $C_{\Sigma,k,t,shed}$ needed to be disconnected is calculated based on the consumption forecast $C_{f,\Sigma,t}$ for the distribution network obtained from TSO. It is assumed to have low error since consumption does not generally have large variation in considered time window of 5 minutes.

Feeder Selection Algorithm finds out the feeders for which the sum of the power flows is greater and as close as possible to the total consumption to be disconnected $C_{\Sigma,k,t,shed}$. This is basically a combinatorial optimization problem which can be modelled as "0/1 Knapsack Problem" [95].

"0/1 Knapsack Problem" for Feeder Selection Algorithm can be modelled as following:

$$\begin{aligned} \max \quad & \sum_{i=1}^{total\_num\_feeders} -P_{m,i,t} * x_{i,t} \\ \text{subject to} \quad & \\ & \sum_{i=1}^{total\_num\_feeders} -P_{m,i,t} * x_{i,t} \leq -C_{\Sigma,k,t,shed} \\ & x_{i,t} \in \{0,1\} \end{aligned} \tag{6.4}$$

where,

- $P_{m,i,t}$: Power flow measurements of feeder i at time t in MW
- $C_{\Sigma,k,t,shed}$: Consumption required to be disconnected for stage k in MW
- $x_{i,t}$: Binary switching status of feeder i at time t

The objective function is to minimize the sum of the power flows through selected combination of feeders subject to the constraint that the sum of the power flows through selected combination of feeders is greater than the total consumption to be disconnected. x_i represents the switching status of the feeders. x_i is 1 if the feeder should

be disconnected or 0 otherwise. The binary vector solution $\underline{x}$ to the Equation (6.4) indicates which feeders to be disconnected based on which signals to trip the relays are sent. However, it should be noted that since "0/1 Knapsack Problem" is a integer programming problem, therefore $P_{m,i,t}$ and $C_{\Sigma,k,t,shed}$ are appropriated up to the second decimal point.

This load shedding scheme has the advantages of improved frequency response as compared to load shedding using static relays. This scheme disconnects required amount of load. However, since this method does not use DG data, it may disconnect substantial amount of generation resulting in shedding consumption more than required. Therefore, this scheme may become less economical while being more stable than previous load shedding schemes.

6.3.4 Load Shedding Algorithm using DG data (LSA-DG)

In order to handle the disadvantage of the previous scheme, a new scheme is proposed. This scheme uses the estimate of the amount of distributed PV and WT generation connected to each feeder. Based on these estimates, all the feeders are prioritized. The feeder selection algorithm selects the feeders to be disconnected considering the priorities assigned to each feeder. The flowchart for this scheme is shown in the Figure 6-5.

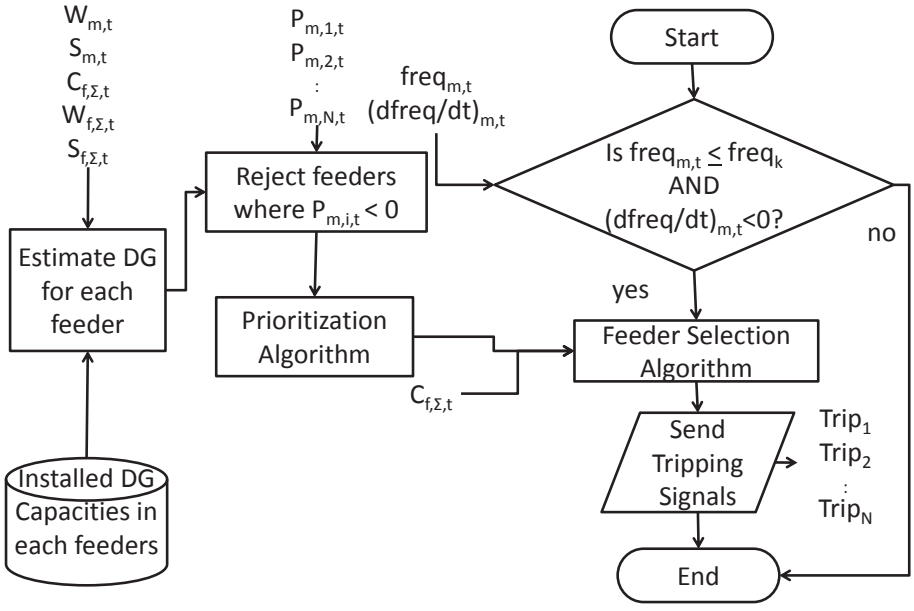

Figure 6-5: Flowchart for Load Shedding using DG Data

The parameters of the flowchart are as following:

- $W_{m,t}$: Generation from "500 kW equivalent WT" the distribution network at time t in MW
- $S_{m,t}$: Generation from "100 kW equivalent PV panel" the distribution network at time t in MW
- $C_{f,\Sigma,t}$: Total consumption forecast for the distribution network at time t in MW
- $W_{f,\Sigma,t}$: Total WT generation forecast for the distribution network at time t in MW
- $S_{f,\Sigma,t}$: Total PV generation forecast for the distribution network at time t in MW
- $P_{m,i,t}$: Power flow measurements of feeder i at time t in MW
- $freq_k$: Load shedding activation frequency for stage k in Hz
- $freq_{m,t}$: Frequency measurement at time t in Hz
- $(dfreq/dt)_{m,t}$: Rate of Change of Frequency measurement at time t in Hz
- $Trip_i$: Trip signal for feeder i

DG Estimation:
It should be noted here that the objective of this work is not to accurately estimate the amount of DG connected to each feeder. If any other algorithm is available which provides the estimation of DG connected to each feeder in real-time, it can be readily used. Remark that any error in estimation algorithm introduces error in prioritization of feeders for disconnection. Therefore, the prioritization algorithm should be robust to take account of the estimation errors so that the error in disconnection of feeders is reduced.

Assumptions:
The assumptions for DG estimation are as follows:

1. Power flow measurements at the resolution of 1 minute is considered. However, the redundancy of the measurements increases if measurements are obtained at faster rate, thereby resulting in better estimation.
2. Wind speed observed in whole distribution network is only differed by certain uncertainties. This implies that if the wind speed measured at DSO control center (or at the location where LSA-DG is hosted) is v_W then wind speed observed at any other location in the network is $v_W + \eta_W$ where η_W is the error in wind speed modelled as white guassian noise with mean $\mu_W = 0$ and standard deviation $\sigma_W = 4\%$
3. Solar insolation observed in whole distribution network is only differed by certain uncertainties. This implies that if the solar insolation measured at DSO control center is I_S then solar insolation observed at any other location in the network is $I_S + \eta_S$ where η_S is the error in solar insolation modelled as white guassian noise with mean $\mu_S = 0$ and $\sigma_S = 4\%$

4. These assumptions do not take in consideration of local phenomena such as clouds, wakes, etc. However, if the amount of DG installed in the distribution network is sufficiently large, the effects of these local phenomenon can be neglected without introducing large error.

5. WTs connected to each feeder is modelled as aggregated wind power generation as integral of 500 kW generation. This means that if the total WT connected to feeder i is 5 MW then it can be assumed that the feeder has 10, "500 kW equivalent WT" connected to it. This is done in order to simulate the wind power generation in the "500 kW equivalent WT" and scale it according to the installed capacity of WT generation in each feeder.

6. Similarly, total PV connected to each feeder is modelled as aggregated generation as integral of 100 kW generation. This means that if total PV connected to feeder i is 5 MW then it can be assumed that the feeder has 50, "100 kW equivalent PV panels" connected to it.

7. No other types of DGs are considered in the system. DGs such as diesel generators, biomass, fuel cells etc. can be neglected since the volume of these generations are in general considerably smaller compared to WT and PV generations in most of the distribution networks.

8. Consumption is assumed to be constant for the selected time window. The total consumption of the distribution network is equal to the consumption forecast from the TSO which is modelled with guassian error η_C with mean $\mu_C = 0$ and standard deviation $\sigma_C = 2\%$

9. Large DGs (large wind farms, CHPs, large biomass plants etc.) are generally connected to dedicated feeders which are exempted from load shedding. It is assumed that feeder with industrial loads in Figure 6-3 represents all those feeders which are not considered for load shedding.

Unknowns:
Number of unknowns for the 10 feeders in each distribution network are as follows:

- $[n_{C,1}, .., n_{C,10}]$: Amount of consumptions connected to each feeder
- $[n_{W,1}, .., n_{W,10}]$: Number of "500 kW equivalent WT" connected to each feeder
- $[n_{S,1}, .., n_{S,10}]$: Number of "100 kW equivalent PV panel" connected to each feeder
- Therefore, the unknown vector comprises of these 3 vectors and given as $\underline{n} = [n_{C,1}, ..., n_{C,10}, n_{W,1}, ...$ is constituted

However, it should be noted that if there is no installed WT or PV generation in feeder i, then corresponding unknown $n_{W,i}$ or $n_{S,i}$ should be removed. The maximum number of unknowns in each considered distribution network is therefore, 30.

Measurement vector:
For a time window of 5 minutes following measurements are considered:

- $[P_{m,1,t}, .., P_{m,10,t}, P_{m,1,t+1}, .., P_{m,10,t+1}, .., P_{m,10,t+4}]$: Power flow measurements for all the feeders for 5 minutes (assumed with time interval of 1 minute).
- $[C_{f,\Sigma}]$: Total consumption forecast of the network obtained from TSO
- $[n_{W,\Sigma,t}]$: Total numbers of "500 kW equivalent WT" connected to the network during the considered time window.
- $[n_{S,\Sigma,t}]$: Total numbers of "100 kW equivalent PV panel" connected to the network during the considered time window.
- The measurement vector $\underline{g} = [P_{m,1,t}, .., P_{m,10,t+4}, C_{f,\Sigma}, n_{W,\Sigma}, n_{S,\Sigma}]$ is constituted

Therefore, the number of elements in the measurement vector for each considered distribution network $\underline{g}$ is 53 ($size_g$) whereas, the number of unknowns are 30 ($size_n$), which makes the system a over-determined system.

Constraints:

- Lower Bound: $\underline{lb}$ = a zero vector of length n, since all the unknowns can have only positive or zero values
- Upper Bound: $\underline{ub}$ = Installed capacities of each unknown

Equations:

$$\begin{aligned}
C_1 - W_{1,t} - S_{1,t} &= P_{m,1,t} \\
C_2 - W_{2,t} - S_{2,t} &= P_{m,2,t} \\
&\cdots\cdots\cdots\cdots\cdots \\
C_{10} - W_{10,t} - S_{10,t} &= P_{m,10,t} \\
C_1 - W_{1,t+1} - S_{1,t+1} &= P_{m,1,t+1} \\
&\cdots\cdots\cdots\cdots\cdots \\
C_{10} - W_{10,t+1} - S_{10,t+1} &= P_{m,10,t+1} \\
C_1 - W_{1,t+2} - S_{1,t+2} &= P_{m,1,t+2} \\
&\cdots\cdots\cdots\cdots\cdots \\
C_{10} - W_{10,t+4} - S_{10,t+4} &= P_{m,10,t+4} \\
C_1 + ... + C_{10} &= C_{f,\Sigma,t} \\
W_{1,t} + ... + W_{10,t} &= W_{f,\Sigma,t} \\
S_{1,t} + ... + S_{10,t} &= S_{f,\Sigma,t}
\end{aligned} \tag{6.5}$$

where,

- C_i: Consumption of feeder i for the considered time window in MW
- $W_{i,t}$: WT generation for feeder i at time t in MW
- $S_{i,t}$: PV generation for feeder i at time t in MW
- $P_{m,i,t}$: Power flow measurements of feeder i at time t in MW
- $C_{f,\Sigma,t}$: Total consumption forecast for the distribution network at time t in MW

- $W_{f,\Sigma,t}$: Total WT generation forecast for the distribution network at time t in MW
- $S_{f,\Sigma,t}$: Total PV generation forecast for the distribution network at time t in MW

Equation (6.5) represents the Kirchoff's Current Law for all the considered feeders for each distribution network. Power flow through each feeder at a given time instant is given as the differences between total consumption and sum of WT and PV generation for that particular feeder. Equation (6.5) also shows that the total consumption, total WT generation, total PV generation in the distribution network is equal to the consumption forecast, WT generation forecast and PV forecast for the considered distribution network respectively.

It can be observed from Equation (6.5) that consumptions do not change with time. This is in accordance to assumption 8. By further considering assumptions 5 and 6, total WT and PV generation are replaced with equivalent "500 kW equivalent WT" generations and "100 kW equivalent PV panel" generations respectively. This is shown in Equation (6.6)

$$
\begin{aligned}
C_1 &= n_{C,1} \\
&\cdots\cdots\cdots\cdots \\
C_{10} &= n_{C,10} \\
W_{1,t} &= n_{W,1} * W_{m,t} \\
&\cdots\cdots\cdots\cdots \\
W_{10,t} &= n_{W,10} * W_{m,t} \\
W_{1,t+1} &= n_{W,1} * W_{m,t+1} \\
&\cdots\cdots\cdots\cdots \\
W_{10,t+1} &= n_{W,10} * W_{m,t+1} \\
&\cdots\cdots\cdots\cdots \\
W_{10,t+4} &= n_{W,10} * W_{m,t+4} \\
S_{1,t} &= n_{S,1} * S_{m,t} \\
&\cdots\cdots\cdots\cdots \\
S_{10,t} &= n_{S,10} * S_{m,t} \\
S_{1,t+1} &= n_{S,1} * S_{m,t+1} \\
&\cdots\cdots\cdots\cdots \\
S_{10,t+1} &= n_{S,10} * S_{m,t+1} \\
&\cdots\cdots\cdots\cdots \\
S_{10,t+4} &= n_{S,10} * S_{m,t+4}
\end{aligned}
\tag{6.6}
$$

where,

- C_i: Consumption of feeder i for the considered time window in MW
- $n_{C,i}$: Amount of consumption connected to feeder i in considered time period in MW
- $W_{i,t}$: WT generation for feeder i at time t in MW
- $n_{W,i}$: Number of "500 kW equivalent WT" connected to feeder i in considered time window
- $W_{m,t}$: Generation from "500 kW equivalent WT" at time t in MW

- $S_{i,t}$: PV generation for feeder i at time t
- $n_{S,i}$: Number of "100 kW equivalent PV panel" connected to feeder i in considered time window
- $S_{m,t}$: Generation from "500 kW equivalent PV panel" the distribution network at time t in MW

Equation (6.6) represents the total WT and PV generations for each feeder based on measurements from a "500 kW equivalent WT" and a "100 kW PV panel" placed on a central location. Total generation is equal to total number of equivalent generators times the measurements of the equivalent generations.

Substituting the values from Equation (6.6) to Equation (6.5), including the constraints, and rearranging in matrix form gives;

$$\mathbf{E} * \underline{n} = \underline{g} + \eta \text{ such that } \underline{lb} \leq \underline{n} \leq \underline{ub} \tag{6.7}$$

where,

- **E**: Matrix of co-efficients between measurement and unknown vectors
- $\underline{\text{n}}$: Unknown vector
- $\underline{\text{g}}$: Measurement vector
- η: Combination of all the errors η_W, η_S, η_C
- $\underline{\text{lb}}$: Vector of lower bounds of unknowns
- $\underline{\text{ub}}$: Vector of upper bounds of unknowns

Solution:
Since Equation (6.7) is basically a constrained Linear Least Square Problem (LLSP) [96], its solution can be found by computing the smallest norm of the error η, i.e.

$$\begin{aligned} \min_{\underline{n}} \quad & \frac{1}{2}||\mathbf{E} * \underline{n} - \underline{g}||_2^2 \\ \text{subject to} \quad & \\ & \underline{lb} \leq \underline{n} \leq \underline{ub} \end{aligned} \tag{6.8}$$

Feeder Prioritization:
The idea of providing priorities to feeders is that some of the feeders will have high priority loads like hospitals, traction, dedicated feeder with distributed generation etc. as compared to other feeders. Scores of the feeders can be selected based on following parameters:

- Type of loads connected to the feeder
- Amount of generation connected to the feeder

- Amount of consumption connected to the feeder

Generally, scores or weighage are given by Distribution System Operator (DSO)s based on their experiences [94]. In our studies, equal priorities are assumed for the feeders with residential and commercial loads based on load type. If there are any priority / weighage among the feeders based on load type, then those weighage can simply be multiplied with assumed scores.

Feeder i is prioritised based on estimated consumption C_i, PV generation S_i and WT generation W_i obtained from the solution of Equation (6.8). In order to make the prioritization algorithm robust against errors in DG estimation, feeders are only classified into three groups based on their Generation/Consumption ratio.

Priority or score for each feeder is defined in Table 6.4, where, generation for feeder i

Table 6.4: Prioritization of feeders based on DG

Generation / Consumption Ratio	Score (Sc_i)
≤ 0.2	1
0.2 - 0.5	2
≥ 0.5	4

is calculated as $S_i + W_i$ and consumption for feeder i is C_i. Scores of all the feeders for the considered distribution system constitutes Score vector, $\underline{Sc}$.

Feeder Selection Algorithm:
Feeder selection algorithm discussed with regards to LSA-PF is adjusted here to take Score vector, $\underline{Sc}$ into consideration. Therefore, the cost function in Equation (6.4) is multiplied with Score vector, transforming Equation (6.4) to Equation (6.9).

$$\begin{aligned} \max \quad & \sum_{i=1}^{total\_num\_feeders} -Sc_{i,t} * P_{m,i,t} * x_{i,t} \\ \text{subject to} \quad & \\ & \sum_{i=1}^{total\_num\_feeders} -P_{m,i,t} * x_{i,t} \leq -C_{\Sigma,k,t,shed} \\ & x_{i,t} \in \{0,1\} \end{aligned} \tag{6.9}$$

where,

- $Sc_{i,t}$: Score (priority) of feeder i at time t
- $P_{m,i,t}$: Power flow measurements of feeder i at time t in MW
- $C_{\Sigma,k,t,shed}$: Consumption required to be disconnected for stage k in MW
- $x_{i,t}$: Binary switching status of feeder i at time t

This load shedding scheme is expected to provide better frequency response as compared to other load shedding schemes since this scheme prioritizes the feeders with least amount of DG connected for load shedding. Therefore, this method disconnects minimum amount of DG while disconnecting required amount of consumption.

6.3.5 Considerations for Practical Implementation

While LSA-Directional scheme can be implemented at relay level, LSA-PF and LSA-DG schemes are developed aiming to have them implemented as centralized control methods at DSO control center which can send automated trip signals to the relays connected at the feeders. In modern TSOs many solutions are available such as Distributed Generation Management systems [97], Network management solutions [98], etc.which can provide the measurements and consumption, WT, PV forecasts to be used in the load shedding schemes. LSA-PF and LSA-DG schemes can obtain measured power flow data from the feeders and use the data from TSO to execute the schemes. Following the computations LSA-PF and LSA-DG schemes can send tripping signals to the relay to the selected feeders. Substation automation infrastructure can be used for data communication. The automation systems generally have fast communication links using IEC 61850 standard [99].

The advantages of LSA-PF and LSA-DG schemes shown in Figure 6-4 and Figures 6-5 are that feeder selection algorithm, DG estimation, DG prioritization are independent of frequency or RoCoF measurements. As a result, these two schemes can be run independent of frequency event and prioritise the list of feeders to be disconnected. This list will be ready even before the frequency event happens and as frequency reaches shedding frequencies, the feeders can be disconnected based on the already developed list.

LLSP of Equation (6.8) is a well known problem of state estimation and has been thoroughly studied and implemented [100], [101]. The advantage of Equation (6.8) is that number of unknowns are $3 * total\_num\_feeders$ which is much smaller than number of unknowns in traditional state estimation algorithms, which reduces the space and time complexity of DG estimation algorithm.

Time Complexity of "0/1 Knapsack problem" of Equation (6.4) and Equation (6.9) can be given by the big O notation as $O(total\_num\_feeders * C_{\Sigma,k,t,shed})$. Since $C_{\Sigma,k,t,shed}$ is in p.u., it is sufficiently small. Consequently, $O(total\_num\_feeders * C_{\Sigma,k,t,shed})$ becomes linear and only dependent on number of feeders. For example, if the capacity of distribution network is 1000 MW (and can be chosen as base power); then in order to shed 5% of total consumption in this network, $C_{\Sigma,k,t,shed}$ can have a maximum value of $0.05 * 1000/1000 = 0.05p.u.$ Since, "0/1 Knapsack problem" is an integer programming problem, all the variables are approximated as integers to second decimal point by multiplying them by 100. Therefore, $C_{\Sigma,k,t,shed}$ becomes $0.05 * 100 = 5$. Consequently, time complexity becomes $O(5 * total\_num\_feeders)$, which is linear. This implies that it is possible to implement LSA-DG for very large distribution systems.

Another important point to note that is the modularity of the schemes. If communication failures happen for the flowchart shown in Figure 6-5 and any signal among $W_m, S_m, C_{f,\Sigma}, W_{f,\Sigma}, S_{f,\Sigma}$ is lost, the feeder prioritization can set equal score for all the feeders and the flowchart of Figure 6-5 falls back to that of Figure 6-4. Similarly, if $C_{f,\Sigma}$ is not available due to some reason, a pre-decided prioritised set of feeders can be selected for tripping and LSA-PF works similar to LSA-Directional. This shows that in case of unavailability of certain signals, the advanced load shedding schemes can always fall back to a simpler load shedding scheme thereby, improving the reliability of the protection system.

6.4 Results

Performance indices are defined in order to quantify the benefit of using one scheme over another. The different proposed load shedding schemes are compared with respect to frequency responses and the following different performance indices.

6.4.1 Performance Indices

The following indices are defined in order to evaluate the performance of each scheme:

- ConsReduction: This parameter defines the total reduction in consumption in the transmission network which is caused due to load shedding as well as change in frequency. This is defined in p.u. considering 1000 MVA as base MVA.
- GenReduction: This parameter defines the total reduction in DG in the transmission network which is caused due to disconnection of feeders during load shedding. This is defined in p.u. considering 1000 MVA as base MVA.
- FreqNadir: This is the minimum value of the frequency reached in Hz.

Initially simulation is run for a single time window of 5 minutes. However, in order to test the performance of the schemes over large WT and PV generation scenarios, 400 simulations of 5 minute windows are run for randomly selected WT and PV scenarios over a span of 1 meteorological year.

6.4.2 Single Time Window

Feeder Selection Algorithm for LSA-PF

Table 6.5 shows generation and consumption for all the feeders for a distribution network for a specific instance for both LSA-PF and LSA-DG. It can be observed from Table 6.5 that all the feeders have same priority/score (since generations from DG are

Table 6.5: Generation and consumption in each feeder for LSA-PF and LSA-DG

Feeder i	Power flow P_i [MW]	Consumption C_i [MW]	DG $S_i + W_i$ [MW]	Score for LSA-PF Sc_i	Score for LSA-DG Sc_i
1	9.760	10	0.24	1	1
2	8.076	10	1.924	1	1
3	4.147	5	0.853	1	1
4	2.698	5	2.302	1	2
5	2.189	5	2.811	1	4
6	2.952	5	2.048	1	2
7	3.694	5	1.306	1	2
8	3.242	5	1.758	1	2
9	7.917	10	2.083	1	2
10	8.602	10	1.398	1	1

not known) based on which "Feeder Selection Algorithm" is run for LSA-PF. The outcome of this algorithm is [0 0 1 0 0 1 0 0 0 0], which means that feeder 3 and feeder 6 should be disconnected.
Therefore, total load disconnected = 10 MW and total generation disconnected = 2.901 MW

DG Estimation for LSA-DG

Table 6.6 shows the estimated power flow and measured power flow for all the feeders of a distribution network for a specific instance, based on which Root Mean Square Error (RMSE) and Normalised Root Mean Square Error (NRMSE) are calculated.

Table 6.6: Estimated and measured power flow for all the feeders for a distribution network

Feeder i	Measured Power flow $P_{m,i}$	Estimated Power flow $P_{e,i}$
1	9.76	9.7535
2	8.076	8.2791
3	4.147	4.3070
4	2.698	2.9022
5	2.189	2.3945
6	2.952	3.1573
7	3.694	3.8605
8	3.242	3.4140
9	7.917	7.9675
10	8.602	8.8045

$$RMSE = \sqrt{\frac{\sum_i (P_{m,i} - P_{e,i})^2}{total\_num\_feeders}} = 0.1713MW$$

$$NRMSE = \frac{RMSE}{(max(P_{m,i}) - min(P_{m,i}))} = 0.0226$$

It can be observed from Table 6.6 and RMSE & NRMSE values that DG estimation has low estimation error.

Feeder Selection Algorithm for LSA-DG

Table 6.5 also shows generation and consumption for all the feeders for a distribution network for a specific instance used for LSA-DG.

Priority/score for each feeder (based on Table 6.4) that can be observed in Table 6.5 is used to run "Feeder Selection Algorithm" for LSA-DG. The outcome of this algorithm is [0 1 0 0 0 0 0 0 0 0], which means that feeder 2 should be disconnected.
Therefore, total consumption disconnected = 10 MW and total generation disconnected = 1.924 MW. Therefore, it can be observed that for the same consumption and generation scenario, LSA-DG disconnects less amount of DG than LSA-PF ($= 2.901MW$).

Frequency Response

In a single time window of 5 min, the frequency response for all the load shedding schemes are compared as shown in Figure 6-6 and performance indices are given in Table 6.7. It can be observed from Figure 6-6 that FreqNadir values for the LSA-DG and

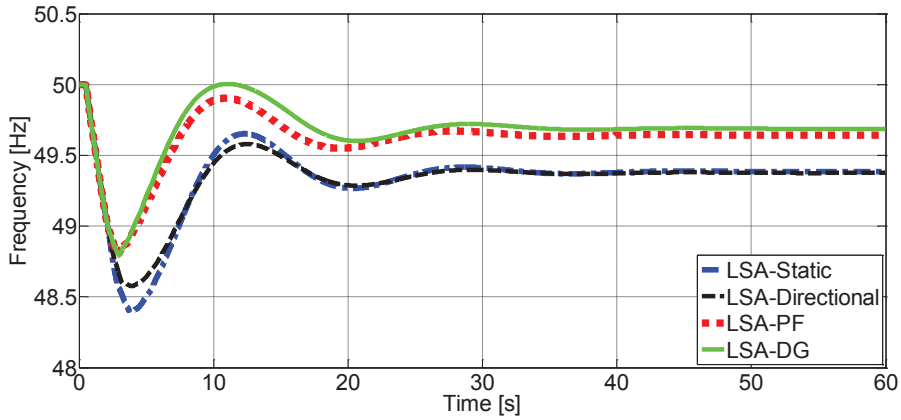

Figure 6-6: Frequency responses for different load shedding schemes

LSA-PF are higher than LSA-Static and LSA-Directional. From the FreqNadir values of Table 6.7, it can be observed that for LSA-Static, frequency goes down to 48.39 Hz.

Table 6.7: Performance of different Load Shedding Schemes

Load Shedding Algorithm	ConsReduction Abs. [p.u.]	ConsReduction Improvement over Static Relay [%]	GenReduction Abs. [p.u.]	GenReduction Improvement over Static Relay [%]	Relative Load Disconnection [p.u.]	FreqNadir Abs. [p.u.]	FreqNadir Improvement over Static Relay [Hz]
LSA-Static	1.4288	-	1.0802	-	0.3486	48.39	-
LSA-Direct.	0.862	38.67	0.5055	53.20	0.3565	48.57	0.18
LSA-PF	0.9994	30.05	0.3975	63.20	0.6019	48.81	0.42
LSA-DG	0.7665	46.35	0.1123	89.60	0.6542	48.805	0.415

This implies that there have been 4 stages of load shedding at 49 Hz, 48.8 Hz, 48.6 and 48.4 Hz. The reason for this is quite a lot of generation is disconnected by this scheme as a result the relative load disconnected (given by, ConsReduction-GenReduction) is less. For LSA-Directional consumption shedding is reduced and one less stage of load shedding than LSA-Static can be observed. However, since the frequency nadir is low, it is evident that amount of relative load disconnected in these stages is not adequate. Table 6.7 depicts that although absolute amount of consumptions disconnected are quite high for LSA-Static and LSA-Directional but relative loads disconnected are much less than LSA-PF and LSA-DG. Since, LSA-PF and LSA-DG have similar amount of relative loads disconnected and same number of load shedding stages (at 49 Hz), therefore the frequency responses are quite similar. However, it can be observed that LSA-DG scheme disconnects much less consumption and generation than other schemes.

6.4.3 Multiple Random Simulations

It should be noted that the results shown in Figure 6-6 and Table 6.7 are for specific generation and consumption scenario in a certain time window of 5 minutes. In order to validate the performance over all possible generation scenarios simulations, several wind and solar generation scenarios are randomly generated over a profile of 1 meteorological year. For each of these scenarios, same underfrequency event as discussed before is simulated. It should be noted that consumptions are assumed constant for all these simulated scenarios. For each scenario, ConsReduction, GenReduction and FreqNadir values are observed. Maximums, minimums and averages of these performance indices observed over 400 such simulations are shown in Table 6.8. RMSE and NRMSE for DG for 400 simulations are found to be 0.2827 MW and 0.0353 respectively.

It can be observed from Table 6.8 that LSA-DG performs much better statistically com-

Table 6.8: Performance Indices for 400 simulations

Load Shedding Algorithm	ConsReduction			GenReduction			FreqNadir		
	Max. [p.u.]	Min. [p.u.]	Avg. [p.u.]	Max. [p.u.]	Min. [p.u.]	Avg. [p.u.]	Max. [Hz]	Min. [Hz]	Avg. [Hz]
LSA-Static	1.48	0	1.027	1.108	0	0.473	49.06	47.94	48.32
LSA-Direct.	1.22	0	0.724	0.665	0	0.232	49.06	48.32	48.54
LSA-PF	1.025	0	0.712	0.496	0	0.154	49.06	48.35	48.76
LSA-DG	0.907	0	0.461	0.213	0	0.044	49.06	48.62	48.82

pared to other load shedding schemes.

6.5 Summary

- Traditional UFLS scheme (LSA-Static) tends to disconnect large amount of DG resulting in disconnection of consumptions more than requirement.
- LSA-Static may disconnect certain feeders with more generation than consumption. This has negative impact in terms of load shedding and may even invoke frequency instability.
- LSA-Directional incorporates directional element in traditional LSA-Static relay thereby preventing disconnection of feeder with generation greater than consumption.
- LSA-Directional may disconnect substantial amount of DG and not disconnect required amount of consumption.
- A novel algorithm called LSA-PF is proposed which uses combinatorial optimization to select feeders for disconnection based on their power flow data.
- LSA-PF has the advantages of improved frequency response as compared to LSA-static relays. This scheme disconnects required amount of load. However, this scheme may disconnect substantial amount of DG resulting in shedding consumption more than required.
- A novel algorithm called LSA-DG is proposed. This scheme uses the estimate of the amount of distributed PV and WT generation connected to each feeder along with the power flows through the feeders.
- LSA-DG performs much better as compared to other load shedding schemes.

Chapter 7

Conclusions and Future Research

This chapter summarizes the conclusions of the PhD thesis. Directions for future work in the field are also suggested.

7.1 Conclusions

This PhD project "Integration of renewable generation in power system defence plans" investigates how wind power and other renewable generation can contribute to the power system defence plans ensuring that major disturbances in the power system do not develop into system blackouts. The focus is especially on impacts of renewables on power system frequency stability. Reserve requirements in terms of volume, speed and technology of deployment in order to prevent frequency emergencies are proposed, developed and recommended. Defence plans against frequency instability are proposed, discussed and developed for power systems with large penetration of renewable generations.

The overall conclusions of this PhD study are given in the following:

- Risks of imbalances due to wind forecast errors exceeding designed frequency containment reserves of 3000 MW for Continental Europe network reduce exponentially with increase in volume of frequency restoration reserves and do not depend on speed of frequency restoration reserves activation. Power imbalances due to wind forecast errors for Continental Europe network in 2020 can be handled with reserves dimensioned as today. However, power imbalances due to wind forecast errors in 2030 can be high and cannot be handled by reserves dimensioned as it is in present scenario. Therefore, frequency restoration reserves for countries with high wind power penetration in 2030 should have additional volume of frequency restoration reserves (at least 2 times higher than the volume in present scenario).

- Fast deployment of reserves is required in preventing frequency instability if the system inertia is low. A mathematical analytical approach for frequency containment process demonstrates that the droop, system inertia and technology providing frequency containment reserves are deciding factors in containing the frequency following a large disturbance. Time to reach peak frequency (frequency nadir for underfrequency) is independent of the size of the disturbance. Following a large disturbance, frequency oscillates sinusoidally with an exponential decay depending on attenuation value. Attenuation of frequency oscillation is independent of size of disturbance and dependent on system inertia and droop.

  Hydro and Nuclear generators are unsuitable for providing frequency containment process since they are too slow. Fossil fuel steam, cross-compound steam generator and wind turbine are capable of providing frequency containment process. Proper droop settings for these technologies are designed for different system inertia . Both peak frequency (or frequency nadir) and attenuation are determining factors while designing the droop settings. For low inertia systems, droop should be high in order to prevent oscillatory instability. Wind turbines are capable of providing better response in terms of frequency containment process than conventional generators. It is feasible to operate the power system with lower inertia if frequency containment process is provided from wind turbines as compared to conventional generators.

- Proper protection settings for wind turbines are necessary but not sufficient to prevent frequency instability following a large disturbance, especially when wind power penetration is high. Therefore overfrequency emergency control from wind turbines is required.

  Overfrequency controls from wind turbines are dependent on droop settings, activation delays and ramp rate capabilities. Ramp rate should be at least 0.3 p.u./s or greater in order to obtain maximum support from wind turbines. Low droop settings for wind turbines are recommended in low wind power penetrated high inertia system, while high droop settings are recommended for high wind power penetrated low inertia system. Droop based frequency control may not be sufficient to prevent frequency instability if wind power penetration is as high as 80%. In such cases, virtual inertia supports from wind turbines are essentially required.

- Novel algorithms are proposed and developed for underfrequency load shedding considering high penetration of distributed generations. Traditional underfrequency load shedding scheme (LSA-Static) tends to disconnect large amount of distributed generation resulting in disconnection of consumptions more than requirement. This scheme can even disconnect certain feeders which has more generation than consumption. Underfrequency load shedding scheme incorporating directional relay (LSA-Directional) prevents disconnection of feeder with generation greater than consumption. However, LSA-Directional still can disconnect substantial amount of distributed generation without disconnecting the required amount of consumption. Underfrequency load shedding scheme using power flow data (LSA-PF) has the advantages of improved frequency response as compared to traditional relay. Although this scheme can disconnect required amount of consumption, however, this scheme may disconnect substantial amount of distributed generation. Underfrequency load shedding scheme using distributed generation data (LSA-DG) performs better than other load shedding schemes. This scheme disconnects minimum amount of distributed

generation while disconnecting required amount of consumption.

7.2 Future Research

There are always open questions at the end of a research work. Some suggestions for future work are:

- The adequacy of reserve requirements for future European networks is studied only to handle power imbalances caused by wind power forecasts. Therefore, the imbalances caused from other sources like contingencies, load, other stochastic generations like solar photovoltaics etc. could be added with these imbalances for future studies.
- It will be interesting to test the overfrequency control capabilities in terms of ramp rates and droop settings on a real wind turbine.
- Economic analysis and reliability studies of the proposed underfrequency load shedding schemes could be performed in future. Economic analysis could include implementation cost of the proposed underfrequency load shedding schemes and benefits of reduction in disconnections of distributed generations & consumptions. Further, the proposed distributed generation estimation scheme could be validated with real data from Distribution System Operators in future.
- Defence plans and strategies could be investigated and developed for voltage and rotor angle stability for future power systems with high penetration of renewable generations.

This page would be intentionally left blank if we would not wish to inform about that.

Appendix A

CorWind

Wind power prediction for different time horizons are performed using software called CorWind. CorWind is developed by Wind Energy Department at Technical University of Denmark. is used to simulate wind power time series ($P_{realtime}$) with realistic fluctuations for a large area and from time scales of a few seconds to a couple of hours [102], [103], [104]. An overview of CorWind is shown in Figure A-1. CorWind is also used to estimate wind power forecasts with short horizon like hour-ahead forecasts, P_{HA} and online forecasts, P_{online}.

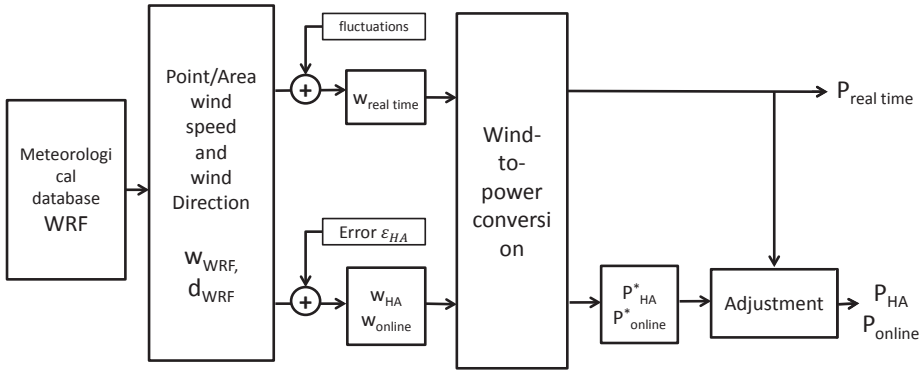

Figure A-1: Overview of Corwind

The input to CorWind is the wind speed from a meteorological model. Currently, the Weather Research and Forecasting (WRF) mesoscale model is used to provide the wind speed values at specified WRF grid points at an hourly resolution. CorWind interpolates these values to the location of the points in this study. The wind speed value w_{WRF} and wind direction d_{WRF} at each point for an hour is used to estimate a power spectral density (PSD) for that hour. In order to account for the observed correlation between the wind speed values at two points, the PSD for all the points are prepared such that the point-to-point coherence is consistent with an empirically derived function. The

coherent PSDs are then transformed into wind speed time series $w_{real\ time}$ for each point. The wind power $P_{real\ time}$ arising from a given wind speed condition is estimated using a wind-to-power conversion module.

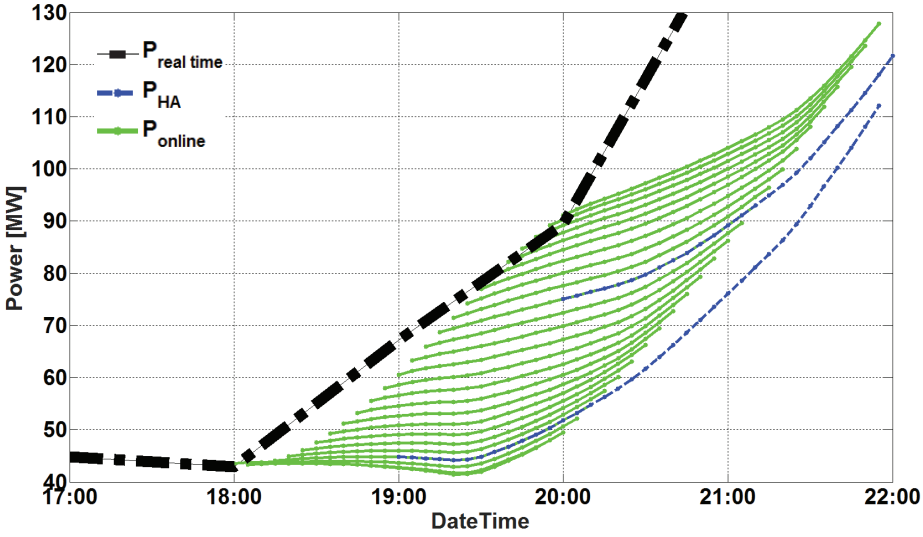

Figure A-2: Available Power, Hour Ahead and online forecasts

The wind speed w_{WRF} is also used to generate a wind speed forecast by adding a wind speed error from an autoregressive and moving average (ARMA) random process with a specified short term horizon. Like for $P_{real\ time}$, the corresponding wind power forecast is estimated by a wind-to-power conversion module to give an the intermediate wind power forecast P^*_{HA} or P^*_{online}. CorWind uses an adjustment procedure that aligns the initial part of a forecast with the values of the real wind power $P_{real\ time}$ near the time of the update, to give the output forecast P_{HA} or P_{online}. Hour-ahead forecasts are assumed to be calculated 30 minutes before the hour of operation, while the online forecasts are calculated close to real time. The other difference between P_{HA} and P_{online} is that P_{HA} is updated hourly while P_{online} is updated every 5 minutes, as illustrated in Figure A-2. These mean that the P_{online} is able to follow more closely the changes in $P_{real\ time}$.

The method has been optimized using measurement and historical forecast data such that the difference between the P_{HA} with $P_{real\ time}$ gives a realistic estimate of the hour-ahead wind power forecast error.

Appendix B

Classical thermal unit governor model

Classical thermal unit governor model as shown in Figure B-1 is developed based on the model provided by EUROSTAG library [105]. The model takes into account the following features : the governor, the turbine and the reheater and the boiler with its controls. The high pressure turbine represents a constant proportion (α) of the total mechanical power and is directly proportional to the valve position and the drum pressure. The low pressure turbine represents also a constant proportion (1 - α) of the total mechanical power. The position of the low pressure valve depends on the high pressure valve by a non-linear function. The reheater is represented by the integration of the difference between the high pressure and low pressure flow. The governor characteristic is defined by: reference power + $\Delta\omega/droop$ where $\Delta\omega$ is the speed deviation and $droop$ is the speed droop. The speed deviation is filtered by a dead band.

The drum pressure is defined as the integration of the difference between the input and output of heat. The turbine/boiler control is always the boiler following turbine mode.

The parameters for the model are described in Table B.1.

Table B.1: Parameters for classical thermal unit governor model

Parameter	Description
$droop$	Speed droop value
dB	Speed deviation dead band
DB_{ON}	"0" - dead band not active "1" - dead band active
MAX_{INT}	Governor power maximum limiter or steam generation high limit
$GOMP$	Coefficient of the LP valve position function
T_{SM}	Valve positioning servomotor time constant
V_O	Valve maximum opening speed
V_{FN}	Valve minimum closing speed
α	Contribution of the HP turbine to the mechanical power
T_{RES}	Reheater time constant
T_CH	Boiler storage time constant
P_{MAX}	Maximum boiler pressure
P_{MIN}	Minimum boiler pressure
T_{DELAY}	Fuel and waterwall equivalent time constant if coal fired boiler
G_{PVAR}	"1" - sliding pressure control mode not active "0" - sliding pressure control mode active
P_{VARMAX}	Maximum pressure
P_{VARMIN}	Minimum pressure
K_{CR}	Fuel controller gain
T_{CR}	Fuel controller integrator time constant
MIN_{FUEL}	Fuel input and steam generation low limit
T_{FV}	Derivative time constant
V_{FR}	Fast valving closing speed
$f(\omega, \frac{d\omega}{dt})$	Piecewise function delimiting the fast valving

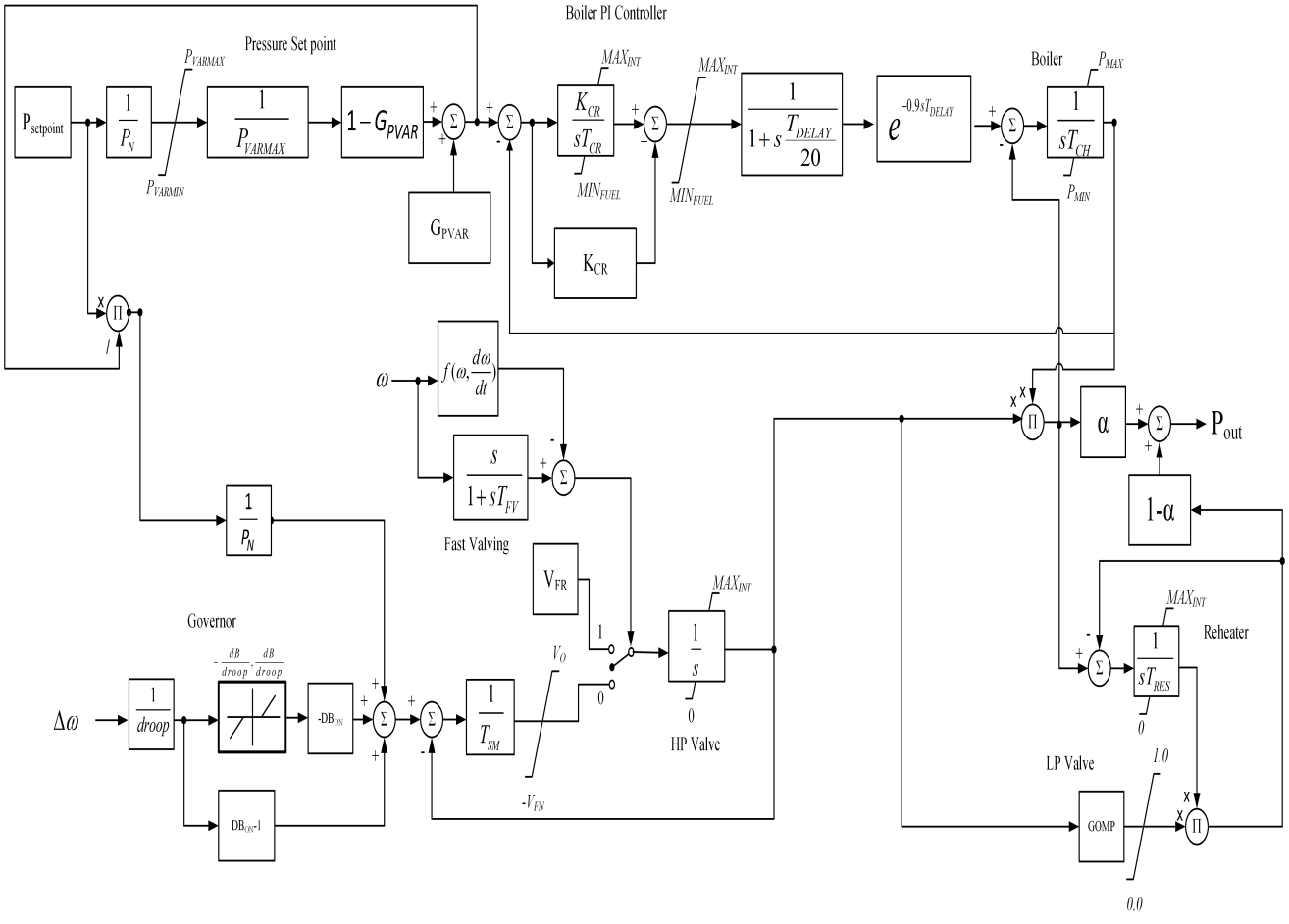

Figure B-1: Classical thermal unit governor model

This page would be intentionally left blank if we would not wish to inform about that.

Appendix C

Hydraulic turbine and governor model

Hydraulic turbine and governor model as shown in Figure C-1 is developed based on the model provided by EUROSTAG library [105]. The model takes into account the following elements :

- the turbine and penstock dynamics through a linear lead-lag transfer function;
- the valving circle and the water flow versus the gate characteristic;
- the speed governor represented by a proportional - integral regulator and the speed droop characteristic represented by $\Delta P + \Delta\omega/droop$;

The parameters for the model are described in Table C.1.

Table C.1: Parameters for hydraulic turbine and governor model

Parameters	Values
$droop$	Speed droop value
K_P	Proportional gain of the proportional integral controller
K_I	Integral gain of the proportional integral controller
T_C	Valving circle motor gain
V_O	Valving circle maximum opening speed
V_F	Valving circle maximum closing speed
T_{CE2}	Hydraulic system time constant (generally equal to the water starting time constant)
T_{CE1}	Hydraulic system time constant (generally equal to the half of the water starting time constant)

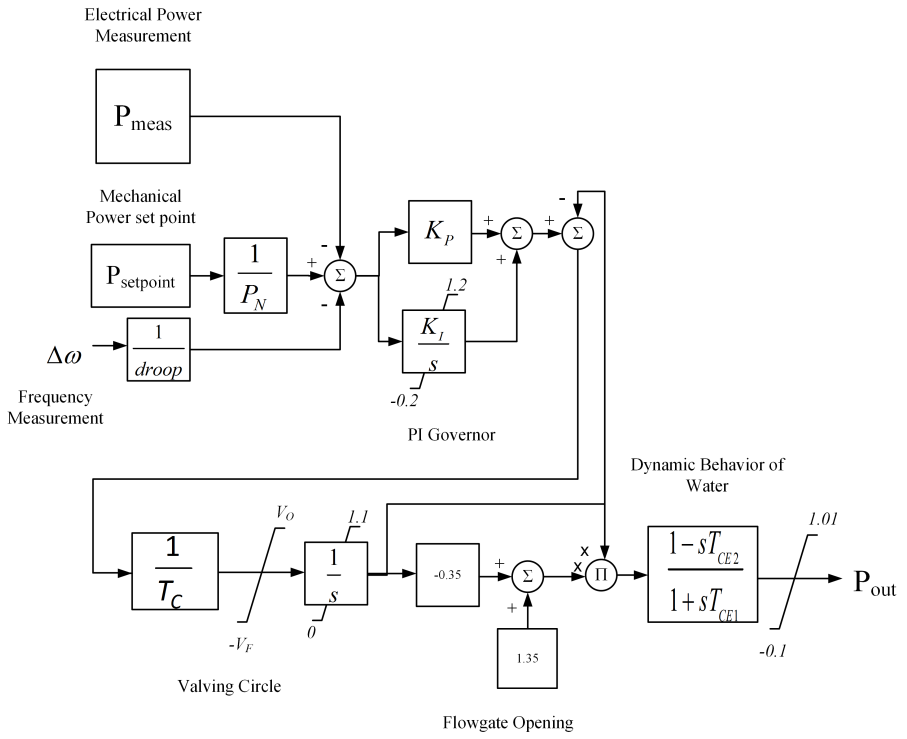

Figure C-1: Hydraulic turbine and governor model

Appendix D

Nuclear unit governor model

Nuclear unit governor model as shown in Figure D-1 is developed based on the model provided by EUROSTAG library [105].

The model takes into account only the turbines, the governor and the rate of power increase behaviours. The turbine and the governor models (speed droop, dead band) are identical to those of the classical thermal unit ones.

The parameters for the model are described in Table D.1.

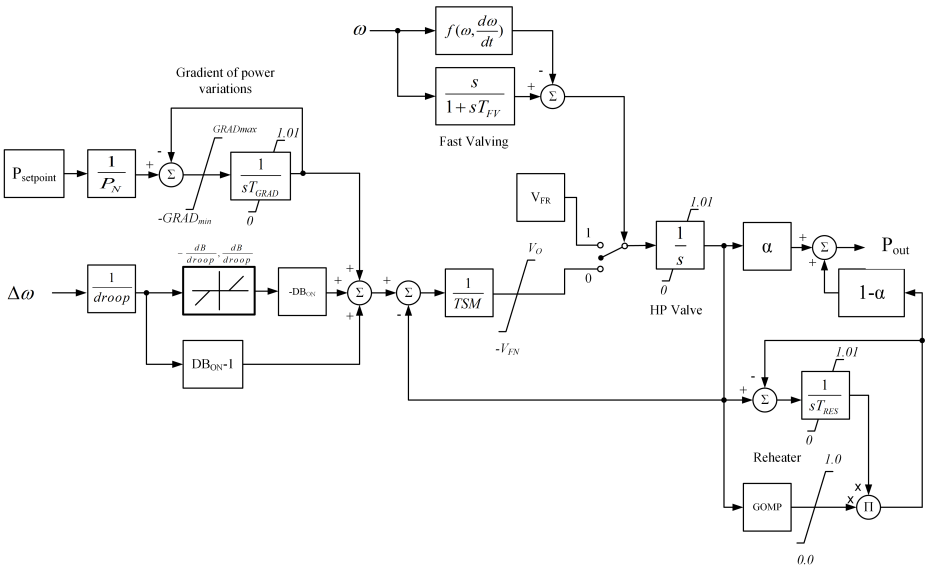

Figure D-1: Nuclear unit governor model

Table D.1: Parameters for nuclear unit governor model

Parameters	Description
$droop$	Speed droop value
dB	Speed deviation dead band
DB_{ON}	"0" - dead band not active '1" - dead band active
$GRAD_{MAX}$, $GRAD_{MIN}$	Maximum power increase and decrease gradient (assumed 0.5 MW/s for a 1 000 MW unit)
T_{GRAD}	Power gradient time constant
α	Contribution of the HP turbine to the mechanical power
T_{RES}	Reheater time constant
$GOMP$	Coefficient of the LP valve position function
T_{SM}	Valve positioning servomotor time constant
V_O	Valve maximum opening speed
V_{FN}	Valve minimum closing speed
T_{FV}	Derivative time constant
V_{FR}	Fast valving closing speed
$f(\omega, \frac{d\omega}{dt})$	Piecewise function delimiting the fast valving action in the plan $(\omega, \frac{d\omega}{dt})$

Appendix E

Wind Turbine Model

IEC 61400-27-1 Type 4A Wind Turbine Model [1]

Type 4 WTs are connected to the grid through a full scale converter as shown in E-1.

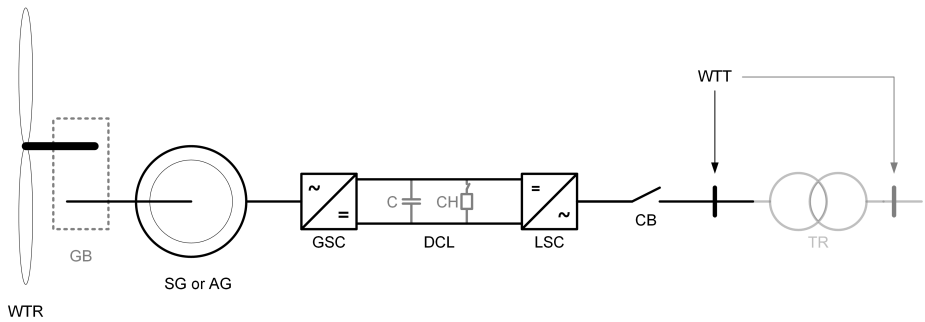

Figure E-1: Type 4 Wind Turbine

The generic modular structure of WT model is shown in E-2. Small description of modular structure is given as following:

- Electrical Equipment Block: which consists of Circuit Breaker and Transformer model for Type 4A WT.
  - Circuit breaker: which is standard circuit breaker model in the simulation tool is used. The circuit breaker model must open the circuit breaker when it receives the F_{OCB} flag.
  - Transformer: which is standard transformer model in the simulation tool is used.
- Grid Protection Block: which includes protection against over and under voltage, and against over and under frequency.

[1] IEC 61400-27-1 ed.1.0 "Copyright ©2015 IEC Geneva, Switzerland. www.iec.ch"

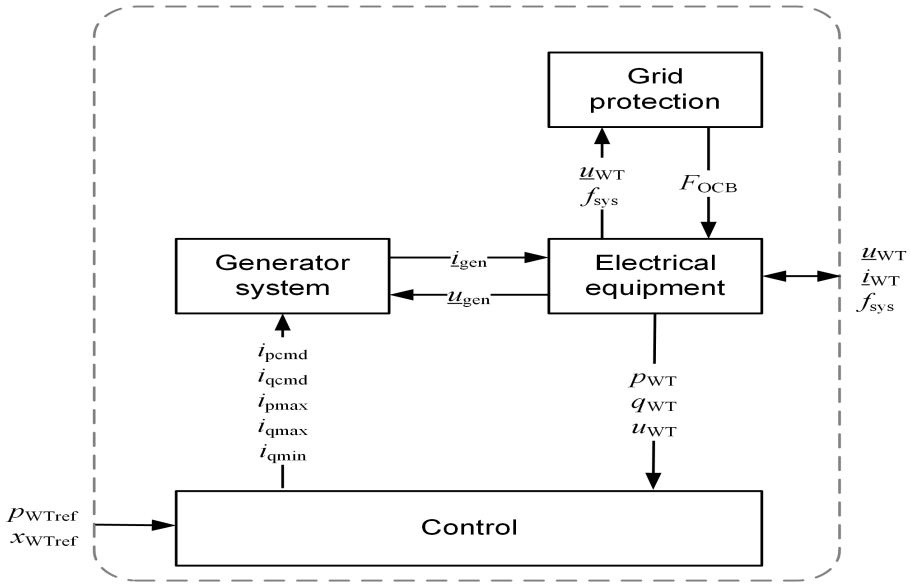

Figure E-2: Modular structure of Type 4A Wind Turbine

- Generator Block: which is modeled via a static generator component, including a current limiter, which has as inputs the current command signals generated by the control block. The generator model is shown in Figure E-3. Table E.1 gives the descriptions and values of different parameters for Type 4 generator set model.

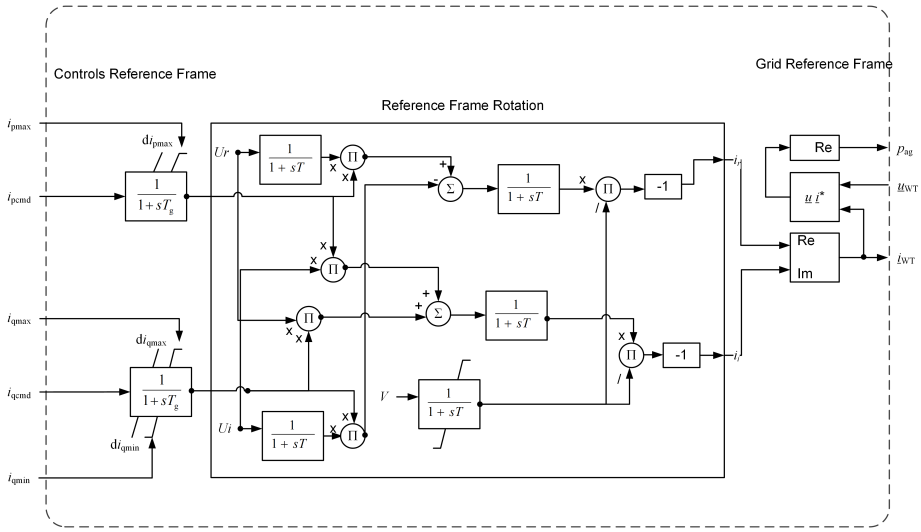

Figure E-3: Generator model of Type 4A Wind Turbine

- Control Block: which consists of several sub-blocks like Current Limiter, P control, and Q control. Modular control structure of Type 4A Wind Turbine is shown in Figure

Table E.1: Parameter list for Type 4 generator set model

Symbol	Base Unit	Description	Values
T_g	s	Time constant	0.005
di_pmax	I_n/s	Maximum active current ramp rate	99
di_qmax	I_n/s	Maximum reactive current ramp rate	99
di_qmin	I_n/s	Minimum reactive current ramp rate	-99

E-4.

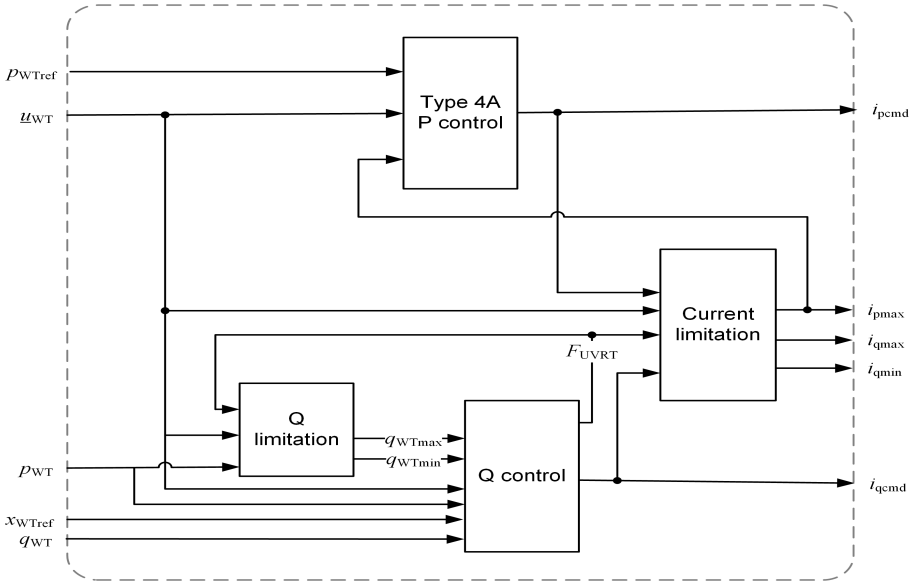

Figure E-4: Modular control structure of Type 4A Wind Turbine

- Current Limiter: which are generated as signals input to P control and Q control blocks. Based on current command signals, voltage and generator speed, maximum and minimum limiting current signals are generated which are further input to active power P control and reactive power Q control blocks.
- P Control Block: which generates current command signal for active power based on the active power reference signal from WPP controller and generator speed. It also generates the aerodynamic power signal.
- Q Limitation Block: which is modelled as constant maximum and minimum reactive power output.
- Q Control Block: which generates current command signal for reactive power. There are 4 different Q control modes - Voltage control, Reactive power control, Open loop reactive power control and Power factor control.

This page would be intentionally left blank if we would not wish to inform about that.

Bibliography

[1] "Final Report on System Disturbance on 4 November 2006," by UCTE. [Online]. Available: https://www.entsoe.eu/fileadmin/user_upload/_library/publications/ce/otherreports/Final-Report-20070130.pdf

[2] "Special Protection Schemes," Prepared by ENTSO-E subgroup "System Protection and Dynamics", ENTSO-E, March 2012.

[3] ENTSO-E, "NC Load Frequency Control & Reserve: Overview last Developments." [Online]. Available: https://www.entsoe.eu/fileadmin/user_upload/_library/resources/LCFR/120925__ENTSO-E_presentation_on_NC_LFC_R_update_final.pdf

[4] Energinet.Dk, "Technical regulation 3.2.5 for wind power plants with a power output greater than 11 kW," Technical report, Tech. Rep., 2010.

[5] EirGrid, "Grid code version 6," Tech. Rep., 2015.

[6] "Technical Background and Recommendations for Defence Plans in the Continental Europe Synchronous Area," Prepared by the Sub Group 'System Protection And Dynamics' Under Regional Group Continental Europe, ENTSO-E, Oct 2010.

[7] V. Akhmatov and A. H. Nielsen, "Simulation model of the transmission grid for a large offshore windfarm, used in education and research at the technical university of denmark," *Wind Engineering*, vol. 30, no. 3, pp. 255–263, 2006.

[8] ENTSO-E, "Supporting Document for the Network Code on Load-Frequency Control and Reserves." [Online]. Available: http://networkcodes.entsoe.eu/wp-content/uploads/2013/08/130628-NC_LFCR-Supporting_Document-Issue1.pdf

[9] ENTSO-E, "Scenario Outlook & Adequacy Forecast (SO&AF) 2014-2030." [Online]. Available: https://www.entsoe.eu/publications/system-development-reports/adequacy-forecasts/Pages/default.aspx

[10] ENTSO-E, "Assessment of the system security with respect to disconnection rules of Photovoltaic panels." [Online]. Available: https://www.entsoe.eu/publications/system-operations-reports/Documents/120530_Assessment_of_the_System_security_with_respect_to_disconnection_rules_of_PV_Panels.pdf

[11] P. Kundur et al., "Definition and classification of power system stability," *IEEE Transactions on Power Systems*, vol. 19, no. 3, pp. 1387–1401, Aug. 2004.

[12] CIGRE Task Force C2.02.24, "Defense Plans Against Extreme Contingencies," Technical Brochure, April 2007.

[13] T. Inoue, H. Taniguchi, Y. Ikeguchi, and K. Yoshida, "Estimation of power system inertia constant and capacity of spinning-reserve support generators using measured frequency transients," *IEEE Transactions on Power Systems*, vol. 12, no. 1, pp. 136–143, Feb 1997.

[14] S. Corsi and C. Sabelli, "General blackout in Italy Sunday September 28, 2003, h. 03:28:00," in *IEEE PES General Meeting*, Denver, 2004.

[15] S. Larsson and E. Ek, "The blackout in Southern Sweden and Eastern Denmark, September 23, 2003," in *IEEE PES General Meeting*, Denver, 2004.

[16] A. D. Hansen, P. Sørensen, F. Iov, and F. Blaabjerg, "Centralised power control of wind farm with doubly fed induction generators," *Renewable Energy*, vol. 31, no. 7, pp. 935–951, June 2006.

[17] A. D. Hansen, F. Iov, F. Blaabjerg, and L. H. Hansen, "Review of contemporary wind turbine concepts and their market penetration," *Wind Engineering*, vol. 28, no. 3, pp. 247–263, 2004.

[18] V. Madani, D. Novosel, S. Horowitz, M. Adamiak, J. Amantegui, D. Karlsson, S. Imai, and A. Apostolov, "IEEE PSRC report on global industry experiences with system integrity protection schemes (SIPS)," *IEEE Transactions on Power Delivery*, vol. 25, no. 4, pp. 2143–2155, 2010.

[19] P. M. Anderson and B. K. LeReverend, "Industry experience with special protection schemes," *IEEE Transactions on Power Systems*, vol. 11, no. 3, pp. 1166–1179, 1996.

[20] C. W. Taylor and S. Lefebvre, "HVDC controls for system dynamic performance," *IEEE Transactions on Power Systems*, vol. 6, no. 2, pp. 743–752, 1991.

[21] UCTE, "Operation Handbook," Union for the Co-ordination of Transmission of Electricity, Tech. Rep., June 2004.

[22] ENTSO-E, "Network Code on Load Frequency Control and Reserves (LFCR)." [Online]. Available: https://www.entsoe.eu/major-projects/network-code-development/load-frequency-control-reserves/Pages/default.aspx

[23] Nordel, "Nordic Grid Code (Nordic collection of rules)," 2007. [Online]. Available: https://www.entsoe.eu/fileadmin/user_upload/_library/publications/nordic/planning/070115_entsoe_nordic_NordicGridCode.pdf

[24] M. Milligan *et al.*, "Operating Reserves and Wind Power Integration:An International Comparison," in *Proceedings of 9th International Workshop on Large-Scale Integration of Wind Power into Power Systems*, Oct 2010.

[25] E. Ela, M. Milligan, and B. Kirby, "Operating Reserves and Variable Generation," NREL/TP-5500-51928, August 2011.

[26] E. Ela, B. Kirby, E. Lannoye, M. Milligan, D. Flynn, B. Zavadil, and M. O'Malley, "Evolution of Operating Reserve Determination in Wind Power Integration Studies," in *Proceedings of IEEE PES General Meeting*, July 2010.

[27] H. Holttinen *et al.*, "Methodologies to Determine Operating Reserves due to Increased Wind Power," *IEEE Transactions on Sustainable Energy*, vol. 3, no. 4, pp. 713–723, 2007.

[28] J. Kiviluoma, M. O'Malley, A. Tuohy, P. Meibom, M. Milligan, B. Lange, H. Holttinen, and M. Gibescu, "Impact of wind power on the unit commitment, operating reserves, and market design," in *Proceedings of IEEE PES General Meeting*, July 2011, pp. 1–8.

[29] A. Botterud, Z. Zhou, J. Wang, J. Valenzuela, J. Sumaili, R. J. Bessa, H. Keko, and V. Miranda, "Unit commitment and operating reserves with probabilistic wind power forecasts," in *Proceedings of IEEE PowerTech*, Trondheim, 2011.

[30] N. Menemenlis, M. Huneault, and A. Robitaille, "Computation of Dynamic Operating Balancing Reserve for Wind Power Integration for the Time-Horizon 1-48 Hours," *IEEE Transactions on Sustainable Energy*, vol. 3, no. 4, pp. 692–702, 2012.

[31] I. D. Margaris, S. A. Papathanassiou, N. D. Hatziargyriou, A. D. Hansen, and P. Sørensen, "Frequency control in autonomous power systems with high wind power penetration," *IEEE Transactions on Sustainable Energy*, vol. 3, no. 2, pp. 189–199, 2012.

[32] EUROPEAN COMMISSION, "Network code on requirements for grid connection of generators: Draft," 2015. [Online]. Available: https://www.entsoe.eu/Documents/Network%20codes%20documents/NC%20RfG/draft_ec_networkCodesJune.pdf

[33] R. Doherty, A. Mullane, G. Nolan, D. J. Burke, A. Bryson, and M. O'Malley, "An assessment of the impact of wind generation on system frequency control," *IEEE Transactions on Power Systems*, vol. 25, no. 1, pp. 452–460, 2010.

[34] TenneT, "Grid code-high and extra high voltage," 2012.

[35] National Grid, "Guidance notes - power park modules," Technical report, Tech. Rep., September 2012.

[36] Nordic Grid Code, "Nordel," 2007.

[37] H. Québec, "Transmission provider technical requirements for the connection of power plants to the hydro québec transmission system," *Montréal, Québec, Feb*, 2009.

[38] ENTSO-E, "Network code for requirements for grid connection applicable to all generators - requirements in the context of present practices," 2012. [Online]. Available: https://www.entsoe.eu/fileadmin/user_upload/_library/consultations/

Network_Code_RfG/120626_-_NC_RfG_-_Requirements_in_the_context_of_present_practices.pdf

[39] "IEEE Guide for the Application of Protective Relays Used for Abnormal Frequency Load Shedding and Restoration," *IEEE Standard C37.117-2007*, pp. c1–43, 2007.

[40] B. Delfino, S. Massucco, A. Morini, P. Scalera, and F. Silvestro, "Implementation and comparison of different under frequency load-shedding schemes," in *IEEE PES Summer Meeting, 2001*, vol. 1. IEEE, 2001, pp. 307–312.

[41] P. M. Anderson and M. Mirheydar, "An adaptive method for setting underfrequency load shedding relays," *IEEE Transactions on Power Systems*, vol. 7, no. 2, pp. 647–655, 1992.

[42] U. Rudez and R. Mihalic, "Analysis of underfrequency load shedding using a frequency gradient," *IEEE Transactions on Power Delivery*, vol. 26, no. 2, pp. 565–575, 2011.

[43] U. Rudez and R. Mihalic, "A novel approach to underfrequency load shedding," *Electric Power Systems Research*, vol. 81, no. 2, pp. 636–643, 2011.

[44] V. V. Terzija, "Adaptive underfrequency load shedding based on the magnitude of the disturbance estimation," *IEEE Transactions on Power Systems*, vol. 21, no. 3, pp. 1260–1266, 2006.

[45] F. Ceja-Gomez, S. S. Qadri, and F. D. Galiana, "Under-frequency load shedding via integer programming," *IEEE Transactions on Power Systems*, vol. 27, no. 3, pp. 1387–1394, 2012.

[46] W. P. Luan, M. R. Irving, and J. S. Daniel, "Genetic algorithm for supply restoration and optimal load shedding in power system distribution networks," *IEE Proceedings - Generation, Transmission and Distribution*, vol. 149, no. 2, pp. 145–151, 2002.

[47] S. Manson, G. Zweigle, and V. Yedidi, "Case study: An adaptive underfrequency load-shedding system," *IEEE Transactions on Industry Applications*, vol. 50, no. 3, pp. 1659–1667, 2014.

[48] C. P. Reddy, S. Chakrabarti, and S. C. Srivastava, "A sensitivity-based method for under-frequency load-shedding," *IEEE Trans. Power Syst*, vol. 29, no. 2, pp. 984–985, 2014.

[49] S. Mullen and G. Onsongo, "Decentralized agent-based underfrequency load shedding," *Integrated Computer-Aided Engineering*, vol. 17, no. 4, pp. 321–329, 2010.

[50] V. Chuvychin and R. Petrichenko, "Development of smart underfrequency load shedding system," *Journal of Electrical Engineering*, vol. 64, no. 2, pp. 123–127, 2013.

[51] Z. Liu, F. Wen, and G. Ledwich, "An optimal under-frequency load shedding strategy considering distributed generators and load static characteristics," *International Transactions on Electrical Energy Systems*, vol. 24, no. 1, pp. 75–90, 2014.

[52] D. Xu and A. A. Girgis, "Optimal load shedding strategy in power systems with distributed generation," in *IEEE Power Engineering Society Winter Meeting*, vol. 2, Columbus, Jan 2001, pp. 788–793.

[53] A. R. Malekpour, A. R. Seifi, M. R. Hesamzadeh, and N. Hosseinzadeh, "An optimal load shedding approach for distribution networks with DGs considering capacity deficiency modelling of bulked power supply," in *Australasian Universities Power Engineering Conference, 2008. AUPEC'08*. IEEE, 2008, pp. 1–7.

[54] P. Mahat, Z. Chen, and B. Bak-Jensen, "Underfrequency load shedding for an islanded distribution system with distributed generators," *IEEE Transactions on Power Delivery*, vol. 25, no. 2, pp. 911–918, 2010.

[55] TenneT, "Requirements for Offshore Grid Connections in the Grid of TenneT TSO GmbH," 2012. [Online]. Available: http://www.tennet.eu/de/fileadmin/downloads/Kunden/tennet_tso_gmbh-asn-eng_21122012_final.pdf

[56] ENTSO-E, "Requirements for Grid Connection Applicable to all Generators," 2013. [Online]. Available: https://www.entsoe.eu/fileadmin/user_upload/_library/resources/RfG/130308_Final_Version_NC_RfG.pdf

[57] L. Zeni, A. J. Rudolph, J. Münster-Swendsen, I. Margaris, A. D. Hansen, and P. Sørensen, "Virtual inertia for variable speed wind turbines," *Wind Energy*, vol. 16, no. 8, pp. 1225–1239, 2013.

[58] M. Altin, R. Teodorescu, B. B. Jensen, U. D. Annakkage, F. Iov, and P. C. Kjær, "Methodology for assessment of inertial response from wind power plants," in *IEEE Power and Energy Society General Meeting*. IEEE, 2012, pp. 1–8.

[59] G. C. Tarnowski, P. C. Kjær, S. Dalsgaard, and A. Nyborg, "Regulation and frequency response service capability of modern wind power plants," in *IEEE Power and Energy Society General Meeting*. IEEE, 2010, pp. 1–8.

[60] F. Díaz-González, M. Hau, A. Sumper, and O. Gomis-Bellmunt, "Participation of wind power plants in system frequency control: Review of grid code requirements and control methods," *Renewable and Sustainable Energy Reviews*, vol. 34, pp. 551–564, 2014.

[61] A. Basit, "Wind power plant system services," Ph.D. dissertation, 2014.

[62] P. Christensen and G. Tarnowski, "Inertia for wind power plants–state of the art review–year 2011," in *proc. 10th International Workshop on largescale integration of wind power into power systems*, 2011.

[63] J. Morren, J. Pierik, and S. W. H. de Haan, "Inertial response of variable speed wind turbines," *Electric Power Systems Research*, vol. 76, no. 11, pp. 980–987, July 2006.

[64] J. F. Conroy and R. Watson, "Frequency response capability of full converter wind turbine generators in comparison to conventional generation," *IEEE Transactions on Power Systems*, vol. 23, no. 2, pp. 649–656, 2008.

[65] N. R. Ullah, T. Thiringer, and D. Karlsson, "Temporary primary frequency control support by variable speed wind turbines-potential and applications," *IEEE Transactions on Power Systems*, vol. 23, no. 2, pp. 601–612, 2008.

[66] P.-K. Keung, P. Li, H. Banakar, and B. T. Ooi, "Kinetic energy of wind-turbine generators for system frequency support," *IEEE Transactions on Power Systems*, vol. 1, no. 24, pp. 279–287, 2009.

[67] M. Fischer, S. Engelken, N. Mihov, and A. Mendonka, "Operational experiences with inertial response provided by type 4 wind turbines," in *13th International Workshop on Large-Scale Integration of Wind Power into Power Systems*, 2014, pp. 457–463.

[68] M. Asmine and C.-E. Langlois, "Field Measurements for the Assessment of Inertial Response for Wind Power Plants based on Hydro Quebec TransEnergie Requirements," in *13th International Workshop on Large-Scale Integration of Wind Power into Power Systems*, 2014, pp. 1–6.

[69] S. Wachtel and A. Beekman, "Contribution of wind energy converters with inertia emulation to frequency control and frequency stability in power systems," in *8th International Workshop on Large-Scale Integration of Wind Power into Power Systems*, 2009, pp. 1–6.

[70] A. D. Hansen, M. Altin, I. Margaris, F. Iov, and G. C. Tarnowski, "Analysis of short-term over production capability of variable speed wind turbines," *Renewable Energy*, vol. 68, pp. 326–336, 2014.

[71] Handbook, UCTE Operations, "P1–Policy 1: Load-Frequency Control and Performance [C]," march 2009. [Online]. Available: https://www.entsoe.eu/fileadmin/user_upload/_library/publications/entsoe/Operation_Handbook/Policy_1_final.pdf

[72] 4COffshore, "Global Offshore Wind Database." [Online]. Available: http://www.4coffshore.com/windfarms/

[73] TheWindPower, "Wind Farms List." [Online]. Available: http://www.thewindpower.net/windfarms_list_en.php

[74] N. A. Cutululis, M. Litong-Palima, L. Zeni, A. Gøttig, N. Detlefsen, and P. E. Sørensen, "Offshore wind power data: Deliverable no: 16.1," Tech. Rep., 2012.

[75] EWEA, "Pure Power," 2011. [Online]. Available: http://www.ewea.org/fileadmin/ewea_documents/documents/publications/reports/Pure_Power_III.pdf

[76] ENTSO-E, "Impact of increased amounts of renewable energy on Nordic power system operation," 2010. [Online]. Available: https://www.energinet.dk/SiteCollectionDocuments/Engelske%20dokumenter/El/Wind%20report.pdf

[77] G. Giebel, R. Brownsword, G. Kariniotakis, M. Denhard, and C. Draxl, "The state-of-the-art in short-term prediction of wind power: A literature overview," ANEMOS. plus, Tech. Rep., 2011.

[78] P. M. Anderson and A. A. Fouad, *Power system control and stability*. John Wiley & Sons, 2008.

[79] P. Kundur, *Power system stability and control*, 2nd ed. McGraw-Hill, 1994.

[80] IEC Standard, "IEC 61400-27-1: Wind turbines - Part 27-1: Electrical simulation models - Wind turbines," pp. 61 400–27–1, 2014.

[81] K. Ogata, *Modern control engineering*. Prentice Hall PTR, 2001.

[82] K. Das, M. Altin, A. D. Hansen, P. E. Sørensen, and H. Abildgaard, "Primary reserve studies for high wind power penetrated systems," in *IEEE PowerTech Eindhoven, 2015*. IEEE, 2015, pp. 1–6.

[83] "Pegase." [Online]. Available: http://www.fp7-pegase.com

[84] Energinet.DK, "TR 3.2.5 Signal list for wind power plants," Technical report, Tech. Rep., 2015.

[85] "Wind turbines. Part 27-1: electrical simulation models for wind power generation-wind turbine models, Technical Report IEC 61400-27-1," *International Electrotechnical Commission*, 2015.

[86] PowerFactory User's Manual, "Digsilent gmbh," *Gomaringen, Germany, May*, 2011.

[87] ELIA, "Solar-PV power generation data." [Online]. Available: http://www.elia.be/en/grid-data/power-generation/Solar-power-generation-data/Graph

[88] Energinet.Dk, "Technical Regulation 3.2.1 for electricity generation facilities with a rated current of 16 A per phase or lower," Technical report, Tech. Rep., 2011.

[89] Energinet.Dk, "Technical regulation 3.2.5 for wind power plants with a power output greater than 11 kW," Technical report, Tech. Rep., 2010.

[90] Energinet.Dk, "Technical regulation 3.2.2 for PV power plants with a power output greater than 11 kW," Technical report, Tech. Rep., 2015.

[91] W. C. New, J. Berdy, P. Brown, and L. Goff, "Load shedding, load restoration and generator protection using solid state and electromechanical underfrequency relays," *General Electric Company, Philadelphia*, vol. 9, 1983.

[92] NERC, "SERC UFLS Standard: PRC-006-SERC-01." [Online]. Available: http://www.nerc.com/files/prc-006-serc-01.pdf

[93] NERC, "SPP Automatic Underfrequency Load Shedding: PRC-006-SPP-01." [Online]. Available: http://www.nerc.com/docs/standards/rrs/SPP_UFLS_Regional_Standard_Draft%207_clean.pdf

[94] R. V. Fernandes, S. A. B. de Almeida, F. P. M. Barbosa, and R. Pestana, "Load shedding - Coordination between the Portuguese transmission grid and the Distribution grid with minimization of loss of Distributed Generation," in *IEEE PowerTech Bucharest, 2009*, 2009, pp. 1–6.

[95] S. Martello and P. Toth, *Knapsack problems: algorithms and computer implementations*. John Wiley & Sons, Inc., 1990.

[96] C. L. Lawson and R. J. Hanson, *Solving least squares problems*. SIAM, 1974, vol. 161.

[97] Energinet.Dk, "Managing the transition towards a sustainable energy system - the role of the electricity sector," 2011. [Online]. Available: http://www.cnred.org.cn/english/jsp/downLoad.jsp?fileName=1-Energinet.dl+Presentations_20111020113102.pdf

[98] Alstom, "Integrating renewable energy resources." [Online]. Available: http://www.gegridsolutions.com/alstomenergy/grid/Global/Grid/Resources/Documents/Automation/NMS/NMS%20HiRES%20Brochure/Smart%20Grid%20renewable%20Brochure%20GB-epslanguage=en-GB.pdf

[99] R. Mackiewicz, "Overview of IEC 61850 and Benefits," in *Power Systems Conference and Exposition, 2006. PSCE'06. 2006 IEEE PES*. IEEE, 2006, pp. 623–630.

[100] A. Abur and A. G. Exposito, *Power system state estimation: theory and implementation*. CRC Press, 2004.

[101] K. Das, J. Hazra, D. P. Seetharam, R. K. Reddi, and A. K. Sinha, "Real-time hybrid state estimation incorporating scada and pmu measurements," in *Innovative Smart Grid Technologies (ISGT Europe), 2012 3rd IEEE PES International Conference and Exhibition on*. IEEE, 2012, pp. 1–8.

[102] P. E. Sørensen and N. A. Cutululis, "Wind farms' spatial distribution effect on power system reserves requirements," in *IEEE International Symposium on Industrial Electronics (ISIE)*, 2010, pp. 2505–2510.

[103] P. Sørensen, N. A. Cutululis, A. Vigueras-Rodriguez, L. E. Jensen, J. Hjerrild, M. H. Donovan, and H. Madsen, "Power Fluctuations From Large Wind Farms," *IEEE Transactions on Power Systems*, vol. 22, pp. 958–965, 2007.

[104] P. E. Sørensen, P. Pinson, N. A. Cutululis, H. Madsen, L. E. Jensen, J. Hjerrild, M. H. Donovan, and A. Vigueras-Rodriguez, "Power fluctuation from large offshore wind farms - Final report," Risø, Tech. Rep., 2009.

[105] Tractebel-RTE, "Standard Models Library, EUROSTAG."

DTU Vindenergi er et institut under Danmarks Tekniske Universitet med en unik integration af forskning, uddannelse, innovation og offentlige/private konsulentopgaver inden for vindenergi. Vores aktiviteter bidrager til nye muligheder og teknologier inden for udnyttelse af vindenergi, både globalt og nationalt. Forskningen har fokus på specifikke tekniske og videnskabelige områder, der er centrale for udvikling, innovation og brug af vindenergi, og som danner grundlaget for højt kvalificerede uddannelser på universitetet.

Vi har mere end 240 ansatte og heraf er ca. 60 ph.d. studerende. Forskningen tager udgangspunkt i ni forskningsprogrammer, der er organiseret i tre hovedgrupper: vindenergisystemer, vindmølleteknologi og grundlag for vindenergi.

Danmarks Tekniske Universitet
DTU Vindenergi
Nils Koppels Allé
Bygning 403
2800 Kgs. Lyngby
Telefon 45 25 25 25

info@vindenergi.dtu.dk
www.vindenergi.dtu.dk